Label-free DNA Sequence Detection Using Oligonucleotide Functionalized Fiber Probe with a Miniature Protrusion

Xingwei Wang

Dissertation submitted to the Faculty of the
Virginia Polytechnic Institute and State University
in partial fulfillment of the requirements for the degree of

Doctor of Philosophy
in
Electrical Engineering

Anbo Wang, Chair
Ira Jacobs
Gary R. Pickrell
Kristie L. Cooper
Ting Chung Poon

August 8, 2006
Blacksburg, Virginia

Keywords: Fiber Optic Biosensor, DNA Sequence Detection, Immobilization, Hybridization, Nano probe, Etching, Layer-by-layer Electrostatic Self-assembly
Copyright 2006, Xingwei Wang

Label-free DNA Sequence Detection Using Oligonucleotide Functionalized Fiber Probe with a Miniature Protrusion

Xingwei Wang

(ABSTRACT)

DNA is the substance that encodes the genetic information that cells need to replicate and to produce proteins. The detection of DNA sequences is of great importance in a broad range of areas including genetics, pathology, criminology, pharmacogenetics, public health, food safety, civil defense, and environmental monitoring. However, the established techniques suffer from a number of problems such as the bulky size, high equipment costs, and time-consuming algorithms so that they are limited to research laboratories and cannot be applied for in-vivo situations. In our research, we developed a novel sensing scheme for DNA sequence detection, featuring sequence specificity, cost efficiency, speed, and ease of use. Without the need for labels or indicators, it may be ideal for direct in-cell application.

The principle is simple. With capture DNA immobilized onto the probe by layer-by-layer self-assembly, the hybridization of a complementary strand of target DNA increases the optical thickness of the probe. Three kinds of sensors were developed. The optical fiber tip sensor has been demonstrated with good specificity and high sensitivity for target DNA quantities as small as 1.7 ng. To demonstrate the potential of this structure for practical applications, tularemia bacteria were tested.

Two other micrometric structures were designed with specific advantages for different applications. The micro-fiber Bragg grating interferometer (Micro-FBGI) has the intrinsic temperature compensation capability. The micro-intrinsic Fabry-Perot interferometer (Micro-IFPI)features simple signal processing due to its simple configuration. Successful DNA immobilization and hybridization have been demonstrated onto the $25\mu m$ Micro-IFPI. Both structures have great potential for nanometric protrusion, allowing future in-cell DNA direct detection. In addition, its quick response

time leads to the potential for express diagnosis. What's more, the idea of nanoscale probe has a broad impact in scanning near-field optical microscopy (SNOM), intracellular surgery in cell sensing, manipulation, and injection.

Keywords: Fiber Optic Biosensor, DNA Sequence Detection, Immobilization, Hybridization, Nano probe, Etching, Layer-by-layer Electrostatic Self-assembly.

Acknowledgments

First of all, I would like to thank Dr. Anbo Wang for bringing me to the Center for Photonics Technology and accepting me as one of your graduate research assistants. I consider myself very lucky and privileged to work in such a state-of-art research center and have the opportunity to contribute to so many different projects, including physical sensors for harsh environments, nanoprobe fabrication, and biosensors for DNA detection. I would also like to thank you for showing such confidence in my abilities and encouraging me to perform to the best of my capabilities. You have seen me grow academically and personally and I thank you for all of the wonderful advice that has shaped me into the professional I am today. Without your professional guidance and enormous encouragement, my research progress and accomplishment of getting my Ph.D. degree within three and a half years would not have been possible. For me, you have not only been a mentor, but also a role model and a friend.

I would also like to extend my gratitude to my other committee members, Dr. Ira Jacobs, Dr. Ting Chung Poon, Dr. Gary R. Pickrell, and Dr. Kristie L. Cooper. Thank you for the many fruitful discussions and for the valuable guidance and support during the preparation of this dissertation. Especially thanks to Dr. Cooper for your help in our technical writing, proposal preparation, and project management. Without you, this document and my success as a research assistant would not have been possible.

I also owe a lot of thanks to the staff and students of the CPT for making CPT a great place for study and research. Very special thanks go to Ms. Debbie Collins. Thank you for all of the administrative support as well as personal advice. Thanks to all the students in CPT. I really

enjoyed the discussions with you that intrigue my inspiration and push me to discover my potential. I am especially grateful to Juncheng Xu for your assistance and encouragement; to Zhuang Wang, Yan Zhang, and Yizheng Zhu for your knowledge and patience. Our happy cooperation has made this an unforgettable and productive experience. I really enjoyed the years working with you.

Personally, I would like to thank my family for their never-ending encouragement, love, and support throughout my life. Thank you for always being there and for being so understanding. You are my inspiration and my joy.

Contents

List of Figures

List of Tables

Chapter 1

Introduction

1.1 Motivation

DNA is an essential biological material whose base sequence controls the heredity of life [1]. The detection of DNA sequences is of particular interest in genetics, pathology, criminology, pharmacogenetics, food safety, and many other fields. Problems associated with the established techniques include the bulky size, high equipment costs, and time-consuming algorithms. Therefore, such systems are limited to research laboratories and cannot be applied for in-vivo situations. The motivation of this research is to develop a fiber probe biosensor with a miniature protrusion for direct in-cell DNA sequence detection without the need for labels or indicators, featuring sequence specificity, cost efficiency, speed, and ease of use.

Identification of the genetic changes that drive cancer progression is providing us with a variety of molecular markers that may be valuable tools for early detection of cancer. Cancer is a heterogeneous group of diseases, each consisting of a series of complex genetic alterations causing uncontrolled growth and spread. The genetic changes during tumorigenesis can be used as indicators for detection of cancer cells in clinical samples. Pioneer studies indicate that these markers can be used for cancer detection in different clinical settings with unprecedented precision.

Diagnosis and management of infectious diseases is another important application for DNA sensors. Infectious diseases are the third leading cause of death in the United States and the first cause worldwide. Since 1992, a greater awareness of emerging infectious diseases and the threat of bioterrorism has developed. Rapid detection of infectious diseases is of essential significance to minimize illness, disability, death, and economic losses.

DNA hybridization sensors hold enormous potential for early cancer detection and rapid diagnosis of infectious diseases. Classical culture procedures, which have been utilized in the clinical microbiology laboratory for a century or more, are labor-intensive and time-consuming. As the urgent need for a safer blood supply and food pathogen identification, and the pressure to reduce the health care costs intensifies the need for less labor-intensive and more rapid clinical microbiology tests increases.

Mycobacterium tuberculosis (TB), the causative agent of tuberculosis, is a good example. In 1993, disease caused by TB was declared a global emergency by the World Health Organization (WHO). Annually TB has a worldwide mortality rate of three million. The emergence of the modern TB epidemic is linked with the HIV epidemic. The compromised immune system of HIV sufferers leaves them more susceptible to the M. *tuberculosis*pathogen, which is highly infectious and transmissible [2]. Current methodologies rely on culture methods and diagnostic techniques, which take up to 30 days to produce definitive results, due to the extremely slow growth rate of M. *tuberculosis* [3]. In a complete genetic analysis system, the direct detection of DNA could be completed in minutes. Rapid diagnostic tests for infectious diseases have been shown to be highly valuable in facilitating major improvements in disease management .

The most promising new technologies are nucleic acid amplification (NAA) methods, which have improved sensitivity and specificity of tests in a format compatible with automation. Polymerase chain reaction (PCR), developed by Roche Molecular Systems (Pleasanton, CA), was the first NAA method and has been the most successfully implemented technology in basic research and clinical application. There are three basic steps: denature target strands, anneal primers, and amplify the strands. With alternating temperatures, the PCR technique creates a double-stranded nucleic

acid product called amplicons. By repeating the cycle several times, large quantities of amplified product are produced.

After PCR amplicons are made, their sequence must be confirmed. A variety of methods have been developed for the detection of the binding of the complementary strand of DNA. Chip-based DNA sensors offer sensitivity, specificity, and parallelization for detection of selected DNA sequences or mutated genes associated with human diseases. This is a solid substrate on which capture DNA is immobilized and after the binding of the complementary target DNA the binding is detected. Fluorescent dyes are the standard label for gene chips. However, these dyes are expensive and they can rapidly photobleach. Also, the readout of those arrays involves highly precise and expensive instrumentation and requires sophisticated numerical algorithms to interpret the data, which makes the analysis time consuming [4, 5].

DNA chip detection schemes that use an electrical signal rather than the optical signal from the fluorescent dyes are being developed by a number of research groups currently. The idea, however, is over 40 years old. The first experiments in this area were performed by Palecek who developed methods to discriminate single as opposed to double-stranded DNA through direct DNA reduction [6]. Current techniques include nanoparticle-based electrical DNA detection, redox-active reporter molecules, enzymes as electrical transducers, direct electrochemical detection, capacitance-based detection, etc. [7].

However, many biological and medical applications require in cell DNA detection. Generally speaking, plant cells are on the order of $100\mu m$, while animal cells are on the order of $10\mu m$. The chip biosensors with millimeter bulky size are no longer sufficient. Our main goal is to fabricate nanometric size DNA sensors that can be inserted into cells for direct detection.

As far as materials are concerned, much effort has been invested in the immobilization of DNA probes onto various solid supports. Glass-slides, nitrocellulose-coated microscope slides, and silicon-based DNA microarrays are widely used. Among the materials, silicon dioxide has a few unique advantages. Firstly, silicon dioxide is biocompatible which makes it suitable for in situ applications. Secondly, silicon dioxide is a durable material that sustains high temperature and

washes of high ionic strength. Thirdly, it is non-porous so the hybridization volume can be kept to minimum thus enhancing the kinetics of annealing probes to target. Finally, optical fiber, whose material is silicon dioxide, is an efficient media to transmit signal. Therefore, in this research, probe DNA is immobilized on the optical fiber tip.

In this research program, a micrometric protrusion was developed and fabricated on the tip of an optical fiber. Then capture DNA was self-assembled onto the fiber probe. Once the complementary DNA was hybridized with immobilized probes, the thickness of the fiber tip increased. Without the requirement for labels or amplification steps, this novel nanoscale DNA sensor will be able to detect specific DNA sequence in seconds. This biosensor technology is promising for rapid, low cost, selective, accurate and reliable in-cell DNA detection.

Such DNA sensors hold a great potential for early diagnosis of cancer and infectious diseases, for on site detection of food contamination, for environmental monitoring, and for forensic studies. A potentially major application could be the detection of the presence of pathogenic microorganism and analytes (carcinogens, drugs, mutagenic pollutants, etc.) with binding affinities for the structure of DNA during the testing of water, food, soil, and plant samples.

1.2 Broader impacts

The DNA sensor is a kind of biosensor. Biosensors, capable of detecting a biological phenomenon by the conversion from biomolecular signals to physical signals, have been developed during the last two decades for environmental, industrial, and biomedical diagnostics. They usually consist of a bioreceptor and a transducer. The bioreceptor can be a bio-sensitive layer containing biological recognition elements attached to the transducer. The transducer converts the physicochemical perturbation produced by the interaction between the target analyte and the bioreceptor into a measurable effect. Bioreceptors provide specificity because they enable binding of the specific analyte of interest to the sensor for the measurement with minimum interference from other components. Biological sensing elements can be either a biological molecular species (e.g. an antibody, an

enzyme, a protein, or a nucleic acid) or a living biological system (e.g. cells, tissue, or whole organisms) that utilizes a biochemical mechanism for recognition.

Extensive research has been devoted to the development of a variety of fiber-optic biosensors that have paved the way for the development of the fiber-optic nanosensors. The development and application of submicron fiber-optic chemical sensors with distal diameters between 20 and 500 nm have been reported [8, 9].

In addition, submicron fiber-optic biological sensors have been developed and used to detect biochemical targets inside single cells [10]. Single-cell analysis (SCA) technology is of great significance. First of all, in addition to providing a complement to conventional bulk cell assays, it can provide dynamic analysis of interactions within individual living cells. Secondly, when the number of sample cells obtained from surgical procedures is limited, and cannot be propagated for study, SCA is especially important.

However, traditional techniques for intracellular analysis require “fixing” cell samples before analysis, which often destroys the viability of the cells and may greatly change cellular architecture. Micron and sub-micron fiber-optic biomedical sensors have been developed and used to detect biochemical targets inside single cells. They could provide the path to investigate important intracellular biological processes in vivo because of the minimally invasive nature of the technique. Fiber optic sensors can consist of a biologically or chemically sensitive layer attached to an optical transducer. The transducer can thus convert the result of the interaction between the sensing layer and the target into a measurable effect such as an electrical signal. The integration of these advances in miniature structure technology and biotechnology could lead to a new generation of biomedical sensors with high sensitivity and good selectivity for probing and sensing of living cells at the molecular level.

In addition, such nanosensors can be very useful in the study of near-field scanning optical microscopy (NSOM). The combination of NSOM and surface-enhanced Raman scattering (SERS) has been demonstrated to detect biochemicals on solid substrates with sub-wavelength 100 nm spatial resolution.

1.3 Outline of dissertation

The major objective was to develop a fiber probe biosensor with a miniature protrusion for in-cell DNA sequence direct detection without the need for labels or indicators, featuring sequence specificity, cost efficiency, speed, and ease of use. The research work described in this dissertation, entitled “Lable-free DNA Sequence Detection Using Oligonucleotide Functionalized Fiber Probe with a Miniature Protrusion”, is focused on the following issues:

1. Design and develop an innovative sensor scheme with high sensitivity, sequence specificity, and rapid response time, to meet the requirements of DNA direct detection applications.

2. Design and develop the miniature sensor probe fabrication techniques and fabrication system to meet the requirements of future in-cell DNA sequence detection applications.

The layout of this dissertation is as follows:

1. The first chapter opens with an introduction to the important needs of the in-cell DNA detection sensors and the problems of current available technologies, followed by the objective and scope of my research.

2. Chapter 2 reviews in detail the existing DNA detection methods, presents the concept of our miniature fiber probe DNA sensor, and discusses the advantages of this novel idea over the conventional ones.

3. In Chapter 3, different current nanoprobe design and fabrication methods are given. Their advantages and disadvantage are discussed.

4. Chapter 4 reviews different capture DNA bonding methods with the L-b-L ESA approach emphasized.

5. In Chapter 5, the main factors that influence DNA immobilization are discussed. The results are based on a series of experiment trials guided by the Taguchi method.

6. Chapter 6 describes the fabrication of an optical fiber DNA sensor. Immobilization and hybridization of DNA onto the fiber tip with L-b-L ESA are demonstrated. The sensor is proven to feature high sensitivity and good specificity. In addition, experiments on bacteria samples are also given.

7. Chapter 7 introduces two kinds of sensor structures for nanoprobe design. Their specific advantages and disadvantages are discussed.

8. Chapter 8 gives the results of immobilization and hybridization of DNA onto the micrometric tip sensor. The results demonstrate great potential for future nanometric-size sensor for in-cell DNA direct detection.

9. Chapter 9 gives the summary and suggestions for the future work.

Chapter 2

DNA Sequence Identification Schemes

With the progress of the Human Genome project and the discovery of the genetic basis of disease, there is a tremendous demand for efficient instruments to analyze DNA-encoded information to improve medical diagnosis and treatment.

DNA hybridization sensors play an important role in identification of causal pathogens and determination of the presence of bacterial and viral species. They are of great significance in food safety, environment monitoring, and public health management. Classical methods are often inconvenient because of their time-consuming process and the requirement for trained personnel and additional reagent preparation. As a result, significant research has been devoted to the development of DNA sensors that are sensitive, selective and relatively simple to use [11, 12].

As a kind of biosensor,a DNA sensor shares a similar simple principle: a specific biochemical receptor is attached to a transducer, which translates the recognition result into a measurable signal [13, 14]. The main challenges associated with these devices are the sensitivity and the specificity of the receptor and the transducer. These problems are often addressed by immobilization of the specific sensing element in relatively high concentration and choice of signal transduction mechanism. A high concentration sensing element near the transducer can serve as a kind of preconcentrating analyte before detection. Transduction mechanisms to detect DNA hybridization

include electrochemical, piezoelectric, and optical systems. The validity of the approach depends on the biochemical materials to be detected. For example, amperometric transducers are particularly suitable for redox enzyme systems, because recognition is through an enzymatic reaction that generates or consumes redox-active species to be detected. However, they are inappropriate for detection of the hybridization of a DNA single strand with its complementary strand since their selective recognition properties are based on affinity.

In order to convert the DNA-encoded information stored in DNA, a number of fundamental issues have to be resolved. In this chapter, the properties of DNA are introduced first. Then the current identification procedures are reviewed followed by their problems and need for improvement. The design and operating principle of our nanoprobe in-cell DNA sensor are presented in the last part.

2.1 DNA properties

DNA (deoxyribonucleic acid) is the chemical responsible for preserving, copying and transmitting information within cells and from generation to generation. Nucleotides are single building blocks of DNA. Since all DNA nucleotides contain a phosphate group and deoxyribose as the sugar, the only difference among them is the nitrogen base. There are four nitrogen bases that can be used to build DNA. Therefore, there are just four choices of nucleotides (symbolized by A, T, G, and C), as shown in Fig. 2.1.

The nucleotides bond to one another by linking up from phosphate group to deoxyribose to phosphate group to deoxyribose. This bonding causes them to form a single chain. However, DNA is actually made up of two chains, the second chain, called the complementary chain, has an order of nucleotides that corresponds in a particular manner to the first chain as shown in Fig. 2.2. They are connected by hydrogen bonding (non-covalent) between paired bases. A and T are connected by two hydrogen bonds (non-covalent). G and C are connected by three.

In a DNA molecule, the two strands, each resembling a helix, intertwine with each other. Therefore, the two strands form a “double helix” structure. This was first discovered by James D. Watson

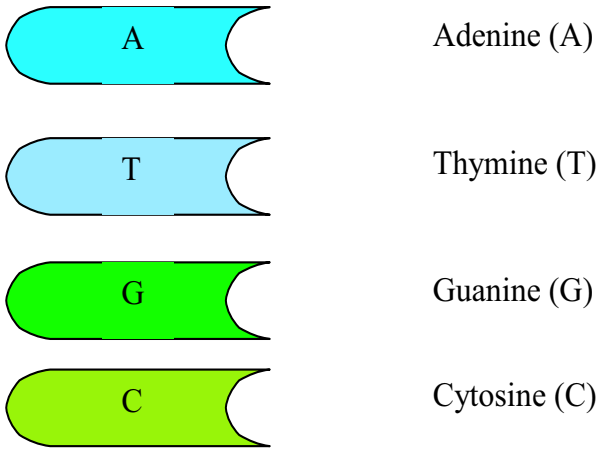

Figure 2.1: Four nitrogen bases of DNA.

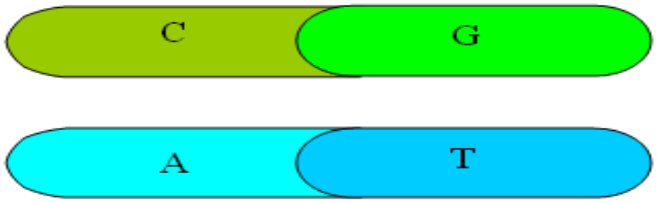

Figure 2.2: Complementary chains of DNA.

and Francis Crick in 1953.

The resulting double helix structure, including the local base pairing and the overall helix pitch is partially defined by base pairing and base stacking, as well as the constraints imposed by backbone conformation and sugar pucker. In solution, DNA is a right-handed double helix structure, also known as the B form. There are about 10 nucleotide pairs per helical turn, and the distance between two neighboring pairs is 0.34 nm. Hence, a turn is about 3.4 nm. DNA structure may be in an A form when salt concentration is high or alcohol is added. It is still right-handed, but there are 11 base pairs per turn, and a turn is 2.3 nm. A third structure is in Z form, which is left-handed. There are 12 base pairs per turn, and a turn spans 4.6 nm.

According to the Watson and Crick model, hybridization of two complementary strands is a very selective recognition process. There are two steps:

1. Nucleation: bonding between two short complementary regions of DNA;
2. Rapid binding of the remaining base pairs to form the strand.

Therefore, when a single chain of DNA is electrostatically self-assembled on silicon or silica surfaces, the complementary chain will be easily bonded to it.

The process of identifying the existence of a certain expression involves 6 steps:

1. Synthesis of the single-stranded capture DNA sequence.
2. Attachment of the capture DNA strand to a probe.
3. Introduction of the samples to be identified to the probes in aqueous form.
4. Hybridization will occur if the sample is complementary with the capture sequence on the probe.
5. Washing away the remaining unattached samples.
6. Decision and measurement. If the targeted DNA samples have the complementary sequence to the immobilized single-stranded DNA probe, then bonding of the bases from the two DNA strands strongly combines the two together. The targeted DNA is hybridized at the surface. Otherwise, the sample will be removed after washing.

2.2 Current DNA sequence identification techniques

In clinical molecular biology, it is often required to find the existence of a certain known DNA expression in a given sample. The important tool for measuring the expression of genes and characterizing complex genetic activity changes is the hybridization of a complementary DNA strand attached to immobilized DNA probe.

A variety of methods have been developed for the detection of the binding of the complementary strand of DNA according to the above steps. The sensors employ single stranded probe DNA that is immobilized on the surface of the transducer and behaves as the biological recognition element [13–16]. DNA biosensors have been based on electrochemical and optical methods, whereby the local hybridization event is converted into an electrical or optical signal and measured. The difference lies in the probe design scheme, the binding method between capture DNA and the probe, and the signal readout technique.

Electrochemical methods have been extensively studied since the electroactivity of nucleic acids was discovered about 40 years ago. Most of them are indirect, using radiochemical, enzymatic, fluorescent, or electrochemiluminescent indicators. [13–15] However, these techniques are inconvenient due to their need for labels as indicators and their excessive pretreatments, which may increase the risk of contamination and preclude in situ monitoring.

In comparison with the existing detection techniques using labels, label-free methods such as field effect detection, surface plasmon resonance, the electrochemical method, QCM, surface stress measurements, and AFM force measurements eliminate the perturbation from these attached labels. In the following sections, different schemes are introduced in detail.

2.2.1 Polymerase chain reaction (PCR)

PCR is not a DNA detection scheme; instead, it is a method to make large quantities of copies of a gene. It is usually necessary to provide enough samples for detection or sequencing.

There are three major steps in a PCR:

1. Denaturation at $94°C$: the double stranded DNA melts into single stranded DNA. At this time, all enzymatic reactions stop.

2. Annealing at $54°C$: At the beginning, ionic bonds are constantly formed and broken between the single stranded primer and the single stranded template. If the primers fit exactly to the

template, the bonds are stable and last a little bit longer. Then the polymerase can attach and start copying the template. Once there are a few bases built in, the ionic bond between the template and the primer has a stronger ionic attraction than the forces breaking them. Therefore, it does not break anymore.

3. Extension at $72°C$: This is the ideal working temperature for the polymerase. Because the temperature is higher, primers that are non-complementary to the template get loose again. Only those bases complementary to the template are coupled to the 3' side.

An exponential increase in the number of copies can be obtained because both strands are copied at the same time. Therefore, after n cycles, there will be 2^n copies. Usually it is repeated for 30 or 40 cycles. The whole process can be performed on an automated cycler, which can heat and cool the tubes quickly.

2.2.2 Fluorescence-based optical DNA detection

Florescence-based optical DNA detection is one of the most popular methods in use. Before the samples are introduced to the probe, some kind of fluorescence label is attached to the samples to be identified. After the immobilization, fluorescence micrographs are taken by CCD camera to illustrate the final result of hybridization.

For example, Texas Red is used in reference [14]. Under illumination of a 100 W mercury lamp with bandpass filter wavelength 595nm, the label emits fluorescence at a wavelength of 615nm corresponding to the red color in the visible spectrum.

However, this fluorescence-based optical detection technique suffers from many problems. First of all, the fluorescent dyes are expensive and can rapidly photobleach. Secondly, the readout involves expensive instrumentation and needs sophisticated numerical algorithms to interpret the data. Thirdly, the process is time-consuming. These problems generally limit its use to research laboratories and make it hard to adapt this detection scheme for on-site or point-of care use.

2.2.3 Nanoparticle-based electrical DNA detection

The basis for this detection is the use of gold and other metal nanoparticles as novel markers. It has been shown that they can be easily modified by DNA, and the conjugates are still able to bind in a sequence-specific manner to complementary DNA [17, 18]. Labeling DNA targets with nanoparticle instead of fluorophore probes greatly alters the melting profiles of the targets from an array substrate, which increases the specificity over three times.

One detection scheme uses the drop in resistance after the binding of gold nanoparticles [19–22].

1. Droplets of capture DNA are deposited and immobilized into the gap between the electrodes.
2. Target DNA is bound with gold nanoparticles.
3. Silver enhancement step is used. Only with gold nanoprticles as seeds can this process occur. The silver particles will grow to the point at which they come in contact with one another and the electrodes, thereby bridging the gap and producing a resistance drop.
4. Decision and measurement step. If no target DNA is present in the gap, then there is no binding of the nanoparticles. Then silver is not deposited across the gap, and the resistance remains high.
5. An electrical readout is connected to a PC and data can be shown on a LCD display.

Another method, called “scanometric DNA array detection with nanoparticle probes”, [11] takes advantage of oligonucleotide-modified gold nanoparticle probes and a conventional flatbed scanner. Two gold particle probes are covalently bound with oligonucleotides that are complementary to a target. When encountering the target, these particle probes are polymerized and make a red-to-blue color change for detection. It is reported that the sensitivity can exceed that of the fluorophore system by two orders of magnitude when coupled with a signal amplification method in which silver ions are reduced by hydroquinone to silver metal at the surfaces of the gold nanoparticles [23–31].

2.2.4 Redox-active reporter molecules

This method takes advantage of labeled redox-active reporter molecules on the target molecule. The charge transport from the reporter molecule to the electrode indicates the existence of hybridization. The charge transport can take place either through: 1) the DNA duplexes; 2) an additional molecular wire; or 3) the surrounding solution [32–35].

Umek et al. describes an electrochemical 'sandwich' assay. Once the target DNA is captured on the electrode, a ferrocene-labeled signal probe is hybridized to the overhanging portion of the probe-target complex. The molecular wire provides a pathway for electron transfer between the ferrocene label and the electrode. The electron transfer between the ferrocene and the gold electrode is detected as a Farradaic current.

Instead of measuring the electron transport after the hybridization, Willner et al. and Patolsky used a system where they blocked the transfer to detect DNA. After the target DNA binds to capture DNA immobilized on a gold electrode surface, a redox-active intercalator electrocatalytically generates peroxide, which is then oxidized by horseradish peroxidase (HRP). The product of this reaction precipitates on the electrode, blocking the reaction.

2.2.5 Enzymes as electrical transducers

There are two different methods to detect DNA based on enzymatic reaction:

1. The product of an enzymatic reaction is used to block the electron transfer between the electrode and the surrounding solution.
2. The product of the enzymatic reaction is reduced and the current is measured.

Willner et al. and Patolsky take the first method. After the target DNA binds to captured DNA immobilized on a gold electrode surface, a phosphate is enzymatically converted into an insoluble indigo product which blocks the reaction.

Lumley-Woodyear et al. and Campbell et al. take the second method. The electrode is modified with an electron conducting redox hydrogen. Capture DNA is immobilized in this hydrogel and then hybridized with biotin-labeled target DNA. A horseradish peroxidase (HRP) complex will then bind to the biotin. Once the enzyme is bound in the hydrogel it is electrically 'wired'. This 'wiring' makes the electrode an electrocatalyst for H_2O_2 electro-reduction to water.

2.2.6 Electrochemical methods

Extensive efforts have been exerted in electrochemical methods for DNA hybridization detection. Detection of variation in capacitance or impedance has been demonstrated.

Pusan National University uses the difference in the impedance before and after hybridization. Tae-Young et al. reported the impedance and admittance changes according to frequency variation before and after hybridization, which may be useful for DNA detection. Lawrence et al. employ impedance measurements on functionalized heterostructures [36]. The decrease of the impedance values by hybridization indicates that double-stranded DNA is more conductive than single-stranded DNA.

DNA chips with metal electrodes of a 40 nm gap were developed to directly measure electrical conductivity of DNA by Shingi Hashioka, et al. They measure the electric currents between two electrodes to detect the existence of DNA. Detection of a very small amount of the DNA, on the order of femtoliter, was demonstrated [37].

Capacitance monitoring is another direct detection method of the hybridization event. When the target DNA species hybridizes with immobilized probes, the thickness of the dielectric layer increases; accordingly, the capacitance decreases. This can be described by the following equation:

$$C = \frac{\epsilon\epsilon_0 A}{d} \tag{2.1}$$

where C is capacitance (F)

ϵ_0 is the dielectric constant of vacuum (F/m^2)

ϵ is the dielectric constant of the layer

A is the active area of the device (m^2)

d is the thickness of the dielectric layer (m).

2.2.7 Surface plasmon resonance (SPR)

Surface plasmon resonance occurs only at a specific angle of incident beam because of the change in refractive index, which depends on the binding of the target molecules. The BIAcore system (Pharmacia Biotech Co.) has been commercially available. Because optical phenomena are influenced by many different factors near the interface of the surface and solution, this method is usually used qualitatively.

SPR is reported to be used to monitor hybridization kinetics on gold with the help of an applied electrostatic field. It was demonstrated that a repulsive potential can denature mismatched DNA hybrids within a few minutes, while leaving the fully complementary hybrids largely intact. By adjustment of the electrode potential, matched and mismatched hybrids can be discriminated. Because the potential changes the shape of the surface plasmon resonance curve, the full curve rather than simply the shift in the resonance minimum is accounted.

2.2.8 Quartz crystal microbalance (QCM)

QCM is a highly sensitive mass measuring instrument that can be used in gas phase and in aqueous solution. A nanogram level increase in mass will induce a linear decrease in the resonance frequency [38]. The core idea for DNA detection is to measure the mass change of the cantilever caused by DNA hybridization through the shift of the resonance frequency. The 27-MHz QCM is reported to be highly sensitive to detect hybridization without using any DNA labeling in ionic aqueous solutions.

2.2.9 Surface stress measurements

Surface stress measurement detects an asymmetric stress within a film due to an appropriate binding event [39]. One side of a microcantilever is functionalized with a selection of biomolecules. DNA hybridization generates a nanomechanical response in the microfabricated cantilevers, which can be optically detected [40]. It is reported that multiple unlabeled biomolecules can be simultaneously detected at nanomolar concentrations within minutes. When multiple binding assays are used in cantilever arrays, detection of femtomoles of DNA on the cantilever at a 75 nM concentration DNA solution is estimated.

2.2.10 Surface vibration spectroscopy in conjugation with electrophoresis

Ko-ichiro Miyamoto, et. al proposed a label-free method to analyze the chemical bonding state of DNA in situ (in vitro). The basis lies in the difference in the spectral features of hybridized DNA and single-stranded DNA (ssDNA). It is detected by electrophoresis in conjugation with infrared absorption spectroscopy in the multiple internal reflection geometry [41].

2.2.11 Atomic force microscopy (AFM)

Atomic force microscopy (AFM) was used to monitor DNA hybridization processes by measuring attractive or repulsive forces between a silica tip and the substrates that are as close to each other as the order of the instrument's resolution to make it possible to take measurements over a small area. For example, if the tip is first treated with negative charge, when surface hybridization occurs, it will increase the substrate surface charge and the repulsive force subsequently. The change can be determined from AFM force-separation curves [42].

In principle, AFM operates like the record player and the stylus profilometer. To achieve atomic-scale resolution, AFM incorporates a number of refinements. However, dull tips and tip-sample interaction forces are the main obstacles for high-resolution imaging of biological structures. Many

attempts have been exerted to develop sharper tips, primarily by improved microfabrication processes. If a modified atomic force microscope tip is used, AFM force measurements may be able to discriminate DNA hybridization with mismatched sequences.

2.2.12 THz technology for label-free genetic diagnostics

Theoretical calculations predict that interbackbone excitations of DNA molecules have a multitude of intrinsic resonances in the THz frequency range. This provides the basis for label-free DNA detection. A number of research groups have performed their investigations on hybridized DNA molecules by Raman, Fourier-transform, or time-domain THz techniques.

M. Nagel, et al. have demonstrated that hybridized DNA generates a stronger shift from the original center frequency than denatured DNA, and the shift is in proportion to the hybridization degree of the DNA molecules. In addition, the hybridized DNA exhibited an increased reactive index, higher absorption, less viscosity, and smaller thickness in comparison to the denatured samples. The THz technique is reported to be able to detect femtomolar level samples and single-base mutation [43].

2.2.13 Combination techniques

In addition to the methods described in the previous sections, many other methods for DNA detection have been reported. Some approaches take advantage of more than one technique to improve the sensitivity. Following are some examples.

- **Microcantilever resonance-based DNA detection with nanoparticle probes**

This method combines the nanoparticle elements and frequency shift of QCM. The hybridization reactions cause the attachment of gold nanoparticles, and the change is amplified by catalyzing the nucleation of silver. The effective mass of the microcantilever is increased accordingly, which shifts the cantilever frequency. The cantilever is 1/100 times smaller than quartz crystal microbal-

ance [44]. The method is reported to reach sensitivity of detection for target DNA at a concentration of 0.05 nM or lower.

□ **Fluorescence modulation of long DNA molecules adsorbed onto a microelectrode surface**

Masanori Udea et al. demonstrated fluorescence modulation of DNA labeled with dye that is adsorbed onto a microelectrode surface. Under potentials greater than about 1 V, the fluorescence of DNA was quenched. By reducing the potentials to lower than 0.6 V, it was recovered. This can be used for selective detection of DNA [45].

2.2.14 Problems of the current DNA sensors

The described methods for DNA detection offer enormous opportunities, but some hurdles remain. For those detection techniques using labels, some kind of fluorescence dye, or enzyme, or other chemical has to be attached to the target before the samples are to be analyzed. This excessive preparatory step not only can make the testing time-consuming, but also increase the risk of contamination, human error, or mechanical damage of the probe. In addition, labeling can modify the DNA strand conformation. Fluctuations and fluorescence efficiency site dependence due to degradation of fluorophore may deteriorate the quantificability and lower the precision of detection. In comparison with this, the label-free methods eliminate the perturbation from these attached labels.

Another main challenge is that the bulky size of the sensor probe makes it impossible for in-cell detection. In general, the sensor size is in the order of millimeter, while the cell size is within 10-100 micrometer.

2.3 Novel fiber probe with a miniature protrusion for DNA detection

The basic configuration of our novel miniature fiber probe for DNA detection is shown in Fig. 2.3. First, we will fabricate a fiber probe with a miniature protrusion on the fiber end. Secondly, capture DNA will be immobilized onto the protrusion. Thirdly, the sensor probe will be inserted into a cell and the sample attached. Finally, we will wash the remaining DNA away. If the target DNA is complementary to the capture DNA and hybridization occurs, the thickness of the fiber probe will increase. Otherwise, if the sample is not the complementary DNA, it will be easily washed away, and the thickness will remain the same.

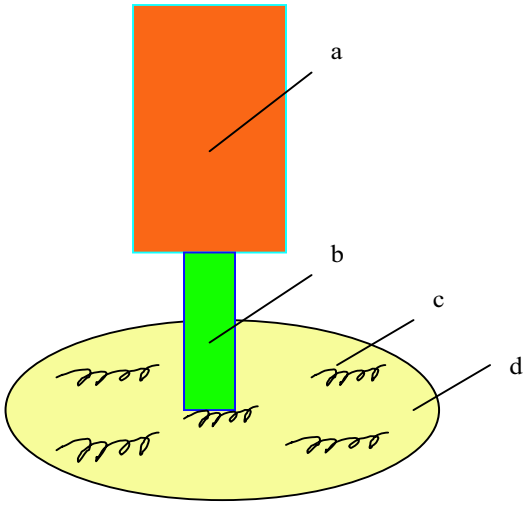

Figure 2.3: Optical fiber probe (a) with miniature protrusion (b) inserted into a cell (d) to detect DNA sequence (c).

Chapter 3

Current Nanoprobe Fabrication Techniques

The fabrication of micro/nano scale probes is essential in intracellular operation, such as our DNA investigation application. There are two primary physical requirements for high quality probes. The first is that the tip should terminate in a well-defined aperture. Secondly, the probe shape must allow access to the specimens of interest. As mentioned in Chapter 2, in order to fulfill the requirement of in-cell DNA detection application, the fiber probe has to be on the order of nanosize. In transmission-mode, light is coupled to the waveguide from an external source (such as a laser) and directed through the tip of the probe. The ideal probe is one in which the incoming electromagnetic radiation passes through only the very tip of the probe. A single-mode optical fiber is the most commonly utilized type and was selected for this project.

This chapter describes the material selection for the sensor probe and current methods for nanoprobe fabrication, including pulling and etching. In addition, advantages and disadvantages of different methods are discussed.

3.1 Material selection

A variety of materials, including cleaved crystals, semiconductor structures, glass pipettes, and tapered optical fibers, have been reported for nanoprobe fabrication [46]. At the same time, much effort has been exerted to immobilize DNA probes onto various solid supports in different applications. Glass-slides, nitrocellulose-coated microscope slides, and silicon-based DNA microarrays are now widely used. Glass microarrays with optical fluorescence detection, pioneered by Patrick Brown's lab at Stanford [47, 48], are now the most popular method because an external CCD camera can be used as the detection system. Recently, in order to facilitate fabrication of "lab-on-a chip" devices, there is surge in the study of silicon-based DNA arrays.

The requirements of material to act as solid fixture for DNA are:

1. Capability for immobilization and then hybridization of readily detectable quantity of functional ;
2. Film stability;
3. Fidelity of the immobilized sequences.

In our study, for in-cell nanoprobe DNA sensor application, silica has a few unique advantages over other materials.

1. Silica is a durable material that sustains high temperature and washes of high ionic strength.
2. It is non-porous so the hybridization volume can be kept to minimum, thus enhancing the kinetics of annealing probes to target.
3. Optical fiber, whose material is silica, is commercially available and common for signal transmission, which can greatly reduce the signal detection complexity.
4. It has been shown that optical fiber can be pulled or etched to nanoprobe, which is required for in-cell applications.

5. Last but not least, silica is biocompatible.

Therefore, our in-cell nanoprobe will be fabricated on the end of optical fiber, whose material is silica.

3.2 Fiber probe fabrication

There are a variety of techniques that have proven useful for fiber tapering down to a fine tip, but the task is commonly accomplished by:

- Heating and pulling with a commercial micropipette puller;
- Chemical etching in a bulk etchant or at the etchant-solvent interface.

3.2.1 Heating and pulling method

The heating-pulling method was developed by E. Betzig. In the heating and pulling method, fiber is locally heated by a CO_2 laser and subsequently pulled apart. A single mode fiber is mounted on a commercial pipette puller (Sutter Instruments) and illuminated by a focused CO_2 laser. When a pre-set pulling velocity is reached, the laser is switched off and after an adjustable delay a hard-pull is exerted on the fiber, pulling both halves apart. The tip shape depends heavily on the temperature and the timing of the heating and pulling, as well as on the size of the heating area. Several groups have studied the fiber pulling process; in particular Valaskovic et al. have performed an extensive study on the optimization of the pulling parameters of the fiber probes.

The major advantage of this method is that the glass surface on the taper is very smooth. Also, once the heating and pulling parameters are optimized, the desired taper and tip diameter can be produced with high reproducibility.

However, it is difficult to produce apex dimensions less than 50 nm by this method. Also, the taper is usually much longer than tips produced by etching, as shown in Fig. 3.1. Probes with a longer, more gradual taper typically have lower transmission efficiencies than those with shorter tapered regions, for a given tip aperture diameter [49]. What's more, the longer taper usually means a less robust structure.

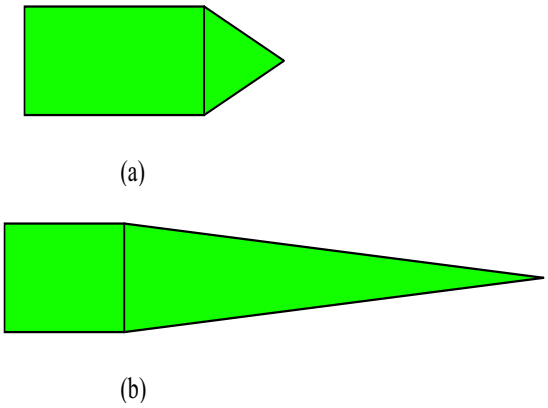

Figure 3.1: Schematic illustration of different shape of fiber tip formed by (a)chemical etching; (b) heating and pulling.

3.2.2 Chemical etching

Chemical etching is dipping the fiber into a hydrofluoric acid (HF) solution. The etching process is influenced by a number of parameters, such as

- the concentration of the HF solution,
- organic solvent on top of the HF solution,
- the etching time and
- the type of fiber or dopant.

The advantage of this method is that quantities of fiber with high tip cone angle and small tip size are obtained easily in a single step.

The major disadvantage of the etching process is the very irregular surface of the fiber after etching.

Among chemical etching, there are five main etching approaches:

- Meniscus etching;
- Selective etching;
- Tube-etching;
- Sealed-tube etching;
- Kwong-Li probes.

Meniscus etching was patented by Dennis R. Turner in 1983. This etching is typically covered by a protective layer of hydrophobic chemical such as tolueneor p-xylene that serves two purposes:

- To form a meniscus along the fiber tip during etching.
- To prevent corrosion of the optical fiber above the tip region by the etchant vapor.

The etching process is shown in Fig. 3.2. The fiber is dipped into a stack solution of etchant and etchant-insoluble organic solvent. Etching occurs at the point where the meniscus is formed along the fiber. At the beginning, the etchant wets the fiber surface with an initial meniscus height, as shown in Fig. 3.2(a). As etching proceeds, the upward pulling force resulting from surface tension decreases due to the reduction of the fiber radius in contact with the etchant, illustrated in Fig. 3.2(b-c). Consequently, the meniscus height reduces progressively until the portion of the fiber below the oil is completely etched, forming the tip.

The properties of the protecting layer determine the shape and contact angle of the meniscus formed, and therefore the choice of this substance determines the cone angle that is produced at

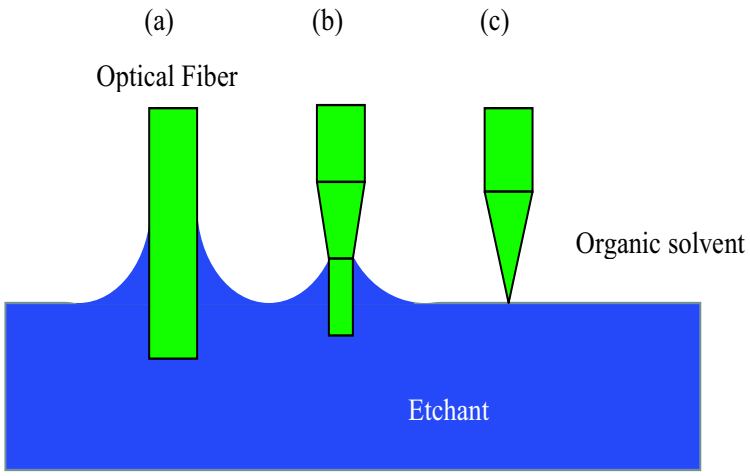

Figure 3.2: Schematics illustrating the formation of a fiber tip.

the fiber tip. Pak at al. [50] have presented a technique based on a theoretical model by a solution of the Young-Laplace Equation to fabricate optical fiber tips with desired geometries. Experiments also show that the final tip shape is governed by the density difference, surface tension and contact angle at the interface. These parameters can be altered by changing the organic solvent, HF concentration, or etching temperature.

The controllable fiber tip discussed above also implies the main drawback of the meniscus etching technique - the tip shape and its surface quality are quite sensitive to the etching environment. Air movement, temperature fluctuations, vibrations, and etchant concentration can have a strong influence on the shape and symmetry of the meniscus-etched probe and its surface roughness. If the surface of the tip is too rough or is marred by other imperfections, then the subsequent DNA immobilization can be unstable, and, therefore, the whole sensor probe will not be robust enough for further detection.

□ **Selective etching (Ohtsu)**

Selective etching takes advantage of the different etching rates exhibited between the core material and the cladding surrounding an optical fiber. The cone-shaped tip is core, and it is formed not at surface but deep inside the etching solution.

♢ Solution of HF:NH_4F:H_2O

For selective etching, a mixture of HF, NH_4F, and deionized (DI) water was used for the etching solution. The volume ratio of these components is critical to the etching rate of core and cladding of optical fiber.

If the etching solution contains a volume of NH_4F more than 1.7 times the others, the etching speed of the core region is slower than that of the cladding region. Therefore, with this method a taper shape can be made on the core region.

On the other hand, if the NH_4F concentration is smaller than 1.7 times that of the others, an inverted cone is made in the core region because the etching speed of the core is faster than that of the cladding.

♢ Geometrical model

When a GeO_2 doped fiber is etched in a BHF:HF:H_2O = X:1:1 (volume ratio)

BHF: buffered HF

NH_4F: $40wt\%$

DI H_2O

X $<$ 1.7 fiber is hollowed as Fig. 3.3(a)

X $>$ 1.7 fiber is sharpened as Fig. 3.3(b)

[R1/R2] decreases with increasing X and converges to a constant value at X = 10 $\sim$ 30. At X = 1.7, the ratio is equal to unity.

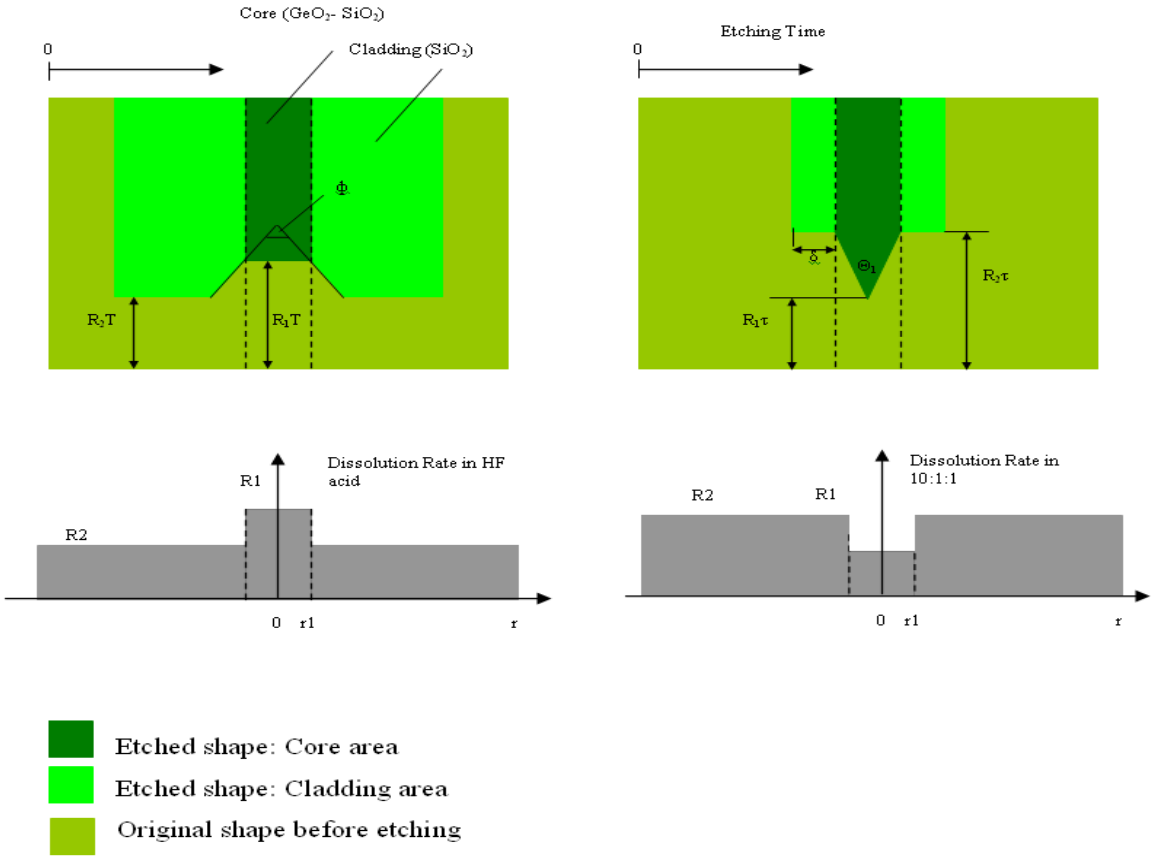

Figure 3.3: Schematic explanation of selective etching of a GeO_2 doped fiber in (a) sharpening the core, (R1>R2) and (b) hollowing (R1<R2). The profile shows the etching rates of the fiber in (a) HF, and (b) $BHF : HF : H_2O = 10 : 1 : 1$.

With geometrical analysis of Fig. 3.3, the following relations between different parameters can be obtained.

The cone angle Φ of the hollow is expressed as

$$\sin\left(\frac{\Phi}{2}\right) = \frac{R_2}{R_1}, \qquad R_1 > R_2\,. \tag{3.1}$$

The cone angle θ_1 and the apex diameter d of the sharpened core are expressed as

$$\sin\left(\frac{\theta_1}{2}\right) = \frac{R_1}{R_2}, \quad R_1 < R_2\,, \tag{3.2}$$

$$d = \begin{cases} 2r_1(1 - T/\tau_1), & T \leq \tau_1\,, \\ 0, & T > \tau_1 \end{cases} \tag{3.3}$$

$$\tau_1 = \frac{r_1}{R_1}\sqrt{\frac{R_1 + R_2}{R_2 - R_1}}\,. \tag{3.4}$$

To fulfill the requirement of size and shape of the final fiber tip, we can select different doping rate materials, different concentration acids, and different etching time [51–53].

T and τ: Etching time

R1 and R2: etching rate of the GeO_2 doped core and the pure silica cladding

r1: radius of the core

Φ: cone angle of the hollow

δ: the cladding thickness

Θ_1: cone angle of the sharpened core.

♢ Multi-step etching

According to the previous theoretical analysis, fiber probe shape and size can be designed and controlled. With one step etching, where only one kind of etching solution is used to sharpen the fiber, it is difficult to obtain a fiber tip sharper than 2 μm. To address this problem, Pangaribuan et al. have put forward a two-step approach [54].

- First step: reduce the cladding diameter;
- Second step: sharpen the fiber.

By this method, the diameter of the apex can be as small as 3 nm with high reproducibility, with control of the cladding diameter. Following this concept, many research groups are working on

different fiber tip shape and size. R. Uma et al. reported in 1995 a method to control the apex shape. Takuya at al. modified the method with photolithography to decrease the surface roughness. Shuji Mononobe at al. expanded the method into a 4-step approach and fabricated a pencil-shaped fiber probe. The apex diameter obtained is less than 10nm [54].

□ **Tube-etching (Zenobi)**

The above etching methods usually suffer from environmental sensitivity. In 1999, Zenobi brought forward the idea of tube etching, which can overcome this problem. Rather than removing the polymer jacket from the fiber prior to etching, the cladded fiber end is immersed in the etchant, which usually consists of a buffered hydrofluoric acid solution. Another difference to Ohtsu's selective method is that the tip is formed at surface instead of in the deep etchant [54].

The fiber jacket is resistant to degradation by the etching solution, and the entire etching process takes place inside the hollow tube formed by the jacket. As shown in Fig. 3.4, initially, the outer regions of the fiber are etched slightly faster than the center, and the formation of a conical shape starts. As soon as a preliminary taper is formed, convection starts to deliver HF to the upper region of the cone. The convection is driven by concentration gradients caused by the etching process itself and the gravitational removal of the reaction products (SiO_2 and H_2SiF_6).

Because of the protective environment of the tube enclosure, the glass surface and taper shape is extremely smooth. This is an obvious advantage over other etching methods.

While still producing large cone angles, tube etching features the following advantages:

1. Tips with reproducible shapes are formed in a high yield;
2. The surface roughness on the taper is drastically reduced;
3. The tip quality is insensitive to vibrations and temperature fluctuations during the etching process.

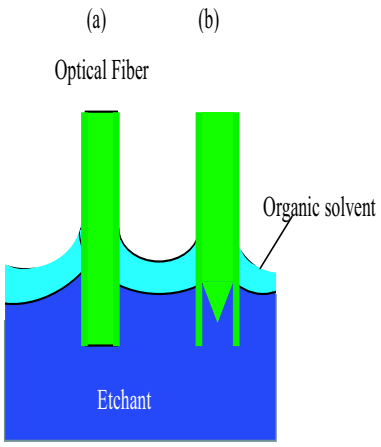

Figure 3.4: Schematics illustrating the formation of a fiber tip.

□ **Sealed-tube etching**

In 2003, J. Shi at al. [54] reported sealed-tube etching. The fiber acrylate jacket is HF permeable and geometrically in a "tube" shape. The key difference lies that the fiber end is sealed with HF-impermeable plastic. The HF acid laterally diffuses into the jacket to etch the glass fiber without dissolving the jacket material, while in conventional tube etching, HF can diffuse both laterally through the jacket wall and vertically from the bottom open end of the tube. As a result, this sealed-tube etching can form two glass tips simultaneously:the upper tip and the lower tip. Fig. 3.5 shows the schematics of the tip formation.

□ **Kwong-Li (KL) method**

In 2003, Kwong et al. developed the KL method. This method has the following advantages:

1. The process is very fast and reliable;
2. Single step etching;
3. Sharp-angled probes $< 2.1\ ^{\circ}$;

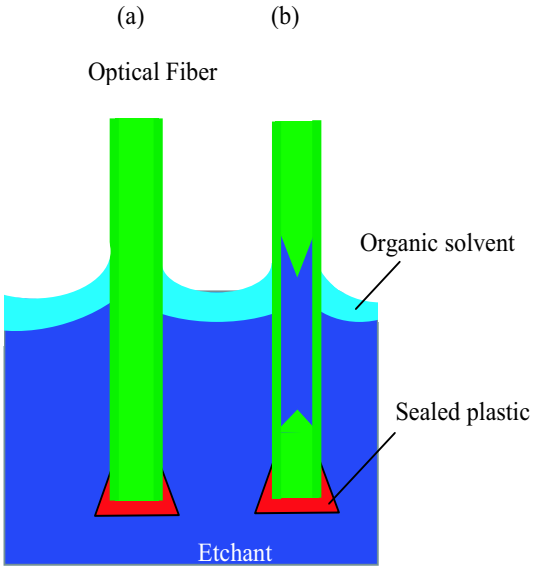

Figure 3.5: Schematics illustrating the formation of a fiber tip in a sealed tube.

4. Nanoscale tip diameters of < 1 μm;

5. Experiments show that KL probes can penetrate through cell membranes with less mechanical resistance than conventional pipettes and probes made from Turner's Method.

The KL method combines a sacrificial boundary etching technique with Turner's method. By controlling the initial etchant height in the sacrificial barrier, final tip profiles can be adjustable.

The key point for KL method is the introduction of glass tubing as the sacrificial barrier to etch the stripped fiber. During etching, HF continues to etch away the inner wall of the glass tubing, so the interfacial meniscus keeps falling. As a result, the final probe formed has a long taper and a pointed tip.

3.3 Other potential applications for nanoprobes

The fabrication of nanoscale probes has become essential in intracellular surgery. Besides in-cell DNA detection, it has broad application in cell sensing, manipulation, and injection.

In addition, nanoprobes have been pursued for Scanning Near-field Optical Microscopy (SNOM) applications since 1984. This technique allows potential optical imaging on the nanometer scale, and its spatial resolution can go down to sub 100 nm, which is far beyond the classical optical microscopy diffraction limit. Like all other scanning probe microscopies, probe profile characterizes the resolution of SNOM. Generally speaking, the smaller the probe-tip diameter, the better the achievable spatial resolution.

This chapter reviews the current methods for nanoprobe fabrication. In general, chemical etching techniques are preferred over the pulling method because of the sharper taper angle and corresponding higher optical transmission efficiencies. In Chapter 7, the design and development of novel nanoprobes will be discussed.

Chapter 4

Layer-by-Layer Self-Assembly of Multilayer Films Containing DNA

As discussed in Chapter 2, one of the key steps for DNA sensor fabrication is to immobilize the capture DNA sequence onto the probe.

Different deposition techniques have been developed to fabricate sensing coatings on optical fiber. For example, sputtering in a radio frequency planar magnetron system, electron beam evaporation, chemical vapor deposition, immersion in gel solutions and many others. However, most of these techniques are neither appropriate to control the thickness of the coatings on the nanometer scale nor to deposit materials on nonplanar substrates.

The reported immobilization methods based on SiO_2 are:

- Covalent bonding formation method.

  In the microarray field, a covalent coupling method has been widely used for the attachment of oligonucleotide or high-molecular-weight probes to planar surfaces. However, this technique requires activation of the underlying planar surface with cross-linking reagents and/or modification of the DNA molecule with amino, thiol, or biotin groups [55–57]. The additional preparatory step increases the complexity of the process and requires technically

well-trained personnel.

- Langmuir-Blodgett (LB) technique.

  The Langmuir-Blodgett (LB) technique is one of the most common methods of nano-film fabrication. One monolayer of the desired substance, originally adsorbed at the gas/liquid interface, is efficiently built at a time to the substrate of choice. The LB apparatus includes a Langmuir trough with a dipping device, an automated movable barrier, and a surface pressure sensor to maintain a controlled surface pressure. Although near-perfect performance has been demonstrated, such as long range ordering of monolayers and multilayers of species that self-assemble at the liquid surface, it is cumbersome, time-consuming and expensive due to the high cost of the required apparatus and maintenance.

- Direct self-assembly method - Layer-by-layer self-assembled-monolayers (L-b-L ESA) [58, 59].

  It is a highly flexible approach for the creation of concentrated planes of functionality.

L-b-L ESA has been widely used in different applications such as non-linear optics, chemical sensing and other functional films and devices. Compared to the first two methods, it is much simpler, more direct and cost-efficient. As opposed to the LB method, L-b-L ESA is independent of the substrate size and topology. In addition, the LB technique typically cannot be used to form films thicker than several monolayers because defects occur and are replicated through the film structure as additional layers are added. Unlike LB schemes, L-b-L ESA processing permits the molecular-level self-healing of defects that may occur in individual monolayers as additional monolayers are gradually added layer by layer to the substrate during the synthesis process [60]. Individual layer thickness is controllable by factors such as concentration, molecular weight, and ionic strength. What's more, the process is performed with water-soluble molecules, which is required for many biological macromolecules. Any solvent-accessible surface is appropriate for the coatings. Last but not least, in comparison with LB or physical vapor deposition techniques, the instrumentation cost is very low. A variety of composite materials have been successfully

assembled with this approach, including organic components, biopolymers and virus particles, and inorganic colloids. Therefore, in our work, immobilization of DNA was carried out by the L-b-L ESA method.

Electrostatic self-assembly was first introduced by Iler in 1966. This is the original idea of constructing multilayer films composed of positively and negatively charged colloidal particles, such as silica and alumina. In 1990s, Decher and Kunitake revisited the concept and reported the fabrication of multilayer polymeric thin films composed of oppositely charged polyelectrolytes. This is the layer-by-layer electrostatic self-assembly method [61].

Simply speaking, it involves the alternate dipping of a substrate into anionic and cationic solutions. Each exposure deposits a reproducible quantity of material and reverses the charge on the surface, leaving it primed for the next layer of polymer. The strong ionic bonds between the oppositely charged species form uniform, sturdy and stable films [61]. Much of the work has generalized and expanded the technique to various combinations of charged components, including synthetic polyelectrolytes, nanoparticles, biopolymers such as proteins, clay minerals , dendrimers, metal colloids, silica, and other inorganic particles. Applications include conducting layers, permselective membranes, enzymeactive thin films, sensors, light-emitting thin films, selective area patterning, electrochromic films, electrocatalysis, and noncentrosymmetric films for nonlinear optics [62–70].

Research and experiments have shown that this remarkably simple technique provides molecular-level control over the thickness, which means that the thickness of each layer can be varied at Angstrom level. Therefore, it will be very promising for direct detection of DNA hybridization. In addition, this approach has the advantages that it is environmentally sound (all water based processing), is readily amenable to automation and integration with current technologies, and can be easily used to fabricate complex multilayer heterostructures with excellent control over molecular architecture [71, 72].

This chapter introduces the basic steps of this self-assembly method, followed by the function principle. Then the factors that control the growth of multilayers are discussed. Finally, the feasibility of DNA immobilization by this method are presented.

4.1 Layer-by-layer self-assembly method

The L-b-L ESA process is based on the electrostatic attraction between oppositely charged polyelectrolytes in each monolayer deposited. The deposition method is described schematically in Fig. 4.1. The process involves following steps.

1. Clean and treat the substrate to create a charged surface. In Fig. 4.1, we assume the outer surface is negatively charged.

2. Dip the substrate into solutions of cationic polymers for a few minutes and by adsorption a monolayer of polyions is formed on the surface. Since the adsorption is carried out at relatively high concentration of polyelectrolyte, a number of ionic groups remain exposed to the interface with the solution, and thus the surface charge is effectively reversed.

3. Remove the substrate and rinse it with water. The substrate has a net positively charged outermost molecular monolayer.

4. Dip the substrate into solutions of anionic polymers. The anionic molecules are adsorbed onto the cationic surface and ionically bonded to the cationic polymer molecules.

Repeat 2) $\sim$ 4) in a cyclic fashion, alternating layer-by-layer molecular self-assembly multilayer films can be obtained, and in principle, there is no limit for the final thickness.

The spontaneous, layer-by-layer self-assembly is based on the ionic attraction developed between the oppositely charged species, which promotes strong interlayer adhesion and a uniform and linear multilayer deposition process. The key to a regular multilayer buildup is the reversal of the surface charge in each adsorbed layer [73–76].

Film properties are determined by the molecular species of the cationic and anionic components. Since the polyanions and polycations overlap each other at the molecular level, the resulting film is a homogenous optical material. The individual layer composition and thickness can be controlled and substrates may include metals, plastics, ceramics, and semiconductors [77, 78].

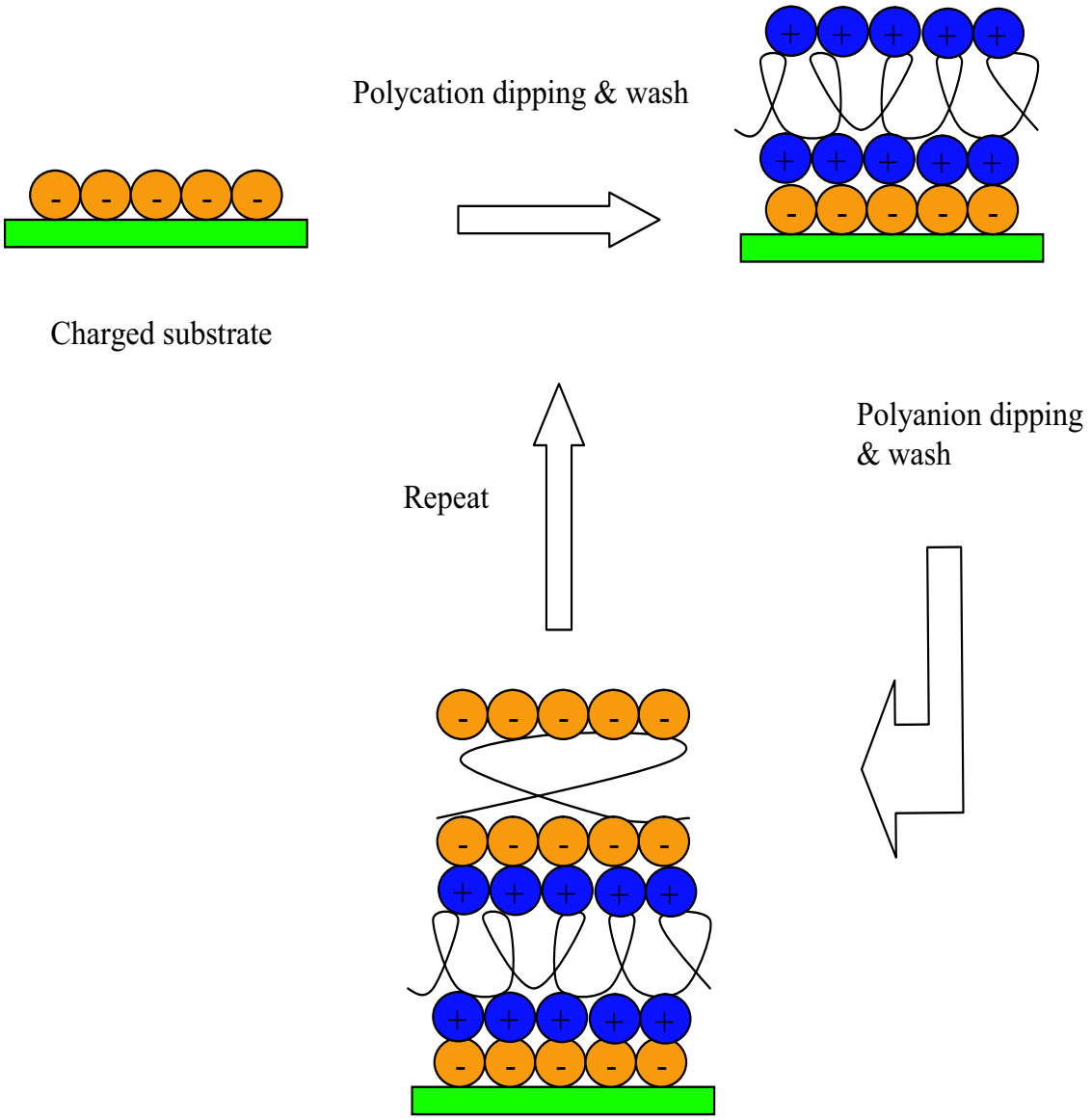

Figure 4.1: Schematics of the L-b-L ESA deposition process. The symbols are over-simplified and not used to represent the conformation of the polyelectrolyte chains.

4.2 Factors controlling the growth of polymer multilayers

As one of the most versatile means available to control structure and properties at the nanoscale level, the processing of polyelectrolytes into thin films one molecular layer at a time has been

introduced in 4.1. At first glance, the electrostatic nature of the assembly process would seem to be intuitive and somewhat trivial. However, it was shown quickly that the polymers are not stratified into well-defined layers but are dispersed and interpenetrating [79]. Much research has been carried out to understand the fundamental issues for better control of the structure, molecular organization, thickness, and properties of the multilayer thin films. Polyelectrolytes perform better than small molecules because of the ionic bonds yielding good adhesion of a layer to the underlying substrate. The conformation of the polymers at the newly created film surface is mostly dependent on the chosen polyelectrolytes and adsorption conditions, and much less dependent on the substrate or the substrate charge density [80], because polymers can bridge over underlying defects. Therefore, the polymer rather than the surface determines the over-compensation of the surface charge by the incoming layer. Accordingly, with the number of deposited layers, the film thickness increases linearly even if different substrates are used. When substrate charge densities are very small, only few groups are bound to the first layer. A larger number of oppositely charged groups are exposed to the solution. In this case, the linear deposition occurs only after a few layers. Experiments have proven that the thickness of the adsorbed layers can be fine-tuned at the molecular level [81, 82].

It is well demonstrated that the organization and thickness of sequentially adsorbed layers are extremely sensitive to dipping solution pH, primarily due to the fact that the charge density can vary with change in pH [83]. For example, the increase in poly(allylamine hydrochloride) (PAH) layer thickness may result from the increasing surface charge density of a previously adsorbed poly(acrylic acid) (PAA) chain with increasing pH. In other words, higher pH results in more highly ionized PAA surface chains, and more oppositely charged PAH molecules are needed to neutralize. It is reported the transitions from very thick adsorbed layers (8 nm) to very thin adsorbed layers (0.4 nm) occur over a very narrow pH range. By controlling pH, the thickness of an adsorbed polycation or polyanion layer can be varied from 0.5 to 8 nm. A variety of groups are working on the explanation of the phenomena and many models have been brought forward [84–86].

In addition, polyelectrolyte multilayer thickness is highly dependent on the salt concentration, salt type, solvent quality, deposition time, and polymer concentration [84–86]. Among these factors, salt has the strongest influence on the amount deposited per cycle, which is directly related to the

layer thickness. Here, the adsorption of polyelectrolytes onto an oppositely charged surface is regarded as an ion exchange phenomenon where charged segments replace small ions compensating the surface charge [87]. The charged polymer segments compete with added salt ions for charged surface sites.

In addition, there is a tendency toward a certain value of the interfacial overlap between a polyanion layer and a polycation layer and a certain roughness at the film-air interface. Similar surface roughness of the polyelectrolytes multilayers is observed regardless of the roughness of the underlying substrates. The cause lies on the property dependence on the polymers rather than the substrate, similar to the self-regulation of thickness increments per layer. Immersion of films in solutions of salt and pure water "anneals" the surface and reduces the roughness to smaller values. It is hypothesized that the salt breaks and removes some of the anion-cation bonds during the dipping and rinsing steps. Therefore, a more equilibrated conformation of the polymer chain is reformed.

Other research has focused on the compositional and structural details. Stephan T. Dubas et al. evaluated the way net charge neutrality is maintained and found that small ions do not participate in charge balance [88]. Lowack and Helm, investigated steric and electrostatic interactions between multilayer-bearing surfaces and concluded that ion pairing causes attraction between oppositely charged polymers and an electrostatic barrier limits the amount adsorbed [80, 89–92].

4.3 Assembly of thin film of DNA

The main idea of L-b-L ESA consists of alternation of the terminal charge after every layer deposition. This implies that in principle there is no restriction to certain polyelectrolytes and that the construction of multilayer assemblies should also be possible by using DNA as a polyanion and poly(allylamine) as a polycation. This is the key for immobilization DNA onto our probe.

DNA is generally considered as polyanion due to the negative charge of their sugar phosphate backbone. Moreover, experiments have shown successful adsorption to positively charged lipid monolayers .

Chapter 5

Polymer and DNA self-assembly on wafer

As discussed in Chapter 4, many factors, such as pH and salt concentration, can influence the surface quality of polymer and DNA films assembled onto the substrate. The development of biosensors based on DNA hybridization requires consideration of the hybridization conditions such as the density of DNA, as well as the temperature, pH, and ionic strength. Careful control of these parameters may therefore enhance the selectivity, sensitivity and speed of the sensor for DNA sequence detection.

The effects of the local environment, such as the nature of the solid substrate used, may directly influence the nature of the selective binding interaction. Commonly used materials include gold, silica, and polymeric substrates. In aqueous solution, different substrates have distinctly different interfacial properties, which can cause false-positive signals due to non-selective adsorption of materials from solution. In addition, the substrates may alter the structure of immobilized biomolecules since it may provide sites for adsorptive interactions between the immobilized biomolecules themselves and the substrate surface. This effect will influence the ability of the immobilized biomolecules for the following selective binding.

According to the electrochemical method, the hybridization efficiency of immobilized single-stranded DNA to complementary strands exhibits a maximum with increasing immobilized DNA

surface density. [93]

To maximize the surface concentration of the DNA immobilized onto the final sensor head, optimal parameters of the experiment environment need to be investigated. Since the fiber sensor head is in such a miniature size, from 125 μm to 5 μm to nanometric size, it is very cumbersome and difficult to handle such tiny sensors in the execution of a test sample matrix. Therefore, we took advantage of 1-inch by 1-inch silicon wafers as the testing sample to investigate the influence of different factors. This demo experiment is meaningful for two reasons: 1) the similar properties of the sample silicon wafer and the fused silica sensor head; 2) the similar immobilization principle and mechanism of polymer and DNA sample assembly onto the surface.

The surface concentration of DNA immobilized onto the surface is affected by the parameters of both the precursor polymer and the DNA sample. Therefore, in our experiments, both contributions were investigated. In the following paragraphs, we discuss our experiment design, and then introduce our experiment methods and setups; finally we analyze our results and select the optimal parameters to maximize the DNA immobilization concentration onto the surface. These results are very meaningful for the guidance of our further experiments.

5.1 Polymer self-assembly on wafer

Polymer self-assembled thin film serves as a precursor layer. To increase the sensitivity of a biosensor, such as our DNA sensor, it is important to control the thickness and refractive index of the film. Applying the DNA alone, it is impossible to change these parameters in a large range. Fortunately, the assembly of polymer films can fulfill this task while retaining the biological activity of the biomolecules. Previous work has shown that varying the polymer species, the salt concentration, the polymer concentration, the pH value, and the immersion time seems to change the thickness and refractive index of the film [94]. Those factors are normally studied separately not systematically. In this study, experimental design methods are applied to determine the relative effect of each of the factors.

5.1.1 Experiment design

Experiment design is a method to organize the experiments properly and efficiently to answer a question or achieve a goal with enough of the right type of data. In our research, the effects of several factors need to be investigated. Instead of running separate experiments for each variable, it is more efficient to manipulate these variables in one experiment. Moreover, when interactions among variables are considered, experiments with more than one independent variable are necessary. A full factorial design with all possible combinations can solve the problem. However, a more efficient design, called fractional factorial designs, can also provide meaningful results with fewer runs or combinations. We take the advantage of the Taguchi method to analyze the data. In this study, the requirement of the design can be described as follows.

- The number and levels of factors that are of interest: 7 two-level factors.
- The number of trials that can be afforded: less than 30.
- The desired resolution of the design: Major effects and no interactions.

With an L-8 array, a fractional factorial design with 7 factors and 8 runs is more appropriate than the full factorial design. For each trial, we repeat the experiments on 3 identical substrates. Therefore, there are totally 24 samples.

Several studies show that there are two steps during polyion adsorption [95]:

1. Polymer chains are anchored to the surface by some segments. This is a fast process.
2. Dense packing the surface. This is a slower step.

Polyelectrolyte concentration plays a weak influence on the adsorption if it exceeds a critical threshold value. [96, 97]

The effect of salt concentration and pH is pronounced. In general, higher ionic strength increases the thickness and density of the film [96–98]and roughness of the surface [98, 99]. Adsorption can

Table 5.1: Factors and levels.

Factor	Level 1	Level 2
pH:DNA	5.5	7.4
C_{salt}:DNA	0M	0.1M
C_{salt}:polymer	0M	1M
pH:polymer	5.5	3.0
Cation species	PAH	PDDA
Buffer	Water	TE
Number of polymer layers	6	12

be sped up by a small amount of salt, but slowed down when salt concentration is high. This can be explained by the competition between polyions and the salt.

There are mainly two effects caused by pH. On the one hand, to establish a given pH, the ionic strength may be increased by addition of acid and base. This may increase the film thickness, as discussed in the previous paragraph. On the other hand, polyelectrolyte charge density may be modified by pH. If the adsorbing polymer charge density is increased, the film will be thinner. Otherwise, if the substrate surface charge density is increased, the film will be thicker. Therefore, there is an optimum pH range [100].

After some deliberation, factors and levels were selected as listed in Table 5.1.

After six (6) or twelve (12) bilayers of polymers were grown onto the sample, it was characterized by variable angle spectroscopic ellipsometry (VASE). Then DNA was immobilized and the sample investigated again by ellipsometry. Finally, the binding capacity was evaluated by ellipsometry using the complementary DNA.

The orthogonal sample matrix (L8) is listed in Table 5.2.

Process:

Table 5.2: Orthogonal Sample Matrix (L8).

Trial	pH: DNA	Csalt: DNA (M)	Csalt: poly. (M)	pH: poly.	Cation	Buffer	Layer No.
1	5.5	0	0	5.5	PAH	Water	6
2	5.5	0	0	3.0	PDDA	TE	12
3	5.5	0.1	1	5.5	PAH	TE	12
4	5.5	0.1	1	3.0	PDDA	Water	6
5	7.4	0	1	5.5	PDDA	Water	12
6	7.4	0	1	3.0	PAH	TE	6
7	7.4	0.1	0	5.5	PDDA	TE	6
8	7.4	0.1	0	3.0	PAH	Water	12

1. Pretreat the silicon substrate: piranha bath for one hour.
2. Grow polymer films onto the substrate.
    - All polymer concentrations are 2 mg/ml.
    - The anion for all samples is PSS.
    - The cation is either PAH or PDDA.
    - Immersion time: For the first two polymer bilayers, use five-minute immersion times for all samples. Remaining bilayers are at 1 minute.
3. Dry with nitrogen gas.
4. Measure the polymer thickness on the substrate with the ellipsometer. (3 different locations)
5. Immobilize DNA onto the substrate.
    - All DNA concentrations are 100 μg/ml.
    - Immersion time: 30min.

6. Dry with nitrogen gas.
7. Measure the DNA film thickness with the ellipsometer. (3 different locations)
8. Analyze the results and obtain information about
    - Main factor influencing the DNA immobilization;
    - Optimal factorial combination to increase the DNA immobilization;
    - Quality and thickness of DNA films.
9. Confirmation test: repeat 1) $\sim$ 8) with the optimal factorial combination.

DNA hybridization test on the substrates obtained from optimal factorial combination parameters.

5.1.2 Materials and sample preparation

All the water utilized during the experiments is Type I reagent grade ultrapure water. It is free of pyrogen, RNase, Dnase and DNA. It is provided by reverse osmosis (Barnstead Diamond RO) followed by ion exchange and filtration (Barnstead Nanopure Diamond UV/UF, $18M\Omega$).

Polyallylamine hydrochloride (PAH), MW 70,000, polysodium 4-styrenesulfonate (PSS), MW 70,000, and poly diallyldimethylammonium chloride (PDDA) Mw 200,000-300,000 were obtained from Aldrich. All polymer concentrations were 2 mg/ml. NaCl (Mallinckrodt) was used to adjust the salt concentration. pH values were adjusted by HCl or NaOH using a Corning 455 Ion Analyzer with ATC probe.

Silicon substrates were cleaned by piranha solution (H_2O_2: H_2SO_4 = 30:70 v/v) at room temperature for one hour in a fume hood. Then the sensor was ultrasonically rinsed in ultrapure water 3 times and dried under nitrogen.

A thin silica layer ($\sim$ 2 nm) is naturally grown on the silicon substrates due to oxidization, and generates negative properties when immersed in water or solutions primarily through the dissociation of terminal silanol groups. After the substrate was cleaned, it was immersed into the positively

charged polymer (PAH) for the first layer assembly. The substrates were alternately immersed in PAH/PDDA or PSS for 5 min for the first 2 bilayers and 1 min for the remaining bilayers. The substrates were rinsed in ultrapure water for 1 min after each layer and then dried in nitrogen.

Samples were investigated by a variable angle spectroscopic ellipsometer (J. A. Woollam VASE) to measure the thickness and refractive index of the self-assembled thin film at three different locations across the surface. A simplified Cauchy model was used to describe the refractive index:

$$n(\lambda) = A + \frac{B}{\lambda^2} \tag{5.1}$$

where A and B are the fitted parameters.

5.2 DNA immobilization on wafer

After testing the polymer films, the wafer was immersed into the DNA sample for 30 minutes. Then the wafer was rinsed with DI water and dried with N_2 flow. Again, they were measured with the ellipsometer.

Taking advantage of the ellipsometer, this experiment can

- Demonstrate the feasibility of DNA immobilization onto the substrate;
- Evaluate the film quality and thickness grown onto the substrate;
- Evaluate the surface concentration of DNA onto the substrate;
- Evaluate the DNA hybridization effect onto the substrate;
- Provide reasonable clues for evaluation of all of the above effects on the 125 μm optical fiber sensor, and the nanoprobe sensor.

5.3 Data analysis

The self-assembled polymer multilayer serves as the precursor film. The variation of the polymer film between each self-assembling process may affect the subsequent immobilization of DNA as well as the hybridization of the complementary DNA. In order to improve the repeatability in polymer self-assembly, high S/N ratios for both thickness and refractive index are preferred.

The results were analyzed in Qualitek-4 (Qualitek Inc). The effect of the factors on thickness and refractive index are considered separately. Quality characteristic (QC) indicates the direction of desirability of the evaluation numbers. According to the criteria, S/N can be:

- Bigger is better;
- Smaller is better;
- Nominal is the best.

In order to control the thickness or refractive index of the polymer self-assembly to a desired value, “Nominal is the best” is selected.

5.3.1 Thickness of DNA immobilized onto the wafer

Our goal is to find the main factors that influence the results, and what the optimal conditions of these factors are. Through the use of Qualitek-4, main effects plots for the thickness analysis are shown in Figure 5.1. When a factor is changed from Level 1 to Level 2, how much the mean changes gives the clue to the relative importance of the factor. Figure 5.2 shows this significance factor in bar chart. For example, the pH of polymer and DNA have much higher effects on the S/N ratios of thickness. Figure 5.3 gives the optimal conditions of factors for the best S/N.

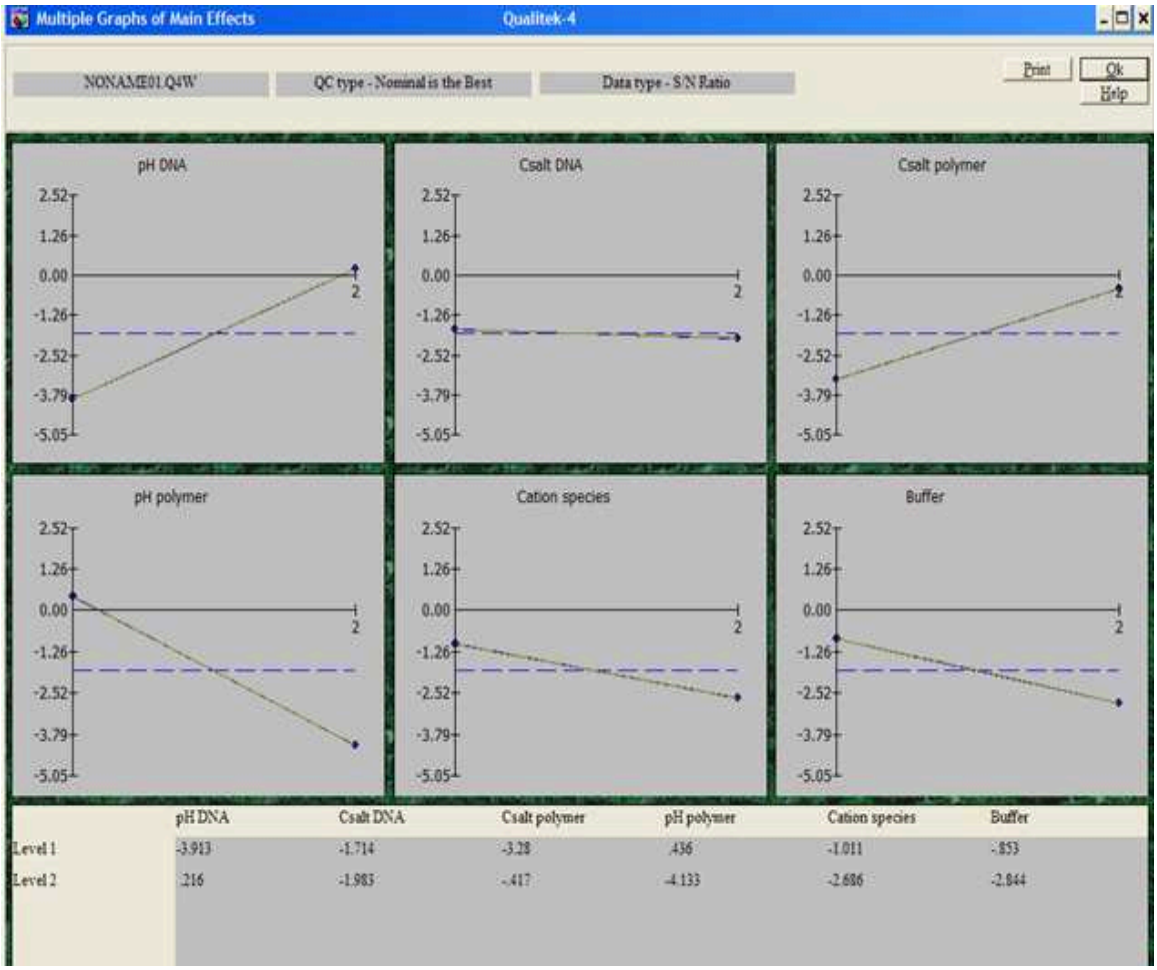

Figure 5.1: Main effects of multiple factors (S/N) for thickness of polymer films.

5.3.2 Refractive index change after DNA immobilized onto the wafer

Figure 5.4 gives the importance of each factor to the refractive index after DNA is immobilized onto the wafer. Figure 5-5 shows that pH of DNA is the dominant factor for the refractive index.

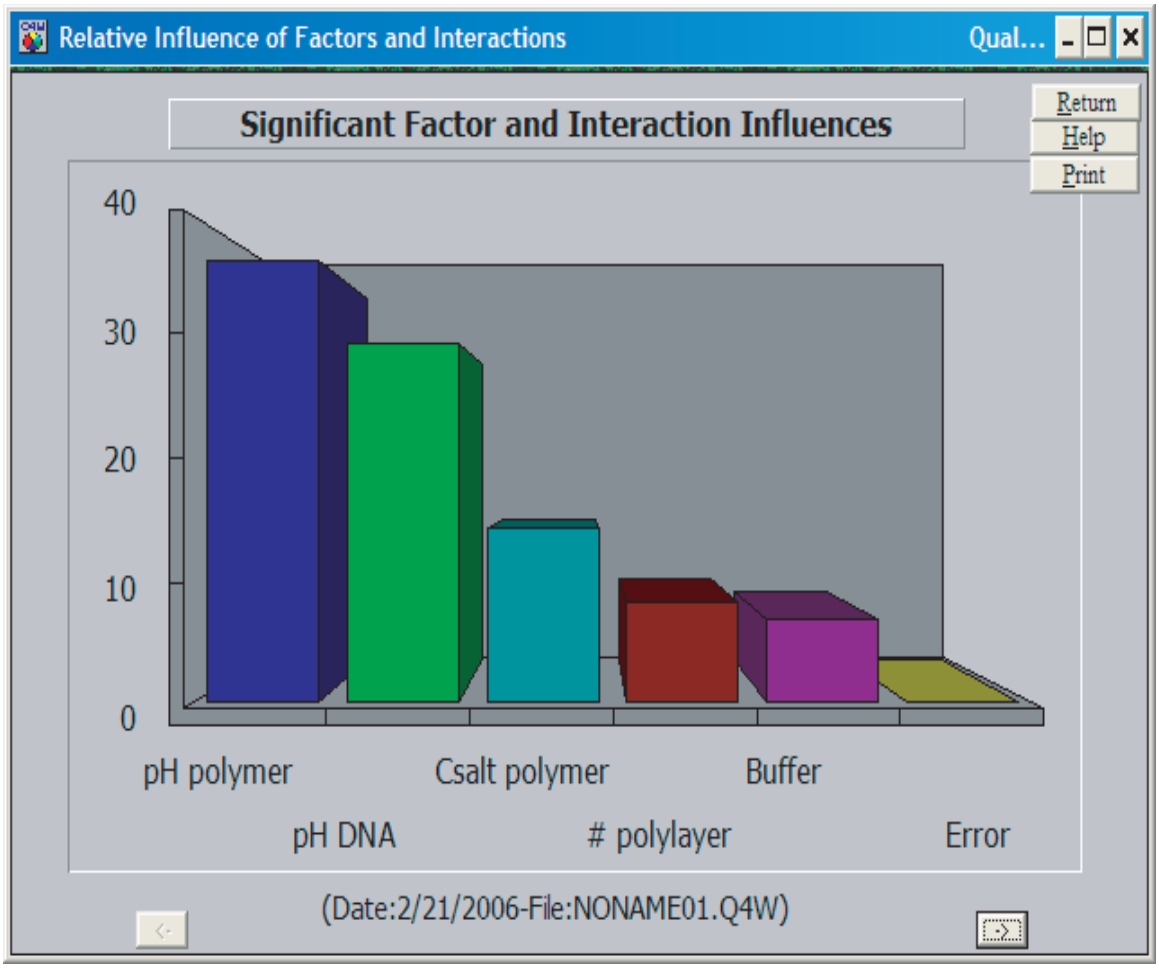

Figure 5.2: Significant factors effect in percentage.

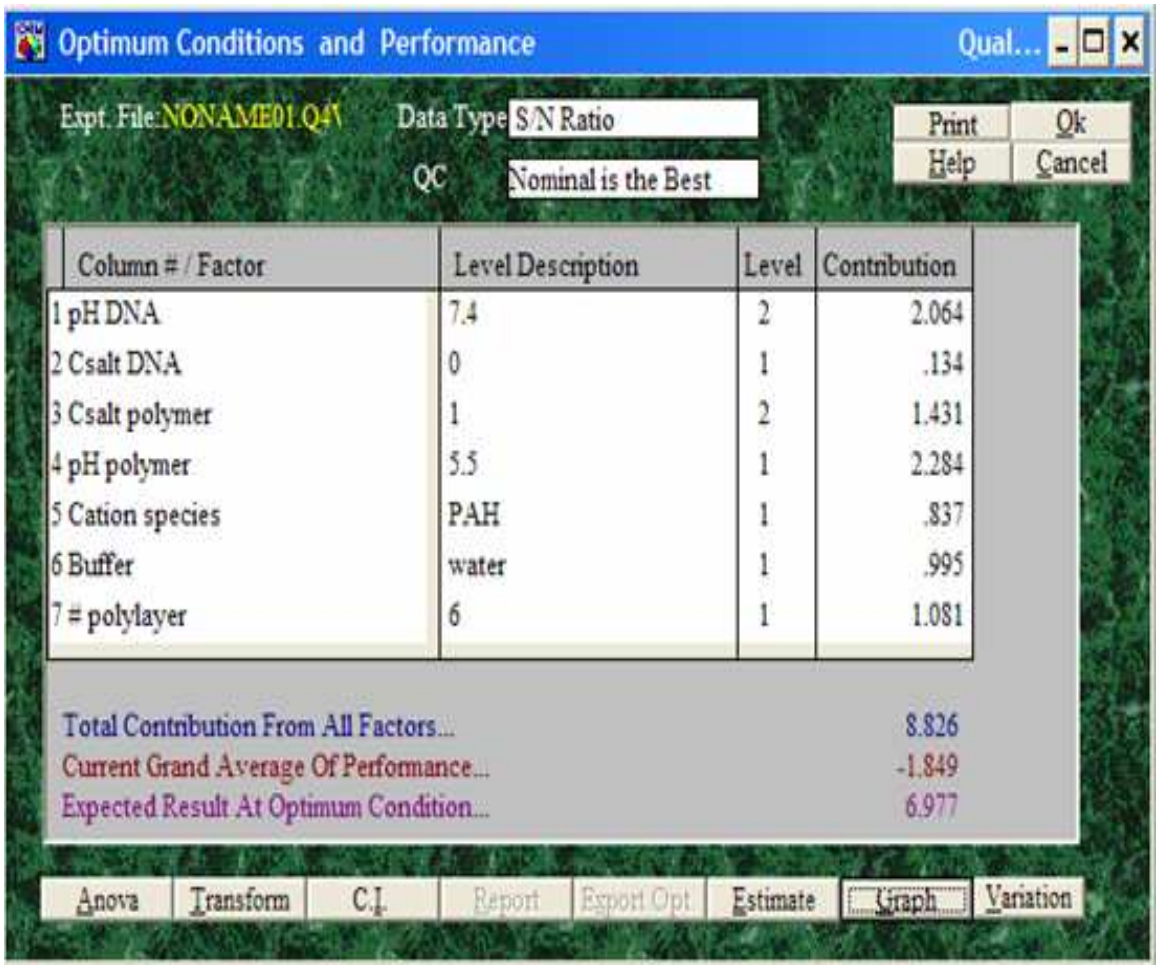

Figure 5.3: Optimum conditions of factors.

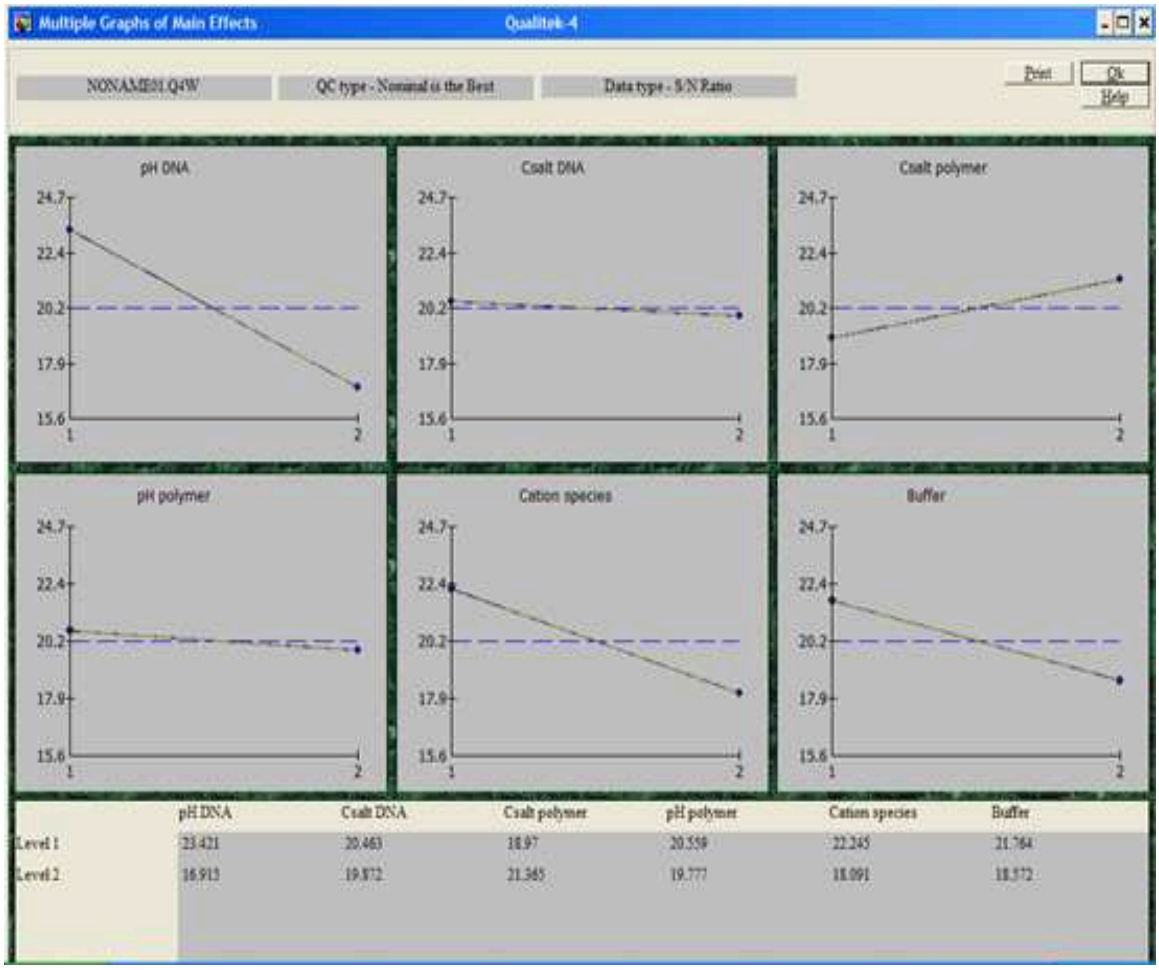

Figure 5.4: Main effects of multiple factors (S/N) for refractive index.

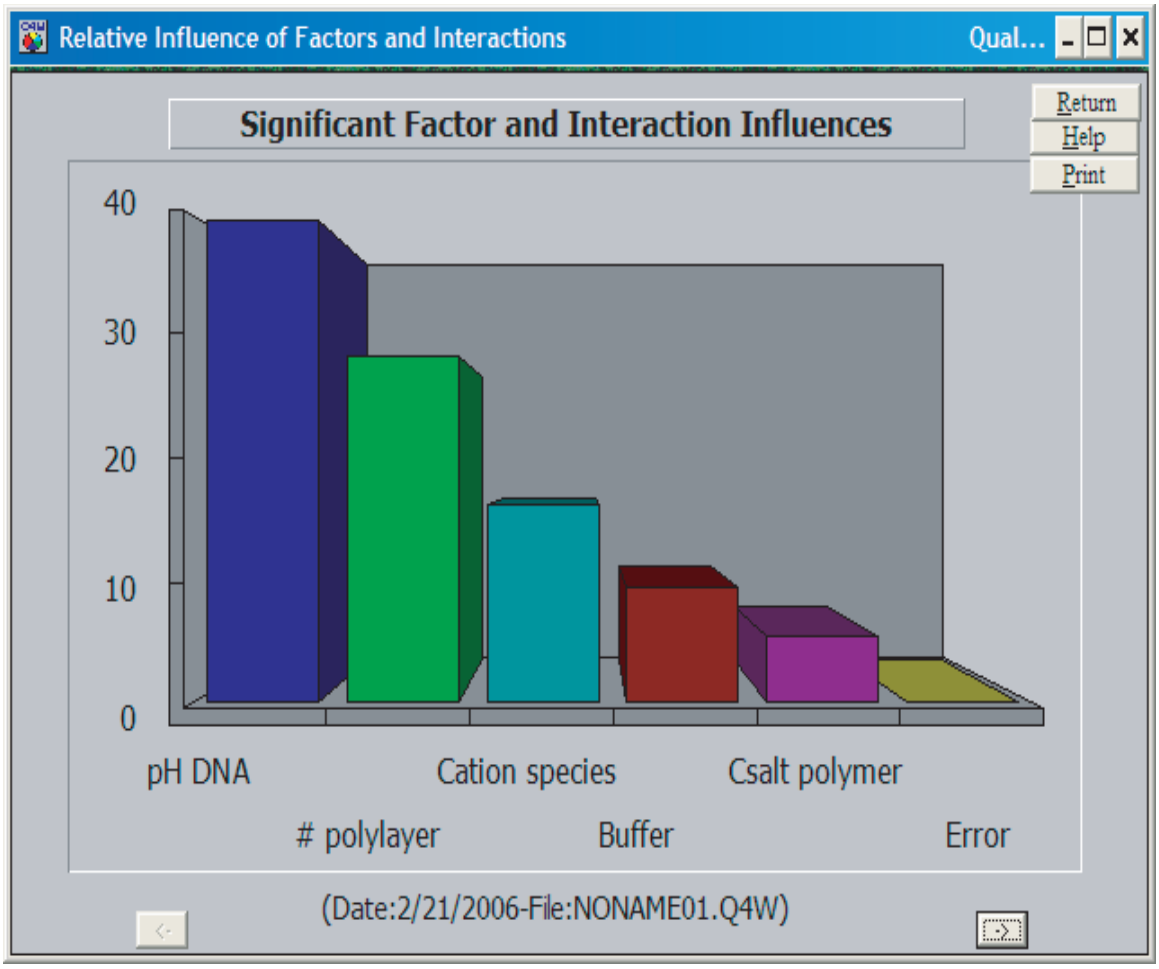

Figure 5.5: Significant factors for refractive index in percentage.

5.4 Conclusion

In order to maximize the surface concentration of the DNA immobilized onto the final sensor head, optimal parameters of the experiment environment were investigated with Taguchi experiment design method. An L-8 array was selected and 24 samples were measured. Taking advantage of the Qualitek-4 software, we find that the main factors that influence the thickness of the immobilized DNA layer is pH of polymer and DNA solution. To control the refractive index of the DNA layer, pH of DNA solution is the main factor. The software also provides the optimal factor levels which can be confirmed in the experiments. These are very meaningful guidance for our future experiments to increase the sensitivity of the sensors.

Chapter 6

Label-free DNA Sequence Detection Using Oligonucleotide Functionalized Optical Fiber

As presented in Chapter 2, our final goal is to design and develop a nanometric scale fiber probe for in-cell DNA detection. The immobilization of DNA will be achieved by the layer-by-layer electrostatic self-assembly (L-b-L ESA) method. To support the feasibility of the concept of our in-cell DNA detection sensor, one of the challenges was to demonstrate successful DNA immobilization to the fiber end. To achieve this goal, a fiber tip biosensor was fabricated, which utilizes a label-free method for direct detection of deoxyribonucleic acid (DNA) sequences. The capture DNA was immobilized onto the surface of a silica optical fiber tip by L-b-L ESA. Hybridization of target DNA with complementary capture DNA increased the optical thickness of the fiber tip. This phenomenon was detected by demodulation of the spectrum of a Fabry Perot (FP) cavity fabricated in the optical fiber.

This chapter presents the experimental results that we have obtained. Sensor design and fabrication are presented. DNA immobilization and hybridization have been achieved. Experimental results demonstrate sequence specificity and high sensitivity to nanogram quantities of target DNA

sequence with short (5 min) hybridization time.

6.1 Fiber tip biosensor

6.1.1 Sensor structure

This is a multi-cavity Fabry-Perot fiber sensor for thin film measurements [101]. Yan Zhang has developed the sensor and the program for signal demodulation. We used this sensor for DNA detection test and thin film measurements. The sensor has a short length of hollow tube sandwiched between two pieces of optical fiber, forming an air cavity between the lead-in and reflection fibers. By cleaving the reflection fiber, a fiber cavity can be formed in addition to the air-cavity. Multiple reflection signals from the interfaces of the air and fiber cavities form the interference fringe pattern. Demodulation of this spectrum can give out an accurate cavity length with high resolution. Therefore, the thickness of the fiber cavity length, which is our focus, can be obtained.

This fiber cavity length acts as the baseline for our further experiments. After growing 5.5 bilayers of polymer films on the sensor, the fiber cavity length will increase. Then the capture DNA sample is immobilized onto the sensor tip. If the immobilization is successful, the fiber tip thickness will increase again. Otherwise, if the film is not strongly bound and easily washed away, the film thickness will not change.

The whole sensor is made of the same material, fused silica, and the glass mechanical bonding can be done by fusion bonding at high temperature. Figure 6.1 shows the basic schematic of the structure. Figure 6.2 to Figure 6.4 are photographs of such a structure.

6.1.2 Sensor fabrication process

The sensor fabrication includes two parts: air-cavity fabrication and fiber cavity fabrication, as illustrated in Figures 6.5 and 6.6. The fusion splice may be formed in a conventional electric-arc

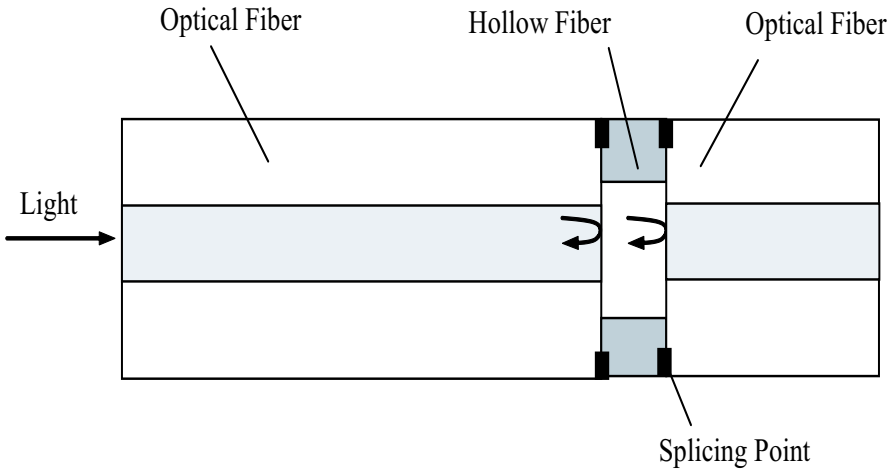

Figure 6.1: Sensor structure.

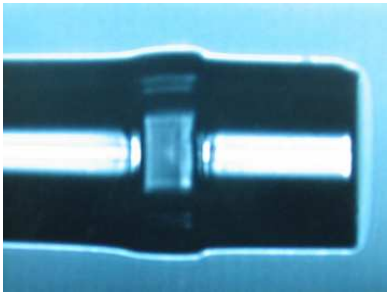

Figure 6.2: Sensor photo taken by an arc fusion splicer (Fujikura FSM-30P).

fusion splicer. The hollow tube fiber may be fabricated from a hollow tube preform drawn into a fiber, in a manner analogous to making conventional optical fiber. Cleaving can be performed with a conventional diamond fiber cleaving tool. Cleaving is performed with high accuracy (within a few microns or less) so that the length of the bonded hollow tube is accurate. To achieve high accuracy, cleaving can be performed under a microscope. Alternatively, after cleaving, the hollow tube can be shortened by chemical etching or polishing.

During fabrication, we utilize the component testing system (CTS, Micron Optics SI720) to mon-

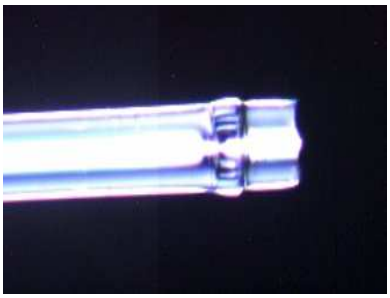

Figure 6.3: Sensor's side view photo taken from a microscope (Zeiss Axiovert 25).

Figure 6.4: Sensor's endface view photo taken from a microscope (Zeiss Axiovert 25).

itor the whole process. After calibration, the standard optical fiber is connected to the CTS. After each step of cleaving and splicing with the hollow fiber, the signal strength is observed to control the process within the error tolerance.

It is noted that the manufacturing process illustrated in Table 6.6 employs conventional and well-known fiber splicing and cleaving tools. Consequently, the present sensor is simple and inexpensive to fabricate. Additionally, the materials required for construction (hollow tubes and solid fibers) are commercially available and very cheap. The present sensor has high mechanical strength and smooth optical surfaces that minimize optical scattering. These features are provided as a result of the cleave and splice manufacturing method.

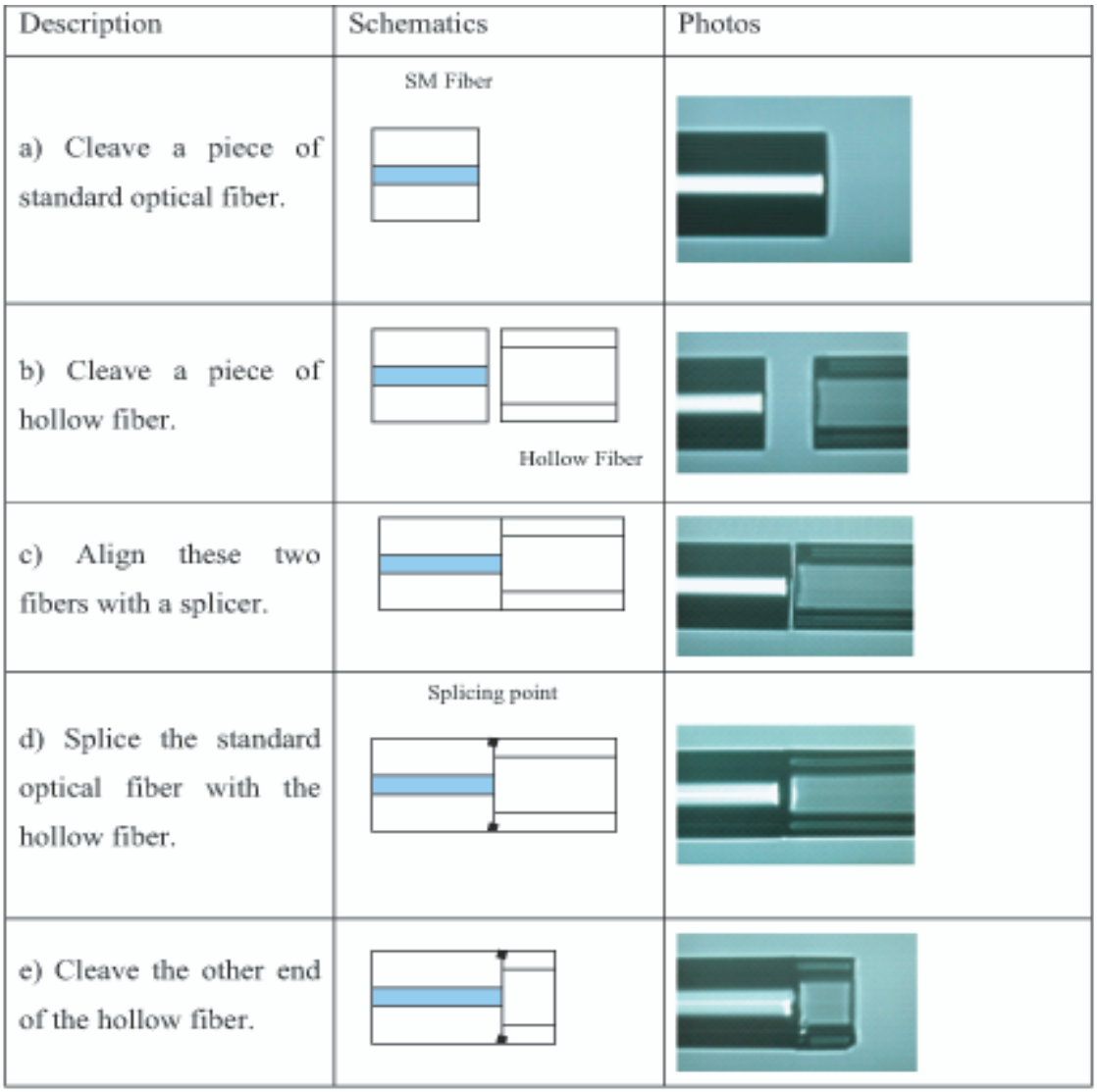

Figure 6.5: Illustration of cavity fabrication.

6.1.3 Sensor's features

In summary, the sensor has the following features:

1. Airgap: (30 $\mu m \sim 45 \mu m$): (Only 2 valleys can be investigated from the CTS)
    - Shorter than this range: CTS cannot see 2 valleys and air gap cannot be calculated

Description	Schematics	Photos
a) Complete air cavity formation.		
b) Align the hollow tube with a piece of fiber.	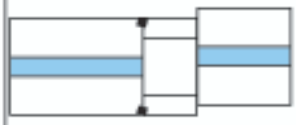	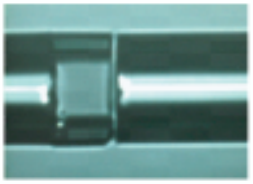
c) Splice the hollow tube with the optical fiber.	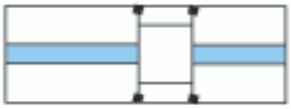	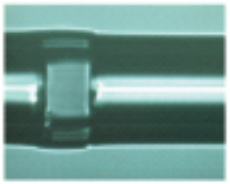
d) Cleave the optical fiber to form the fiber cavity.		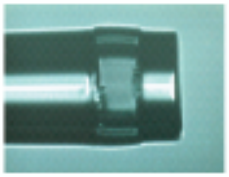

Figure 6.6: Illustration of fiber cavity fabrication.

correctly.

- Longer than this range: Fiber cavity length has to be much longer in order to reduce the interference and the signal separation. This will cause high temperature cross-sensitivity due to the high coefficient of thermal expansion (CTE) of SiO_2.

2. Fiber cavity length: (100 μ m $\sim$ 150 μm)

   - Too short: difficult to separate coupled signals of air cavity, fiber cavity and their mixed frequencies.

- Too long: Temperature cross-sensitivity will be high because of the high CTE of SiO_2.

3. High visibility ($20dB \sim 30dB$): Controlled by the alignment of two SMFs.

4. High light intensity: Peak: $> 2 \sim 3dB$.

6.2 DNA immobilization

6.2.1 Materials and process

The process of identifying the existence of a certain expression of DNA sequence involves immobilization of the single-stranded capture DNA onto the fiber tip, which then becomes the "probe". Then, the probe is immersed into the sample. If the sequence of the sample is complementary to that of the capture DNA, hybridization occurs. Otherwise, if the sample is not complementary, the remaining samples on the probe can be easily washed away by ultrapure deionized (DI) water.

To improve self-assembly growth characteristics, ameliorate denaturation, and allow sufficient configurational freedom for hybridization, a multilayer polyelectrolyte precursor film, polyallylamine hydrochloride (PAH) and polysodium 4-styrenesulfonate (PSS) were deposited by alternately immersing the sensor in the polyelectrolyte solutions for 5 min, as indicated in Table 6.1. The sensor was then rinsed with DI water and dried.

Sample molecules (nucleic acids) used in this study, as indicated in Table 6.2, were purchased from Genosys, and were used without further purification.

Table 6.1: Polyelectrolytes used in immobilization and hybridization experiments.

Name	pH	Concentration (mg/ml)	Salt Concentration
PAH	5.0	2.0	0
PSS	5.0	2.0	0

Table 6.2: Oligonucleotide sequences used in immobilization and hybridization experiments.

Name	Purpose	Sequence (5' - 3')
ssDNA-A	Probe	TCCAGACATGATAAGATACATTGATG
ssDNA-B	Concentration test	CATCAATGTATCTTATCATGTCTGGA
ssDNA-C	Negative control	CTCACGTTAATGCATTTTGGTC

6.2.2 Grow PAH/PSS onto the sensor

□ **Materials and procedures**

Polyelectrolyte solutions are listed in Table 6.1.

Procedure steps:

- Step 1: Agitate the sensor in a hot $H_2SO_4 : H_2O_2$ $(7 : 3)$ mixture for 1 hour and then washed with DI water. The sensor tip is negatively charged.
- Step 2: Immerse the fiber sensor into PAH solution for 5 minutes, and the sensor head is positively charged.
- Step 3: Rinse the fiber sensor with ultrapure water (Barnstead Diamond RO/Nanopure Diamond UV/UF) for 1 minute.
- Step 4: Immerse the sensor into PSS for 5 minutes, and the sensor head is negatively charged.
- Step 5: Rinse the sensor with DI water for 1 minute.
- Step 6: Repeat step 2 $\sim$ step 5 for 5.5 bilayers. The outermost layer is positively charged PAH.
- Step 7: Dry the sensor in a stream of N_2.
- Step 8: Measure the fiber cavity length.

The experiment was carried out at $23°C$. The experiment setup is shown in Figure 6.7.

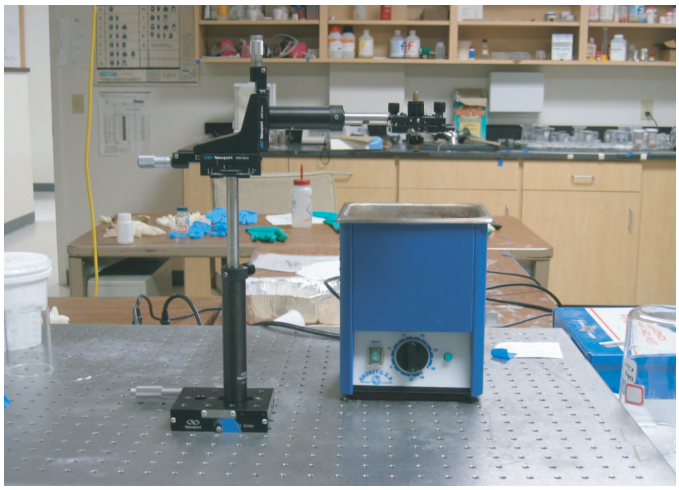

Figure 6.7: Experiment setup.

□ **Results analysis**

Figure 6.8 shows the spectrum of the sensor after growing 5 bilayer PAH/PSS films.

Figure 6.9 shows the fiber cavity length changes according to the layer number. Here, except layer 2, the film growth is linear. This phenomenon is normal in L-b-L ESA technique. The even thickness grown in the following steps indicate its self-healing effect, which is one of the advantages of L-b-L ESA method.

6.2.3 DNA immobilization (DNA immobilization thickness: 3.6nm)

□ **Materials and procedures**

After the polyelectrolyte precursor films were grown on the fiber tip, capture DNA was immobilized to make the DNA sensor probe. The DNA sequence for probe is ssDNA-A in Table 6.2. Its characteristics are listed in Table 6.3. Usually it is stored at $-20°C$. Our experiment was carried out at $21.4°C$.

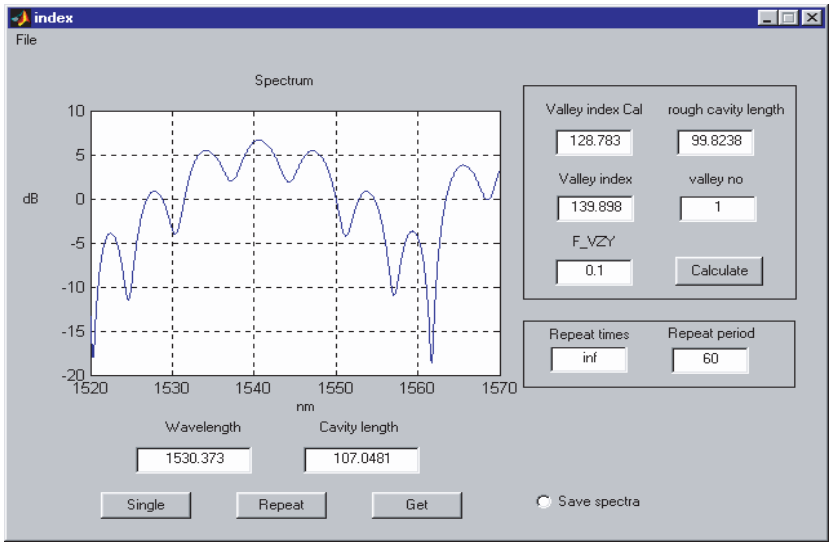

Figure 6.8: Representative spectrum of the sensor after growing 5 bilayer PAH/PSS films.

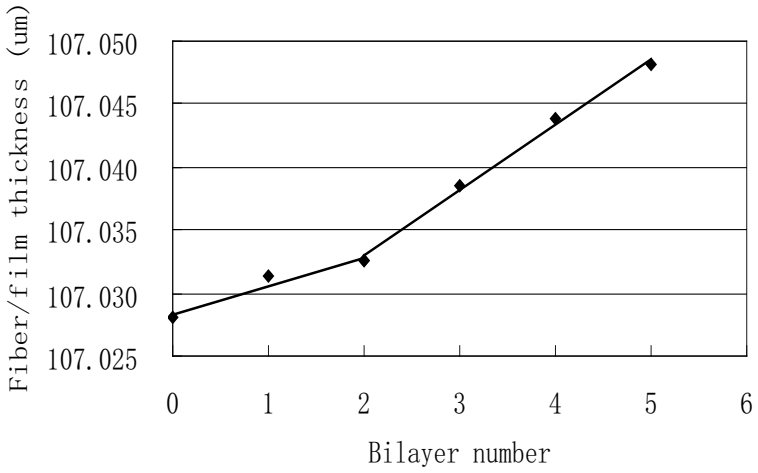

Figure 6.9: Polymer growth. Fiber/film thickness changes according to the bilayer number growth.

Procedure steps:

1. Measure fiber cavity length before DNA is grown.
    - Dip the fiber sensor into DNA solution.

Table 6.3: ssDNA-A used for probe.

Name	pH	Concentration	Salt Concentration
ssDNA-A	5.5	154.17 μg/ml (19.26nM)	0.02 M

- After 5 minutes, draw out the fiber sensor and dry it.

2. Measure fiber cavity length after DNA growth.

3. Plot fiber cavity length change before and after DNA growth in Figure 6.10.

□ **Results analysis**

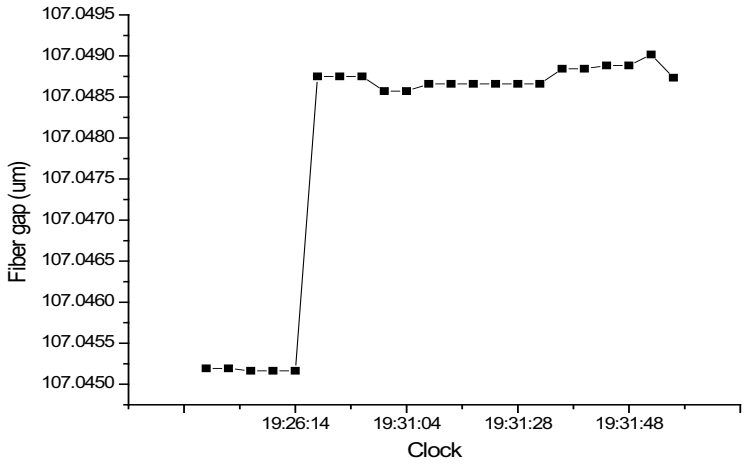

Figure 6.10: DNA immobilization. Fiber cavity length before and after DNA growth. X-axis indicates the time. Y-axis indicates the fiber cavity length in micron.

Analysis:

- DNA growth on the fiber tip is:

$$107.04874 - 107.04518 = 0.00356(\mu m) \approx 3.6(nm). \tag{6.1}$$

- Result agrees well with the result from [102], whose experiment shows DNA layer as thick as 3.3 nm.

6.2.4 Repeatability (DNA immobilization thickness: 3.4nm)

In order to further demonstrate the feasibility of DNA immobilization onto the fiber end with layer-by-layer electrostatic assembly method, the entire experiment was carried out again.

□ **Fabricate fiber sensor for film thickness test**

The fiber cavity length was 112.988 μm.

□ **Grow PAH/PSS, then DNA onto the fiber sensors**

♢ Material and operating environment

All solutions including PAH, PSS and DNA were at the same concentration and pH value as that of the previous experiment, as indicated in Table 6.1, Table 6.2 and Table 6.3. Also, the operating steps were the same to make the results meaningful.

♢ Experiment results

Figure 6.11 plots the fiber cavity length changes according to the film growth. Here, except layer 2, the film growth is linear.

Figure 6.12 plots the fiber cavity length change before and after DNA growth.

Analysis:

- DNA growth on the fiber tip is

$$113.00593 - 113.00255 = 0.00338(\mu m) \approx 3.4(nm). \tag{6.2}$$

- Result agrees well with the result from [102], whose experiment shows DNA layer as thick as 3.3 nm.

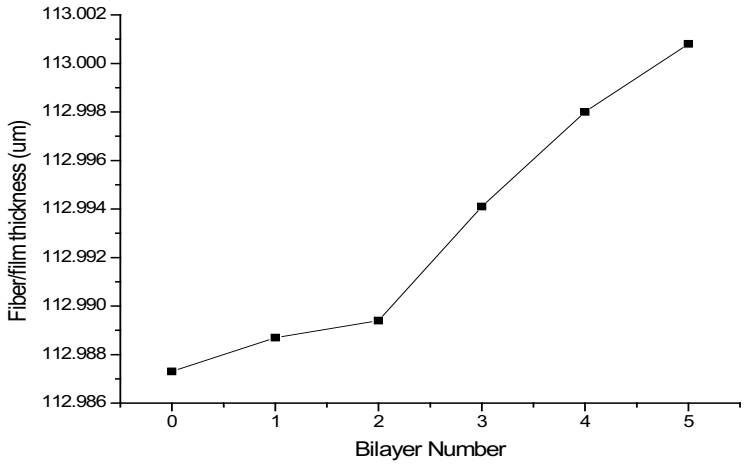

Figure 6.11: Polymer film growth.Fiber/film thickness changes according to the bilayer number growth.

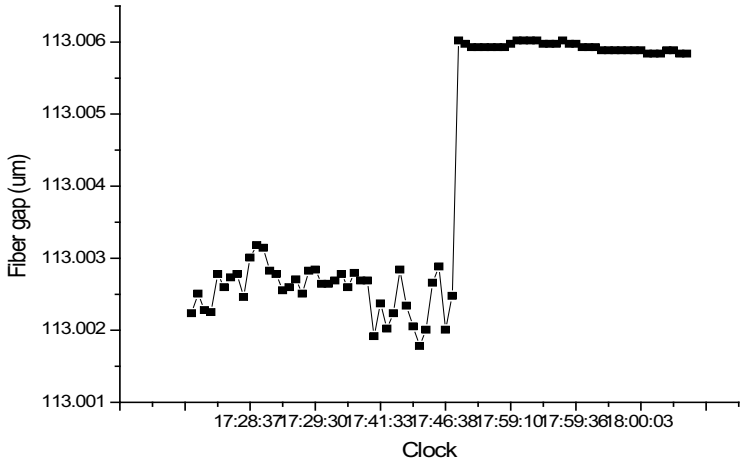

Figure 6.12: DNA immboilizaiton. X-axis indicates the time. Y-axis indicates the fiber cavity length in micron.

- Result also agrees well with the previous experiment.

6.2.5 Summary

Five bilayers of polymer film were grown, with PAH, the positively charged polymer, as the outermost surface. Then the sensor was immersed in ssDNA-A solution for 5 minutes (pH 5.5, concentration 154.17 $\mu g/ml$, $0.02M$ NaCl). Two experiment results, as shown in Figure 6.13, indicate that fiber thickness increases with 3.4 nm and 3.6 nm, which agree well with the result from [7]. This indicates that DNA was successfully immobilized onto the tip of silica fiber. After this step, fabrication of the DNA detection sensor was complete.

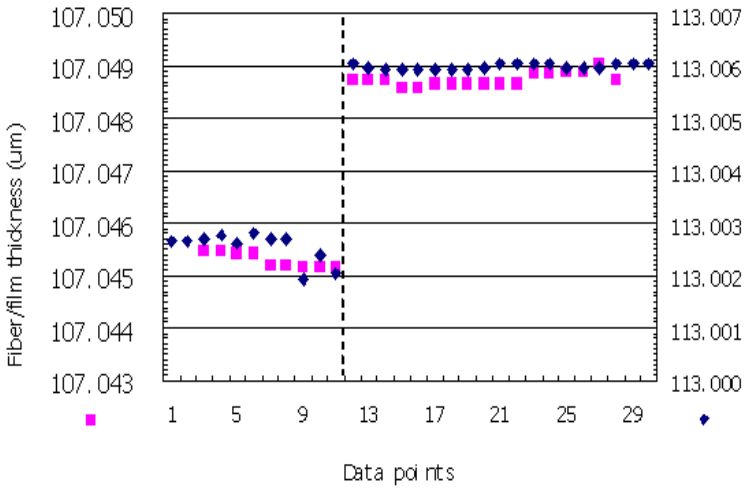

Figure 6.13: DNA was successfully immobilized onto the fiber tip with 3.4nm and 3.6nm thickness respectively.

6.3 DNA sensor test: Hybridization

6.3.1 Specificity

□ **Materials and process**

Table 6.4: ssDNA-B and ssDNA-C used for probes.

Name	pH	Concentration	Salt Concentration
ssDNA-B	5.5	606 μg/ml (76.5 nM)	0.02 M
ssDNA-C	5.5	827.8 μg/ml (123.8 nM)	0.02 M

After the sensors were fabricated, they were tested for specificity in complementary and non-complementary DNA solutions. The complementary DNA sample was ssDNA-B obtained from Genosys. The non-complementary DNA sample was ssDNA-C. The characteristics of these two solutions are listed in Table 6.4.

Two DNA ssDNA-A sensors were immersed into the complementary DNA ssDNA-B solution respectively. After 25 minutes, they were taken out and dried. 4.0 nm and 4.3 nm thickness increases were detected, indicating that the sensor can successfully detect the complementary DNA sequence.

□ **Hybridization**

♢ Hybridization test 1 (DNA hybridization thickness: 4.0nm)

Here, (and in this chapter,) fiber cavity length is the length of the second bonded fiber section, and its unit is micron. Airgap is the length of the hollow fiber in micron.

Figure 6.14 shows the fiber cavity length change after the probe DNA sequence was immobilized and the complementary DNA sequence was hybridized onto the fiber tip.

Analysis:

- Probe DNA layer: 111.0260-111.0220= 0.004 (μm)=4.0 (nm)
- Complementary target DNA layer: 111.0300-111.0260=4.0 (nm)
- DNA was successfully grown onto the fiber sensor head.

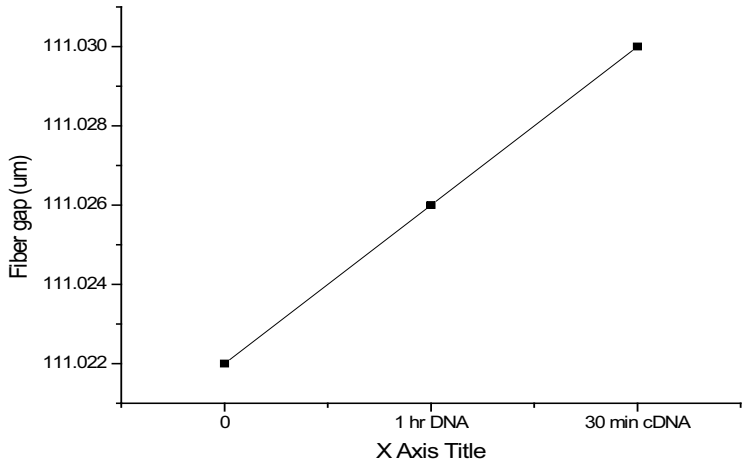

Figure 6.14: Probe DNA immobilization and complementary target DNA hybridization onto fiber tip.

- Complementary DNA was successfully attached onto the DNA layer.

◇ Hybridization test 2 (DNA hybridization thickness: 4.3nm)

We repeated the hybridization test with the same materials and the same process in the clean room.

Figure 6.15 and Figure 6.16 show the fiber cavity length growth of probe DNA immobilization and complementary target DNA hybridization, respectively.

Analysis:

- Probe DNA layer: 105.0413-105.0382=0.0031 (μ m) = 3.1(nm)
- Complementary DNA layer: 105.0456-1105.0413=0.0043(μ m) = 4.3(nm)
- DNA was successfully grown onto the fiber sensor head.
- Complementary DNA was successfully attached onto the DNA layer.

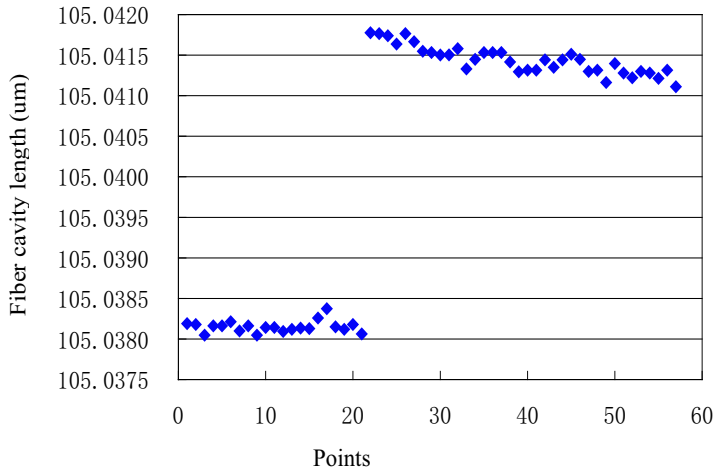

Figure 6.15: DNA immobilization onto the fiber tip to form the probe; DNA thickness is 3.1nm.

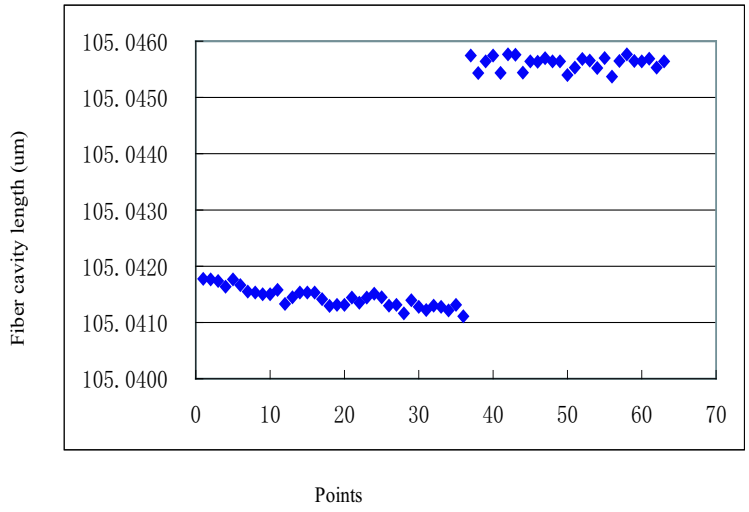

Figure 6.16: DNA hybridization. Complementary DNA is hybridized onto the probe. The thickness is 4.3nm.

The results are consistent with each other, and both agree with the reference. This indicates that the DNA sensor can successfully detect complementary DNA sequence.

□ **Negative control**

In order to prove the sensor will not react to a noncomplementary DNA sequence, a negative control test was carried out. The ssDNA-C sequence listed in Table 6.2 was used. Two sensors were tested using the same solution and process. Both indicate that this kind of DNA sensor does not respond to noncomplementary DNA sequences.

□ **Summary**

For the negative control, two DNA sensors were put into the non-complementary DNA solution for 40 minutes and 1 hour respectively. The concentration of non-complementary DNA was much higher than the complementary ones, and the immersion time was much longer. However, the length of the fiber tip did not change after washing the probe with DI water. This indicates that the non-complementary DNA did not attach onto the probe. The DNA sensor is capable of detecting a specific DNA sequence. This is shown in Figure 6.17.

A novel label-free DNA sequence detection method has been demonstrated. Using the L-b-L ESA method, the capture DNA was immobilized onto the substrate surface. When complementary DNA samples were hybridized, the thickness of the films increased. Otherwise, the non-complementary DNA sample could not be bonded onto the surface tightly and was easily washed away. Detection of the thickness change indicated the successful hybridization.

6.3.2 High sensitivity

To test the sensor's sensitivity, we designed a setup to detect DNA solution within a very small volume.

□ **Syringe bubble**

As shown in Figure 6.18, a small volume of complementary DNA solution was generated by the syringe. Figure 6.19 shows the setup. By decreasing the drop size from 0.8 mm to 0.5 mm, drop volumes of 0.27 μl and 65.4 nl were obtained. Experiments were carried out in a clean room.

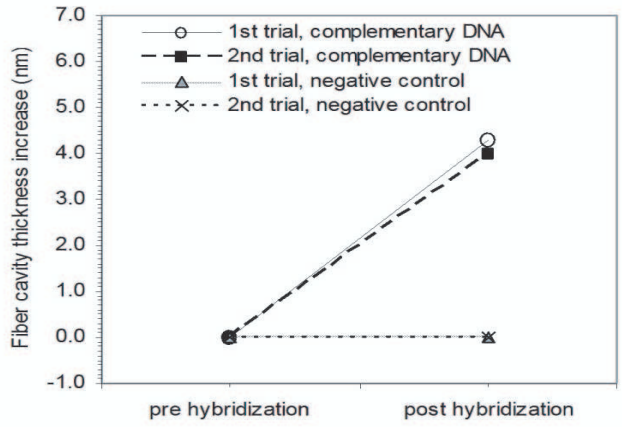

Figure 6.17: Detection of specific hybridization of 26-mer target to immobilized probe; probe: ssDNA-A immobilized on sensor tip; target: ssDNA-B, 76 nmol/ml, pH 5.5, 0.02 M NaCl, immersion time 30 min; negative control: 22-mer ssDNA-C, 123.8 nmol/ml, immersion time 40-60 min. The DNA can successfully detect complementary DNA, whereas no non-complementary DNA attachment is observed.

PAH/PSS and probe DNA solutions are the same as listed in Table 6.1, Table 6.2, Table 6.4, and Table 6.5. Three kinds of complementary DNA sequence were used: ssDNA-B, ssDNA-D and ssDNA-E. ssDNA-D is the mixture of ssDNA-B and ssDNA-C to make the complementary concentration as low as $303\mu g/ml$. ssDNA-E is a mixture of ssDNA-D and ssDNA-C. The characteristics are listed in Table 6.5.

Table 6.5: Complementary DNA solution used in syringe sensitivity test.

Name	pH	Concentration	Salt concentration
ssDNA-D	5.5	303 $\mu g/ml$ (38.2 n M)	0.02 M
ssDNA-E	5.5	151 $\mu g/ml$ (19.1 n M)	0.02 M

♢ 163.6 ng sensitivity

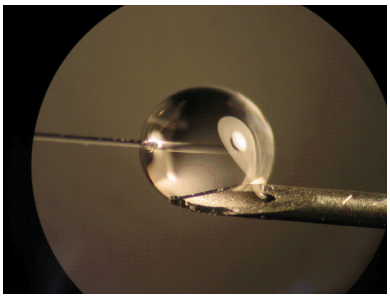

Figure 6.18: Small volume hybridization test. The fiber sensor is inserted into the small drop (nanoliter) of solution generated by the needle tip of a 26 gauge syringe.

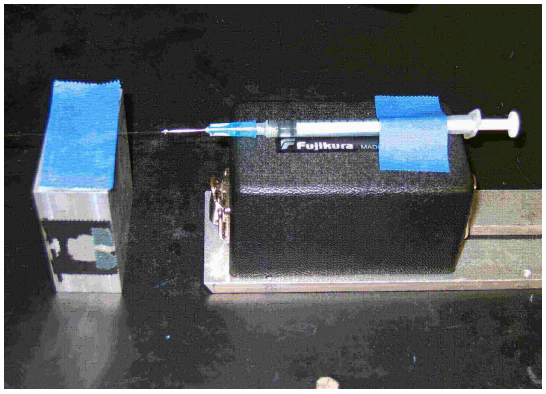

Figure 6.19: Small volume DNA hybridization test setup. A DNA fiber sensor is fastened on a holder on the left. DNA solution bubble is generated by a syringe on the right.

Sensor 4 and Sensor 5 were tested first using ssDNA-B solution. Table 6.6 shows the successful detection of complementary DNA sequence.

Since the diameter of the volume was 0.8mm, the volume of the drop generated by the syringe was

$$V = \frac{4}{3}\pi\left(\frac{0.08}{2}\right)^3 \approx 0.27 \times 10^{-}3(cm^3) = 0.27(\mu l). \tag{6.3}$$

$1ml$=$1cm^3$

1μl = $1mm^3$

Table 6.6: Fiber cavity length change when complementary DNA hybridized onto Sensor 4 and Sensor 5.

	Sensor 4	Sensor 5
Before complementary DNA (μm)	111.5950	111.4100
After complementary DNA (μm)	111.6000	111.4140
Complementary DNA thickness (nm)	5	4

Concentration of complementary DNA was 606 μg/ml The mass of complementary DNA was: $606 \times 0.27 \times 10^{-}3 = 163.62(ng)$ The experiment result indicates that the sensor can detect the complementary DNA mass as small as 163.62 ng.

♢ 19.8ng sensitivity

Sensor 6 was tested first using ssDNA-D solution.

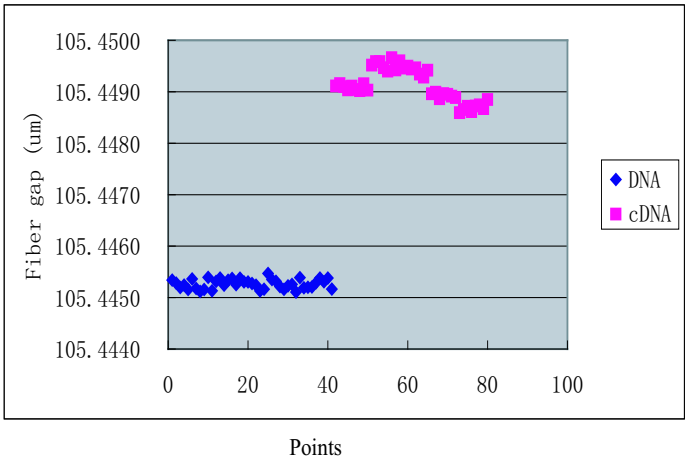

Figure 6.20: Hybridization of complementary DNA (m=19.8ng) onto the fiber tip.

Figure 6.20 indicates the successful complementary DNA hybridization onto the fiber tip.

Since the diameter of the volume was 0.5 mm, the volume is

$$V = \frac{4}{3}\pi\left(\frac{0.05}{2}\right)^3 \approx 65.4 \times 10^{-6}(cm^3) = 65.4(nl). \tag{6.4}$$

Concentration of complementary DNA was $303\mu g/ml$ The mass of cDNA was: $303 \times 65.4 \times 10^{-6} = 19.8(ng)$

The experiment result indicates that the sensor can detect small mass of complementary DNA as low as 19.8 ng.

□ **DNA drip**

To further increase the sensitivity of the sensor, we decreased the volume of the DNA solution with another setup, as shown in Figure 6.21.First we used the syringe to generate a drop of liquid. Then we used the fiber sensor tip to touch and collect the drop from the syringe. Because of the absorption of the liquid onto the solid surface, the liquid will stay on the tip and serves as the container itself for DNA detection. Materials and process are the same as the previous experiments. Experiments were carried out in the clean room.

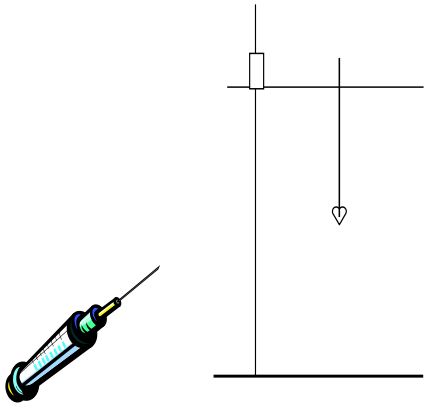

Figure 6.21: Experiment setup. The solution drop is obtained by dipping the sensor tip into the syringe bubble. The bubble can be as small as the size of the fiber tip.

♢ 6.5ng sensitivity

ssDNA-B was used for the complementary DNA solution.

Figure 6.22, and Figure 6.23 show the fiber cavity length change when probe DNA and complementary target DNA were grown onto the fiber tip.

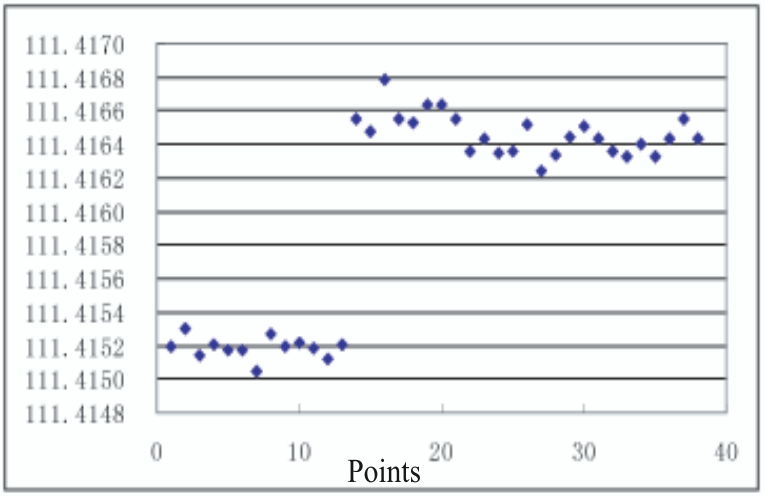

Figure 6.22: Immobilization onto the fiber tip to form the probe; DNA thickness is 1.2 nm.

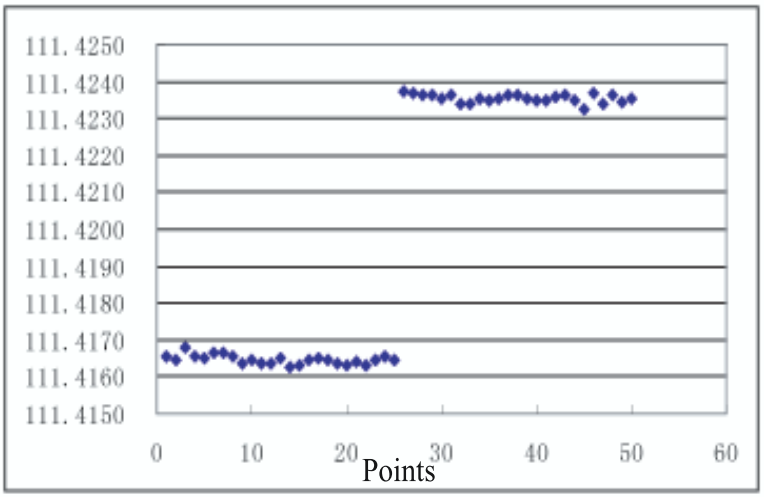

Figure 6.23: DNA hybridization. Complementary DNA (m=6.5ng) is hybridized onto the probe. The thickness is 7.3nm.

Analysis:

- Probe DNA layer: 111.4164-111.4152=0.0012 (μm)
- Complementary DNA layer: 111.4237-111.4164= 0.0073(μm)=7.3 (nm)
- Probe DNA was successfully grown onto the fiber sensor head.
- Complementary DNA was successfully attached onto the DNA layer.

$$V = \frac{4}{3}\pi\left(\frac{0.03}{2}\right)^3 \approx 10.83 \times 10^{-6}(\text{cm}^3) = 10.8(\text{nl}). \tag{6.5}$$

Concentration of cDNA is 606 μg/ml The mass of cDNA is: $606 \times 10.8 \times 10^{-6} = 6.5(ng)$

♢ 3.3ng sensitivity

ssDNA-D was used in this experiment. The experiment was carried out in the clean room.

After dipping the sensor into the ssDNA-A for 40 min, the fiber cavity length was increased to 111.3923 μm. Then the DNA sensor was inserted into the complementary DNA solution for 30 min, the fiber cavity length is increased to 111.3941 μm.

Analysis:

- Probe DNA layer: 111.3923-111.3892=0.0031(μs)=3.1 (nm)
- Complementary DNA layer: 111.3941-111.3923=0.0018(μm)=1.8 (nm)
- DNA was successfully grown onto the fiber sensor head.
- Complementary DNA was successfully attached onto the DNA layer.
- Volume: Since the diameter of the volume was $0.3mm$, the volume was

$$V = \frac{4}{3}\pi\left(\frac{0.03}{2}\right)^3 \approx 10.83 \times 10^{-6}(cm^3) = 10.8(nl). \tag{6.6}$$

Concentration of cDNA was 303 μg/ml. The mass of cDNA was: $303 \times 10.8 \times 10^{-6} = 3.3(ng)$

This experiment indicates that the sensor can detect complementary DNA sequence quantities as small as 3.3 ng.

♢ 1.7ng sensitivity

ssDNA-E was used in this experiment. The experiment was carried out in the clean room.

Analysis:

- Probe DNA thickness: 105.0419-105.0397 = 0.0022(μm)=2.2 (nm)
- Complementary DNA thickness: 105.0435-105.0419=0.0016(μm)=1.6 (nm)
- Volume: Since the diameter of the volume was about 0.3mm, the volume was

$$V = \frac{4}{3}\pi \left(\frac{0.03}{2}\right)^3 \approx 10.83 \times 10^{-6}(cm^3) = 10.8(nl). \tag{6.7}$$

Concentration of cDNA was 151.5ng/ml The mass of cDNA was: $151.5 \times 10.8 \times 10^{-6} = 1.7(\text{ng})$

This experiment indicates that the sensor can detect complementary DNA sequence quantities as small as 1.7ng.

6.3.3 Summary

Good specificity was proven in the hybridization and negative control experiments by immersing two sensors in the complementary and non-complementary DNA solution.

To evaluate the sensitivity of this label-free DNA sequence detection method to small quantities of target DNA, the hybridization was observed in small volumes. The fiber sensor was inserted

into the drop of solution generated from a needle tip and the DNA drip. Sensor fiber cavity thickness changes induced by hybridization shown in Figure 6.24 indicates that the sensor can detect quantities as small as 1.7 ng.

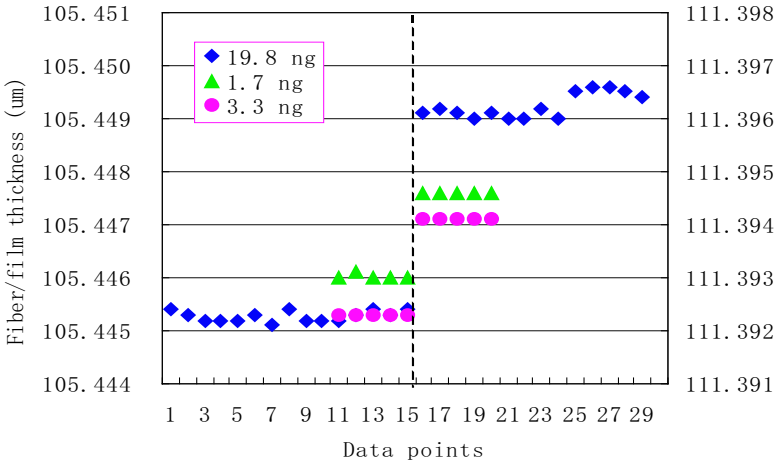

Figure 6.24: Hybridization of small quantities (1.7-19.8 ng) of complementary DNA sequence to ssDNA-A probes immobilized on the sensor interface.

6.4 DNA sensor for detection of bacteria - Tularemia

As presented in the previous sections, our DNA sensor can successfully detect hybridization of complementary DNA samples. This can be utilized as a very useful and efficient tool to detect bacteria, which can be of significance in prevention of the spread of infectious diseases, and defense of biological weapons.

6.4.1 Tularemia

Tularemia (also known as deerfly fever or rabbit fever) is an infectious disease caused by the bacterium *Francisella tularensis* (*F tularensis*). It is the subject of a fifth article in a series pro-

viding recommendations for medical and public health management. As R. R. Parker mentioned, tularemia has the most diverse source among the infection of animals communicable to man. It chiefly affects small mammals such as rabbits, rodents, and hares, as well as the insects that feed on these animals. Through the contact with infected animals, the disease can be transmitted to human beings and characterized by intermittent fever and swelling of the lymph nodes. It can develop severe and sometimes fatal illness. [103]

The causative agent of tularemia, *F tularensis*, is one of the most infectious pathogenic bacteria known. As few as 10 organisms inoculation or inhalation can cause the disease. Due to its extreme infectivity, ease of dissemination, and substantial capacity to cause illness and death, Civilian Biodefense considers *F tularensis* to be a dangerous potential biological weapon. According to an estimation from a World Health Organization expert committee in 1969, if an aerosol of 50 kg of virulent *F tularensis* is dispersed over a metropolitan area with 5 million inhabitants, the result would be 250 000 incapacitating casualties, including 19 000 deaths.

However, presumptive laboratory diagnoses of *F tularensis* are not easy. If routine laboratory procedures are used, isolation and identification of *F tularensis* could take several weeks. Therefore, identification of *F tularensis* in clinical specimens may be missed or delayed for days or weeks. In laboratories, antigen detection assays, enzyme-linked immunoasays, immunoblotting, pulsed-field gel electrophoresis, polymerase chain reaction, and other techniques may be used. Results from antigen detection and polymerase chain reaction analysis can be obtained within several hours after receipt of isolates.

Simple, rapid, and reliable diagnostic tests that could be used to identify persons infected with *F tularensis* in the mass exposure setting need to be developed. Our sensor for DNA detection is an ideal candidate due to its simple principle, ease of use, quick response and low cost.

6.4.2 Experiment

□ **Materials and process**

♢ Heat killed *F tularensis* bacteria (2109 cells/ml, 600nm)

- Blue: Strain TI0902
- Black: Strain LVS

♢ Double stranded probe DNA (2 μg/vial; EDTA buffer)

- schu4-330: 101 bp; complementary to Strain TI0902 (Blue), but noncomplementary to Strain LVS (Black).
- lpnA: 117bp; complementary to both Strain TI0902 (Blue) and Strain LVS (Black).

The materials are provided by the Department of Biomedical Science and Pathobiology in the College of Veterinary Medicine at Virginia Tech.

Pretreatment for bacteria $100°C$ boiled water: 5 min

Pretreatment for DNA

- $100°C$ boiling water: 5 min (separate double DNA into single-stranded DNA)
- Immediately $0°C$ ice with ethanol alcohol poured onto it (keep single-stranded DNA)
- Test during $0°C$ (keep single stranded DNA)

Procedure:

1. Grow 7.5 bilayer PAH/PSS onto the sensor
2. Dip the sensor into the ssDNA for 5 minutes. Rinse for 1 minute. Dry and test.
3. Dip the sensor into the vial of bacteria for 5 minutes. Rinse for 1 minute. Dry and test.

□ **Experiment results**

Figure 6.25 indicates that the polymer is linearly grown onto the sensor with (105.5840-105.5710)/7.5= 0.0017(μm) =1.7(nm) per bilayer.

Figure 6.26 shows the schu4-330 DNA101/ Strain LVS Bacteria test results. DNA growth of 3nm indicating successful DNA immobilization onto the sensor surface; -0.3 nm film thickness change indicating no bacteria is attached.

Figure 6.27 shows the result from schu4-330 DNA 101bp/strain TI0902 bacteria test: DNA growth of 1.6 nm indicating successful DNA immobilization onto the sensor tip; 7.8 nm film thickness growth indicating successful bacteria attachment.

Figure 6.28 shows the result from the lpnA DNA 117bp/strain LVS bacteria test: DNA growth of 1.2 nm indicating successful DNA immobilization onto the sensor tip; 0.8 nm film thickness growth indicating successful bacteria attachment.

Figure 6.29 shows the result from the lpnA DNA 117bp/strain TI0902 bacteria test: DNA growth of 2.2 nm indicating successful DNA immobilization onto the sensor tip; 8 nm film thickness growth indicating successful bacteria attachment.

These results agree with the complementary chain principle.

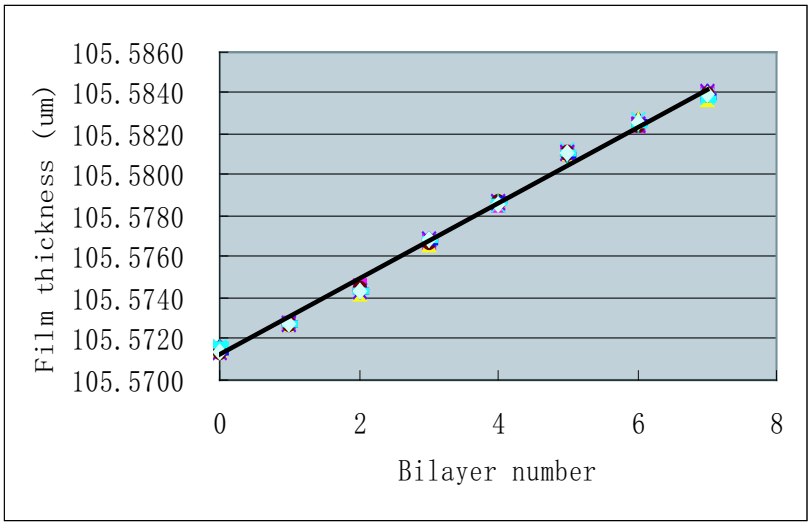

Figure 6.25: $[PAH/PSS]_{7.5}$ growth on the sensor.

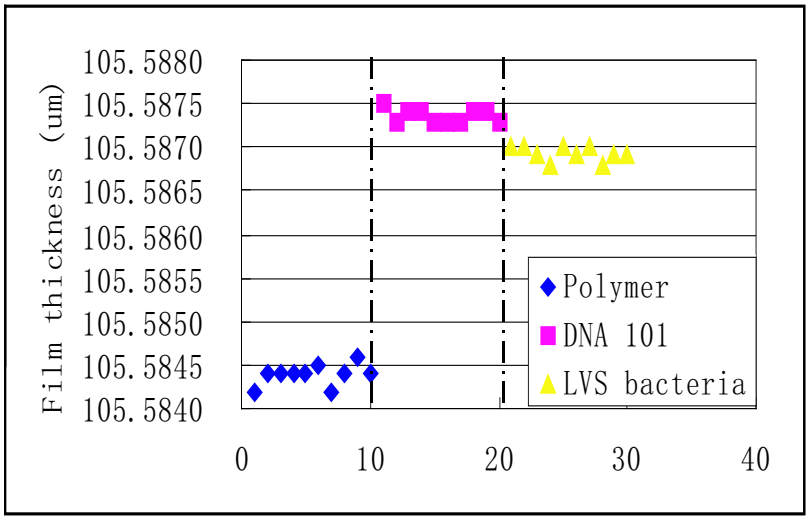

Figure 6.26: DNA101/LVS Bacteria test: DNA growth of 3nm indicating successful DNA immobilization onto the sensor surface; -0.3 nm film thickness change indicating no bacteria is attached.

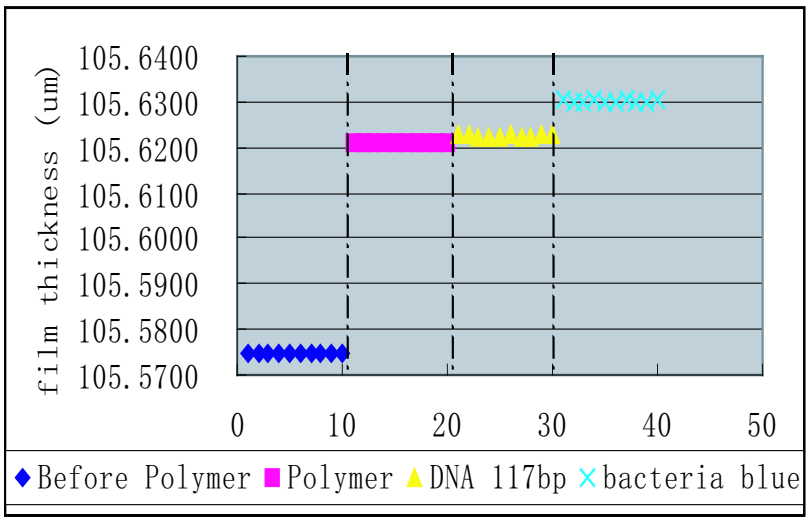

Figure 6.27: Sensor 51 DNA 101bp/strain TI0902 bacteria test: DNA growth of 1.6 nm indicating successful DNA immobilization onto the sensor tip; 7.8 nm film thickness growth indicating successful bacteria attachment.

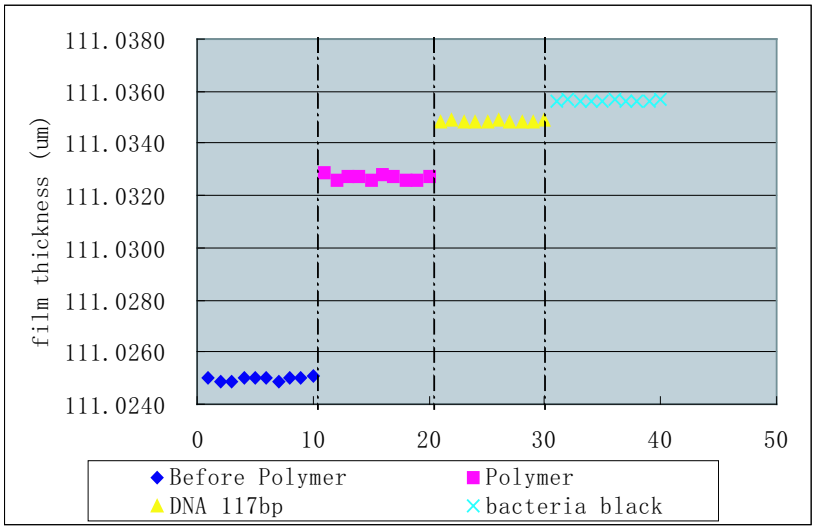

Figure 6.28: Sensor 6 DNA 117bp/strain LVS bacteria test: DNA growth of 1.2 nm indicating successful DNA immobilization onto the sensor tip; 0.8 nm film thickness growth indicating successful bacteria attachment.

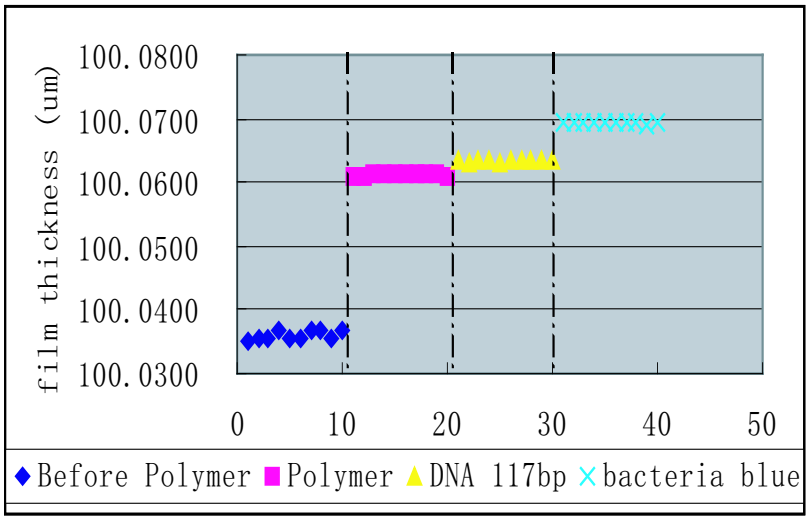

Figure 6.29: Sensor 9 DNA 117bp/strain TI0902 bacteria test: DNA growth of 2.2 nm indicating successful DNA immobilization onto the sensor tip; 8 nm film thickness growth indicating successful bacteria attachment.

6.5 Summary

In summary, we demonstrated a label-free DNA sequence detection method. Using the L-b-L ESA method, the capture DNA was immobilized onto the substrate surface. When complementary DNA samples were hybridized, the thickness of the film increased. Otherwise, the non-complementary DNA sample were not bonded onto the surface tightly and were easily washed away. Detection of the thickness change indicated the successful hybridization.

Experiments show that the method is simple, cost-efficient, sequence specific, and sensitive to nanogram quantities of the target DNA sequence. Moreover, the sensor can be used for detection of bacteria. With different FP cavity designs, this method can be extrapolated into a range of optical sensors for DNA detection featuring miniature size, cost efficiency, speed and ease of use. After optimization, the sensor probe size can be further minimized.

Chapter 7

Nanoprobe fabrication design

Current methods to fabricate nanoprobes, such as heating and pulling, and wet etching, have been described in Chapter 3. Their advantages and disadvantages are also described. Since our potential application is to insert the probe into a cell for direct detection, a strong and robust structure is desired. Accordingly, the probe fabricated by etching, which is shorter and stronger, with a larger tip angle is thus preferred. This chapter describes two novel nanoprobe designs that use etching to narrow the fiber tip into nanosize. The differences lie in the in-fiber Fabry-Perot (FP) structure. These two structures feature unique advantages such as temperature compensation capability or durability, which can fulfill different application requirements.

This chapter introduces two novel intrinsic fiber optic Fabry-Perot (FP) structures, both with a micrometric diameter tip. These structures have great potential for further minimization to nanometric size. With such a tiny protrusion, the sensor can be inserted into micron size cells for intracellular measurements. The possibility of monitoring in-vivo biological processes within single living cells could greatly improve our understanding of cellular function. With the FP cavity inside the fiber, the change in optical path difference (OPD) caused by the environment can be demodulated. This label-free detection method is very useful in biological areas, such as DNA hybridization detection. Compared with the currently available techniques that usually consist of fluorescent dyes, our method greatly reduces the cost and increases the reliability. It provides a

valuable tool for intracellular studies that have applications ranging from medicine to national security to energy production. In addition, the fabrication is simple including only cleaving, splicing, and etching. The signal is stable with high visibility. Last but not least, the structure shows great promise for nanometric protrusion. Once this goal is achieved, the sensor can be inserted into most cells with minimal invasiveness.

7.1 Wet etching

After the intrinsic FP cavity structure is constructed, the fiber sensor tip is on the order of 125 μm diameter. The fiber probe size is reduced to micron to nanometric size by chemical etching (e.g., in HF). For safety considerations, etching is performed in the chemical room with a fume hood as Figure 7.1.

Figure 7.1: Fume hood.

Etching can be described as pattern transfer by chemical/physical removal of a material from a substrate. Compared to dry etching, wet chemical etching provides a higher degree of selectivity. In addition, wet etching often is faster and cheaper. In our research, the wet etching method was chosen.

7.1.1 HF immersion etching

The etching process consists of immersing the complete sensor or the sensor head into $49\% HF$ etchant.

HF-based etchants are used mainly for silicon dioxide, because they were observed to etch polysilicon very slowly. The most significant effects on wet-etch rates are: temperature, impurities in or on the material being etched, and contamination. For fused silica, the etch rate in $49\% HF$ at room temperature is about 1 μm per minute. [104]

For pure HF etching, the overall reaction is

$$SiO_2 + 6HF \rightarrow H_2SiF_6 + 2H_2O. \tag{7.1}$$

HF is a weak acid; it does not completely dissociate into H^+ and F^- ions in water. The etch rate of silicon dioxide increases linearly with the concentrations of both HF and HF_2^- , while being independent of the concentration of F^- ions alone. The HF_2^- complex attacks oxide about 4.5 times faster than HF. Higher-order complexes, such as $H_2F_3^-$, appear to occur at higher HF concentrations (e.g. $49\% HF$) and attack oxide even faster than HF_2^- . Thus, the etch rate increases faster than linearly with HF concentration. [104]

Therefore, the total etch rate curves are not linear. After certain amount of time, the etch rate decreases a little. The reason is that HF molecules and HF_2^- ions are consumed with time and make the HF concentration smaller than it was at the beginning. [105]

In our experiment, the sensor is formed by different kinds of fiber (such as Micro-IFPI, described in 7.2), or fiber with different refractive index (such as Micro-FBGI, described in 7.3). In this case, instead of simply rod etching, fiber etching is needed.

Optical fibers are drawn from fused silica and chemically doped to slightly change the refractive index of either the core or cladding. For 49% HF, the higher the germanium doping, the higher the etching rate. For example, the etching rate of fused silica is about 1 μm per minute. 62.5/125 optical fiber is doped with germanium to increase the refractive index of the core. The etching rate

of the core is about 24 μm per minute, while the cladding (fused silica) etching rate remains 1 μm per minute. The doped core is recessed by etching with an etchant that eats the core faster than the etch-resistant cladding. The depth of the recess can be controlled by the etching time. [106]

7.1.2 HF vapor etching

In order to control the etching results more accurately and precisely, HF vapor was utilized in the second step, similar to "finish machining". In the first step ("coarse machining"), different kinds of etching methods, such as tube-etching, selective etching, etc., can be utilized. In this first step, the etching rate is much faster, and the surface is not easily controlled. In the second step, HF vapor etching, the etching rate is much slower and the vapor can be more evenly evaporated onto the surface. This leads to finer control of the final size and shape of the structure.

7.2 Fiber Bragg grating interferometer with a micrometric tip (Micro-FBGI)

In this structure, a Fabry-Perot cavity is formed by a Bragg grating and the cleaved fiber endface. The whole structure is then immersed into etchant such as HF (hydrofluoric acid) to obtain the taper. Figure 7.2 shows photographs of such a structure. Figure 7.3 shows the spectrum.

The final structure can be different shapes, as illustrated in Figure 7.4. For example, the grating can be far away from the taper, shown in (a) and (c). On the other hand, the grating can be tapered, as (b) and (d). Because most light is still confined inside the core, the signal does not deteriorate much. In addition, the taper can be very long and sharp, which may be beneficial when piercing the cell. Or, it can be short with large cone angle to increase the robustness of the structure.

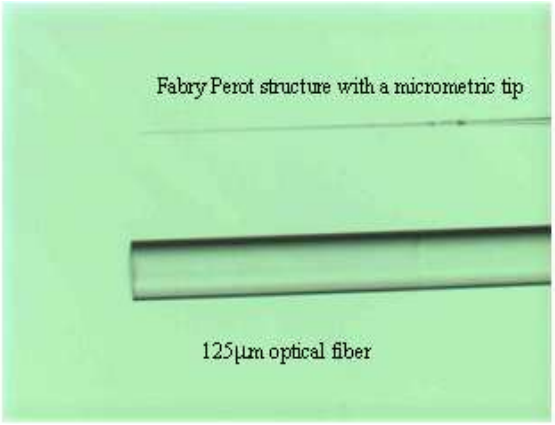

Figure 7.2: Comparison of the Micro-FBGI structure (micrometric tip, upper) with a standard SMF (125 μ m diamater, lower). (Zeiss, Axiovert 25).

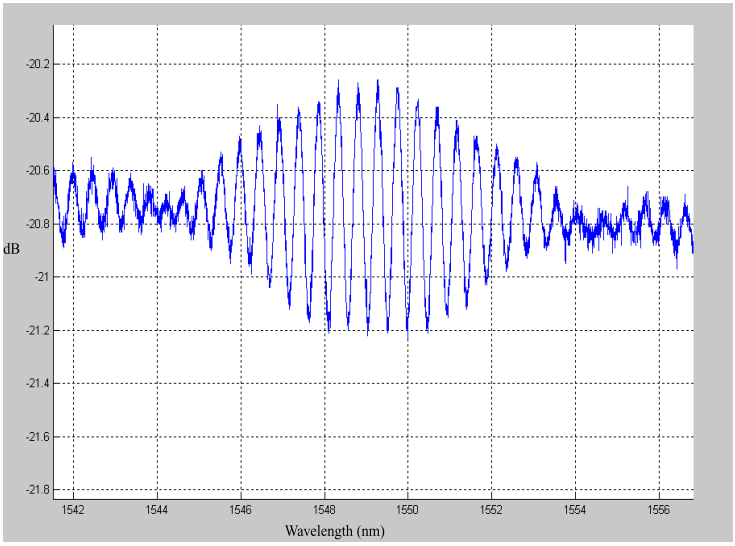

Figure 7.3: Spectrum of Micro-FBGI structure before etching.

7.2.1 Novel features of Micro-FBGI

This micrometric fiber Bragg grating interferometer features:

1. Miniature size: the tip is in micrometric size, and has potential to be decreased to nanometric size.

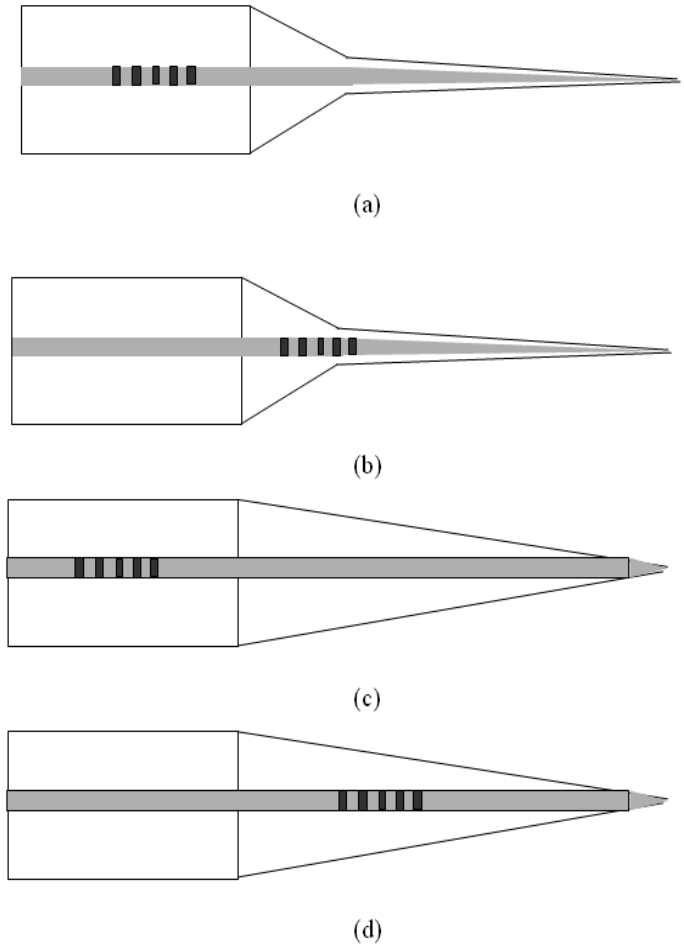

Figure 7.4: Diagram of the novel structure with a tip. (a) Grating is not tapered and the taper is sharp: (b) grating is tapered, and the taper is sharp; (c) grating is not tapered and the taper is not sharp; (d) grating is tapered and the taper is not sharp.

2. Good signal: The cavity and the reflection surfaces are all inside the fiber core. Even when the fiber is etched to nanometer size, the fringes will not deteriorate much. The signal strength and the visibility do not change because of the size. Calculations show that it is easy to trace the fringe and obtain the nanometer change of cavity length.

3. Intrinsic temperature compensation capability: Although the FP cavity length can change when the physical length (e.g. DNA hybridization) or the temperature varies, the envelope

from the FBG is only sensitive to environment temperature. Therefore, the temperature effect can be easily compensated.

4. Compact structure: There is no abrupt step in the structure, which makes it more robust and compact. Also, this leaves less room for contamination. Taking DNA hybridization as an example, most sample (e.g. DNA) will be attached onto the fiber end, with no aggregation on the shoulder of the abrupt step.

5. Simple and efficient fabrication: The process mainly includes FBG lasing, cleaving and etching steps.

6. Biological compatibility: The whole structure is made of fused silica with no impurity, which makes it ideal for medical and biological applications.

7. High temperature capability: The structure can work at more than $600°C$.

8. Low cost: Standard commercially available SMF is the only required material. After hydrogen loading, FBG can easily be formed. There is no need for special fibers.

9. Robust structure: To test its robusticity, the tip of the novel structure was forced on the surface of 125 μm diameter standard SMF many times. It bent with a large curvature but did not break.

10. EMI immunity and electric passivity: Such optical structure is immune to electromagnetic interference.

7.3 Intrinsic Fabry-Perot interferometer with a micrometric tip (Micro-IFPI)

The intrinsic Fabry-Perot interferometer with a micrometric tip (Micro-IFPI) uses two different mode field diameter (MFD) fibers to produce a reflective mirror [107]. An intrinsic Fabry-Perot

interferometer (IFPI) is formed by the reflection from this mirror and the cleaved fiber endface. The whole structure is then immersed into etchant such as hydrofluoric acid (HF), to obtain a micrometric and even nanometric taper.

The mirror is formed utilizing only the splicing technique that fuses two fibers with different MFD. The combinations can be limitless, for example, single mode fiber with multi-mode fiber; single mode fiber with different core sizes; multi-mode fiber with different core sizes; standard fiber with customized fiber; etc..

Figure 7.5 shows the schematic of the FP structure. Figure 7.6 and Figures 7.7(a)-7.7(b) show a photograph of the novel FP structure with a micrometric tip.

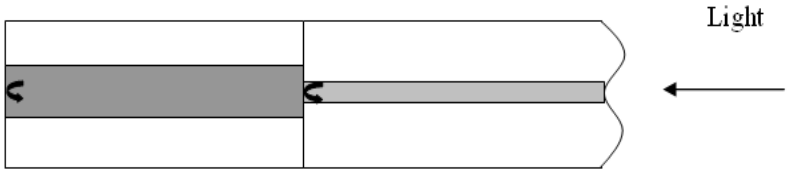

Figure 7.5: Structure of Micro-IFPI structure, fabricated by splicing two fibers with different MFD.

7.3.1 Novel features of Micro-IFPI

This novel intrinsic Fabry-Perot structure has the following advantages:

1. Miniature size: The tip is in micrometric size. Theoretically it can be decreased to nanometric size.

2. Easy signal processing: Conventional analysis for single cavity FP sensor is much easier and faster than demodulation of multi-cavity fringes..

3. Good signal: The fringes are stable with high visibility. The cavity and the reflection surfaces are all inside the fiber core. Even when the fiber is etched to nanometer size, the fringes will not deteriorate much. The signal strength and the visibility do not change because of the

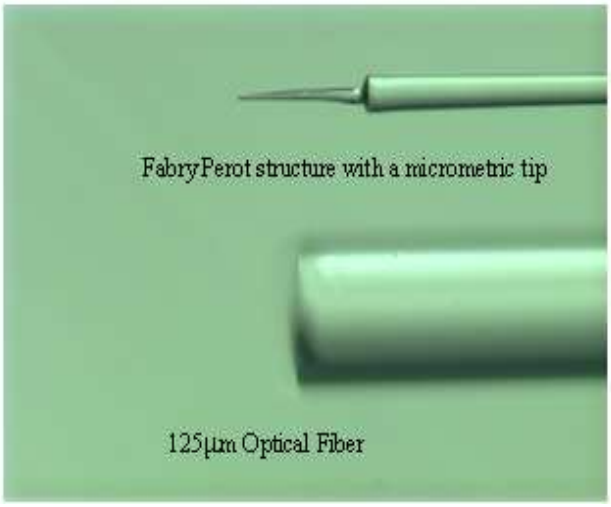

Figure 7.6: Comparison of the Micro-IFPI structure with a standard SMF. The Micro-IFPI structure with a micrometric tip (upper) has a cavity length of 120 μ m; standard SMF has a diameter of 125 μ m (lower). (Zeiss, Axiovert 25)

size. Calculations show that it is easy to trace the fringe and obtain the nanometer change of cavity length.

4. Compact structure: If the junction is not etched, there will not be an abrupt step in the structure, which makes it more robust and compact. Also, this leaves less room for contamination. Taking DNA hybridization as an example, most sample (e.g. DNA) will be attached onto the fiber end with no aggregation on the abrupt shoulder.

5. Simple and efficient fabrication: The process mainly includes cleaving, splicing, and etching steps.

6. Biological compatibility: The whole structure is made of fused silica, which makes it ideal for medical and biological applications.

7. High temperature capability: The structure can work at more than $600°C$.

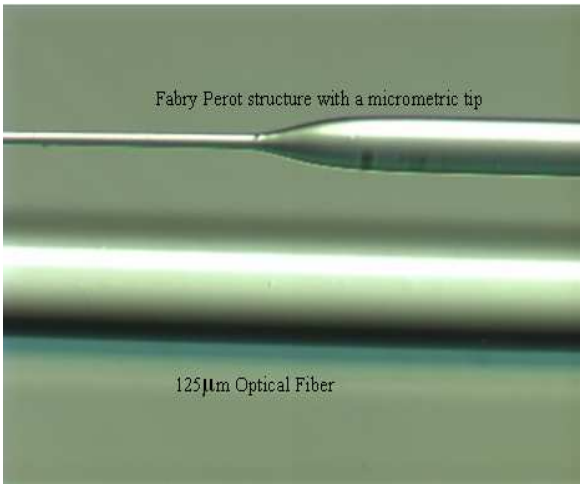

(a) Comparison of the Micro-IFPI structure (junction part) with a standard SMF. The Micro-IFPI structure with a micrometric tip (upper) has a cavity length of 7mm. (Zeiss, Axiovert 25).

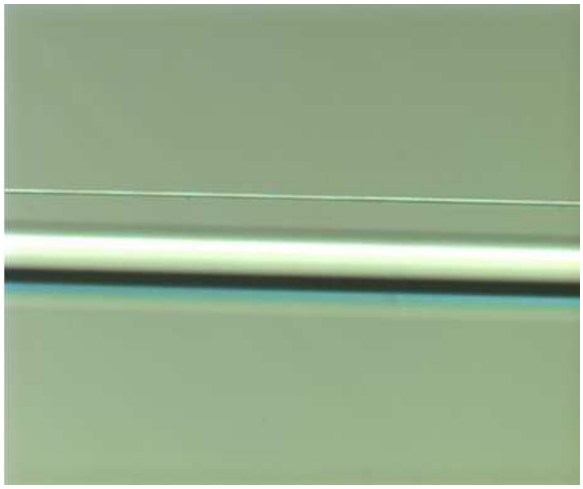

(b) Comparison of the Micro-IFPI structure (middle part) with a standard SMF. The Micro-IFPI structure with a micrometric tip (upper) has a cavity length of 7mm. (Zeiss, Axiovert 25).

Figure 7.7: Overview of the Micro-IFPI structure (Zeiss, Axiovert 25)

8. Low cost: Standard commercially available fibers are sufficient.

9. Robust structure: To test its robustness, the tip of the novel structure was forced on the surface of 125 μm diameter standard SMF many times. It bent with a large curvature but did not break.

10. EMI immunity and electric passivity: Such an optical structure is immune to the electromagnetic interference.

7.3.2 Spectrum of the Micro-IFPI

The spectrum of the novel structure is shown in Figure 7.8. The spectrum shows a strong fringe pattern with high visibility. The cavity length is about 120 μm, which agrees with the measured result from the microscope.

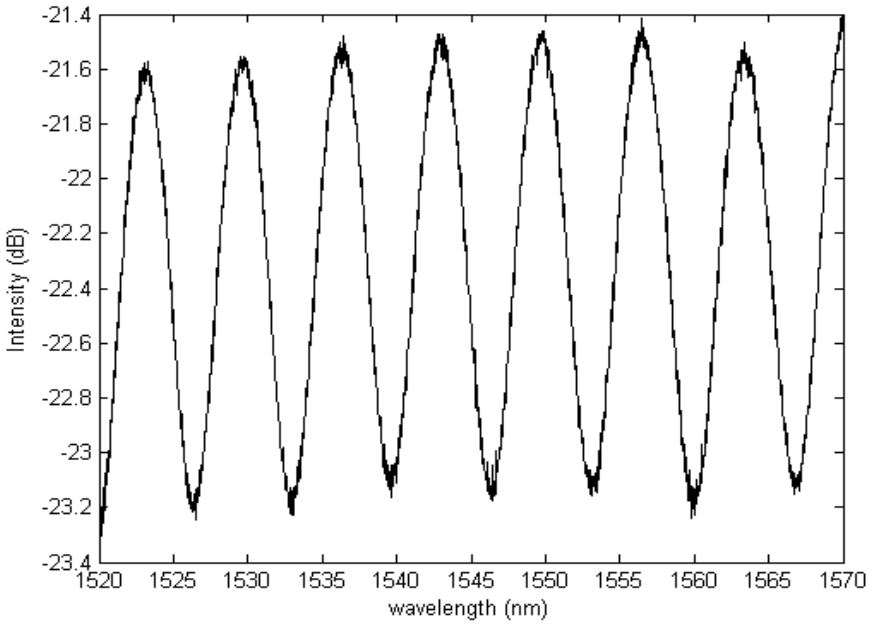

Figure 7.8: Spectrum of the novel FP structure with a micrometric protrusion.

7.3.3 Micro-IFPI sensor tip with 1.7 μm diameter

For our DNA detection application, temperature variation is not big and can be controlled in the lab environment. Therefore, the micro-IFPI sensor is better for its easy signal processing.

□ **Sensor structure**

We fabricated a micro-IFPI sensor in the chemical room under $22.1°C$. After suspending the sensor in HF vapor for 46 minutes, the sensor configuration was as shown in Figure 7.9. After additional 23 minutes, the sensor was as shown in Figure 7.10. Figures 7.11(a)-7.11(b) show the photo of a Micro-IFPI sensor with a 1.7 μm tip compared with a commercial 30 μm fiber.

□ **Summary**

With coarse HF immersion etching, then delicate HF vapor etching, the sensor tip has great potential to be etched down to sub-micron size. Also, this two step etching method taking the

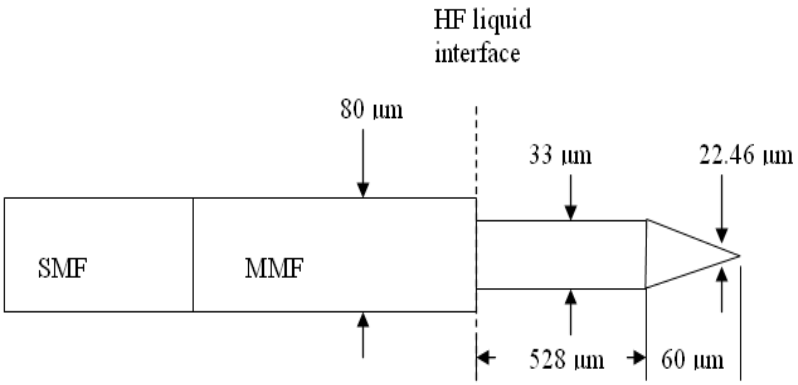

Figure 7.9: Sensor 1 configuration after 46 min HF vapor etching.

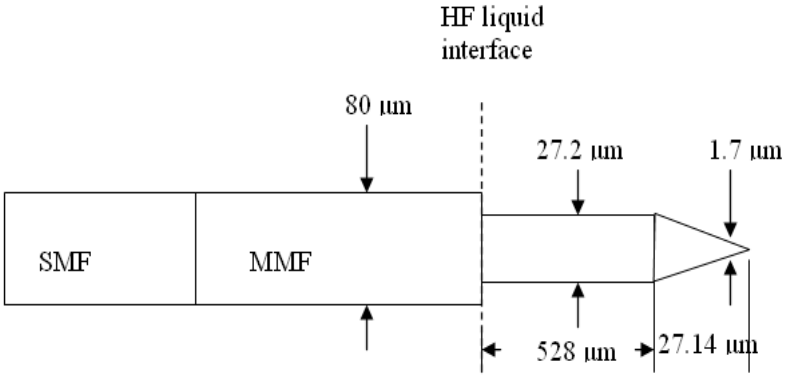

Figure 7.10: Configuration of sensor 1 after an additional 23 min HF vapor etching.

advantage of HF vapor is a new method, which has not been found in the current literature.

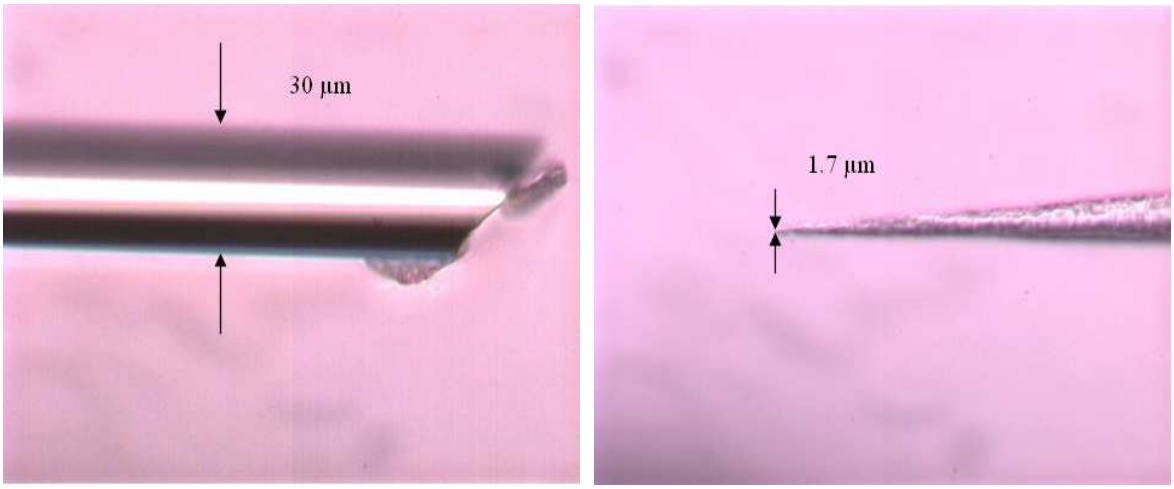

(a) Commercially available 30 μm fiber provided by Miconoptics.

(b) 1.7 μm sensor tip (investigated from 500X microscope).

Figure 7.11: Photos of micron size sensor tip compared with a commercial 30 μm fiber.

7.4 Conclusion

Two novel nanoprobe designs with in-fiber Fabry-Perot (FP) structure are introduced. Featuring unique advantages such as temperature compensation capability or durability, these two structures can fulfill different application requirements.

Sensors with micrometric diameter tip were developed and tested. The sensors hold the potential of further minimization to nanometric size. With such tiny protrusions, the sensor can be inserted into micron size cells for intracellular measurements. The possibility of monitoring in-vivo biological processes within single living cells is of great importance in molecule biology, medicine, national security, and energy production. Experimental results demonstrate that with the FP cavity inside the fiber, the change in OPD caused by the environment can be demodulated. The sensors can serve as refractive index sensors. In addition, fabrication process is simple including only cleaving, splicing, and etching. The signal is stable with high visibility. last but not least, when parameters are finely adjusted, the structures have great potential to be developed into nanometric tips. Once this goal is achieved, the sensor can be inserted into most cells with minimal invasiveness.

Chapter 8

Label-free DNA Sequence Detection Using Oligonucleotide Functionalized Micrometric Tip

In Chapter 6, successful DNA immobilization and hybridization onto the 125 μm diameter fiber sensor end was demonstrated. Chapter 7 presents two novel intrinsic fiber optic Fabry-Perot (FP) structures, both with a micrometric diameter tip. With the FP cavity inside the fiber, the change in optical path difference (OPD) caused by the environment can be demodulated. This label-free detection method is very useful in biological areas. In this chapter, an intrinsic Fabry-Perot interferometer with a micrometric tip (Micro-IFPI) was used to demonstrate DNA hybridization detection. With L-b-L ESA, the capture DNA was immobilized onto the micrometric sensor tip after the precursor polymer films. Hybridization of target DNA with complementary capture DNA increased the optical thickness of the fiber tip, which was detected by the demodulation of the spectrum shift. This demonstrates great potential for future nanometric scale fiber probes for in-cell DNA detection.

8.1 Preparation test and procedure

The fabrication procedures for the Micro-IFPI DNA hybridization sensor, including fiber selection, etching, rinsing, and polymer growth processes, were investigated, and a standard procedure developed.

8.1.1 Sensor structure

As presented in Chapter 7, the intrinsic Fabry-Perot interferometer with a micrometric tip (Micro-IFPI) has a FP cavity formed by the reflection from a reflective mirror and the cleaved fiber endface. The reflective mirror is a splicing point of two different mode field diameter (MFD) fibers. In order to obtain a micrometric and even nanometric taper, the whole structure is then immersed into hydrofluoric acid (HF).

A single mode (SM) fiber (Corning Inc.) and a 105/125 μm step index multimode fiber (Fiberguide Industries, Inc.) were chosen. For the 105/125 optical fiber which has a fluorine-doped cladding with a smaller refractive index than that of the core, the etching rate of the core is smaller than that of the cladding. After about 10 minutes' etching, the cladding of 105/125 is removed, and only the core area is left. Compared with the 62.5/125 graded-index fiber, which has a bowl-shape recess after etching, the 105/125 fiber is much more flat and even because of its step-index configuration. After etching, the whole sensor is made of the same material, fused silica.

8.1.2 Hydrofluoric acid testing

As presented in Chapters 7 and 8.1.1, the sensor must be etched by HF. Therefore, the sensor endface where the probe DNA is immobilized will be treated by HF solution. This surface treatment may cause uneven growth of films. To eliminate this problem, a thorough rinsing procedure was developed to clear the fiber surface after HF etching. Rinsing procedures were compared in the following three tests, which produced sensors of essentially identical size and shape:

Unetched sensor: 125 μ m diameter sensor that was not exposed to HF.

Minimally etched sensor (Rinse Procedure 1): 125 μ m diameter sensor; exposed to HF, but immersed for a very short time (0.1 second); rinsed with running water for 1 minute.

Minimally etched sensor (Rinse Procedure 2): 125 μ diameter sensor; exposed to HF, but immersed for a very short time (0.1 second); rinsed for 7 total minutes as follows.

- Shake drops into the HF beaker;
- Running water, with carrier, 1min;
- Stir with carrier in a beaker, 1min;
- Without carrier, only fiber, running water, 5min.

Films of the structure [PAH/PSS]$_{7.5}$ were grown onto each sensor and the film thickness growth trend was monitored.

□ **Unetched sensor**

There was negligible difference in size or shape of the three sensors tested. Figure 8.1 indicates that [PAH/PSS]$_{7.5}$ is evenly grown onto the sensor tip. The x-axis indicates the number of polymer bilayers. In the top plot, the y-axis indicates the OPD. A linear trend with a slope of 9.3 is observed. The average film thickness per bilayer is about $\frac{9.3}{2 \times 1.45} = 3.2(nm)$. In the lower plot, the y-axis shows the residuals from the fitting line. We can see that the linearity is very good.

□ **Minimally etched sensor (Rinse Procedure 1)**

Figure 8.2 indicates that [PAH/PSS]$_{7.5}$ is unevenly grown onto the sensor tip. The x-axis indicates the number of polymer bilayers. In the top plot, the y-axis indicates the OPD. The average film thickness per bilayer is thicker than the unetched sensor, about $\frac{24}{2 \times 1.45} = 8.3(nm)$. In the lower plot, the y-axis shows the residuals from the fitting line. We can see that the linearity is not very good. The residual is much bigger than that of the unetched sensor. The sensor surface after HF

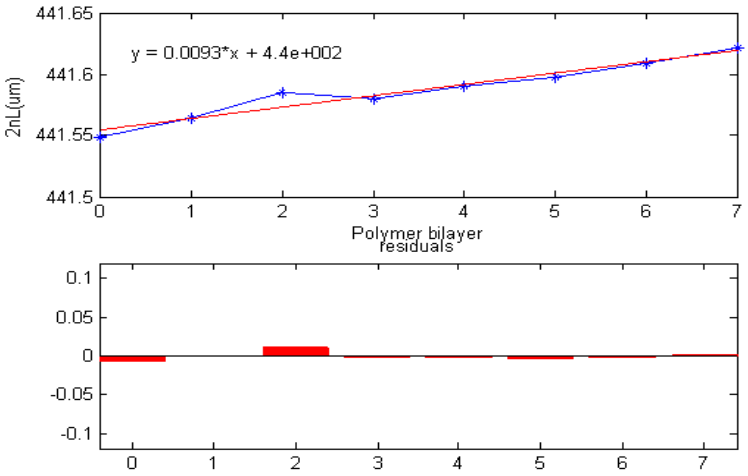

Figure 8.1: Changes in the optical path difference (OPD) as $[PAH/PSS]_{7.5}$ is grown onto the unetched sensor. The average film thickness per bilayer is about $slope/(2n) = (9.3nm/2/1.45) = 3.2(nm)$.

etching the simplified rinse proceure is insufficient quality for polymer film growth, and thus not suitable for the following DNA immobilization.

□ **Minimally etched sensor (Rinse Procedure 2)**

Figure 8.3 indicates that $[PAH/PSS]_{7.5}$ is evenly grown onto the sensor tip. The x-axis indicates the number of polymer bilayers.

The average film thickness per bilayer in the first 2 bilayers is about $\frac{10.5}{2 \times 1.45} = 3.6(nm)$.

The average film thickness per bilayer in the following 4 bilayers is about $\frac{8.5}{2 \times 1.45} = 2.9(nm)$.

Early testing indicated some difficulties in the deposition of L-b-L ESA films on etched fibers. Suspicions that residual HF on the sensor surface was the cause were confirmed in these tests. It is evident that the unetched and thoroughly rinsed sensors have a more linear trend, indicating successful film growth. In addition, the bilayer thickness is reasonable. Therefore, the 7 minute rinse procedure was adopted.

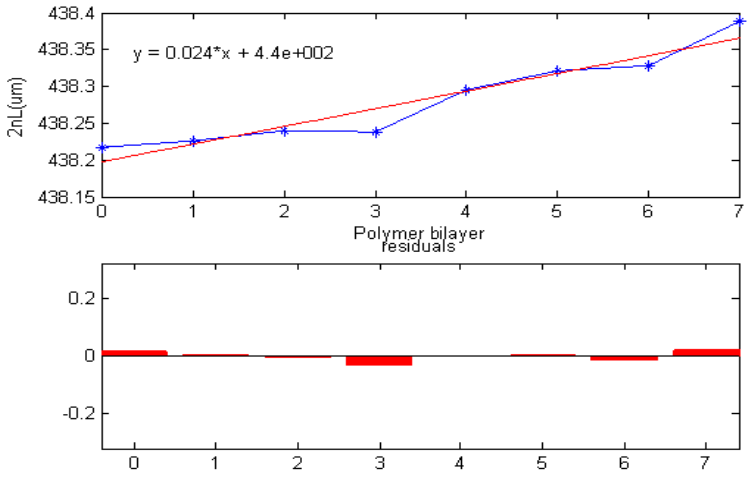

Figure 8.2: Changes in the optical path difference (OPD) as $[PAH/PSS]_{7.5}$ was grown onto the minimally etched sensor, Rinse Proc. 1 (less rigorous rinsing).

8.1.3 Polymer materials

Similar to Chapter 6, polyallylamine hydrochloride (PAH) and polysodium 4-styrenesulfonate (PSS)(2.0 mg/ml, pH 5.0) were used as a multilayer polyelectrolyte precursor film. Nucleic acid sequences used in this study, as indicated in Table 8.1 were purchased from Genosys, and were used without further purification.

Table 8.1: Oligonucleotide sequences used in immobilization and hybridization experiments.

Name	Purpose	Sequence (5’ - 3’)	pH	Con.(nmol/ml)	Salt(M)
ssDNA-A	Probe	TCCAGACATGATAAGATACATTGATG	5.5	13.14	0.02
ssDNA-B	Target sequence	CATCAATGTATCTTATCATGTCTGGA	5.5	10.50	0.02
ssDNA-C	Negative control	CATCAATGTATCTTATCATGTCTGGA	5.5	89.8	0.02

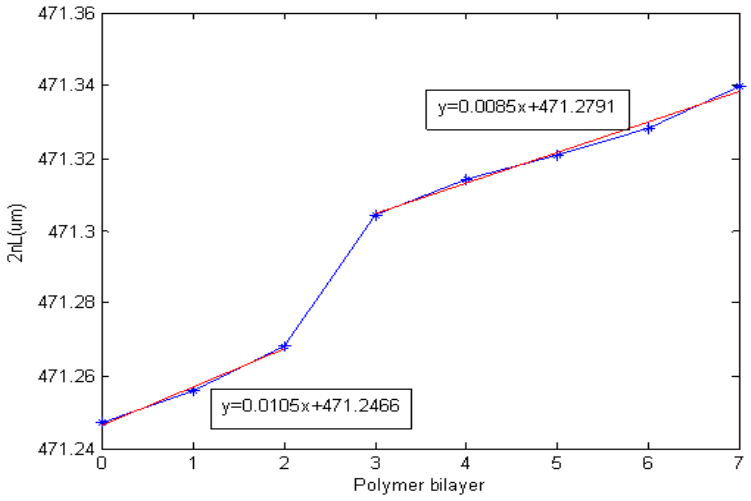

Figure 8.3: Change in optical path difference (OPD) as $[PAH/PSS]_{7.5}$ was grown onto the minimally etched sensor (Rinse Procedure 2). The average film thickness per bilayer in the first 2 bilayers is about 3.6nm. The average film thickness per bilayer in the following 4 bilayers is about 2.9nm.

8.1.4 Rinsing procedure

Two types of rinsing methods were investigated for L-b-L ESA film growth:

- Manually rinsing;
- Ultrasonic rinsing.

Ultrasonic rinsing can result in better repeatability. However, the mechanical strength of the resulting sensor is our first concern. Ultrasonic rinsing was tested 10 μm diameter SMF and 25 μm diameter Micro-IFPI sensors for 1 minute durations, and the structure investigated under a microscope. No visible damage occurred; the sensors are quite robust. However, we have found that for thinner tips, ultrasonic rinsing may cause detachment of the films, especially when the bilayer number is greater than 2. Therefore, in the remaining experiments, we used manual rinsing.

8.1.5 Procedures

Based on the results of the experiments described above, we developed the following standard procedure for the fabrication of micrometric tip DNA hybridization sensors.

1. Sensor fabrication
    - Step 1: Fabricate the sensor with SMF and 105/125 MMF.
    - Step 2: Etch the sensor with HF in the fume hood.
    - Step 3: Rinse the sensor thoroughly using the 7 minute procedure (Rinse Proc. 2).
    - Step 4: Photography the sensor. Record the sensor spectrum and the OPD (at least 300 data points).
2. Polymer growth
    - Step 1: Immerse the fiber sensor into PAH solution for 5 minutes.
    - Step 2: Rinse the fiber sensor manually with ultrapure water (Barnstead Diamond RO/Nanopure Diamond UV/UF) (DI water) for 1 minute. Dry in air.
    - Step 3: Record the sensor spectrum and the OPD (at least 300 data points).
    - Step 4: Immerse the sensor into PSS for 5 minutes.
    - Step 5: Rinse the sensor with DI water for 1 minute. Dry in air.
    - Step 6: Record the sensor spectrum and the OPD (at least 300 data points).
    - Step 7: Repeat step 5 $\sim$step 10 for 7.5 bilayers. The outermost layer is positively charged PAH.
    - Step 8: Plot the spectra shift of the sensor.
    - Step 9: Plot the OPD change after polymer growth.
3. DNA immobilization

- Step 1: Immerse the sensor into ssDNA-A for 5 minutes.
- Step 2: Rinse the sensor with DI water for 1 minute. Dry in air.
- Step 3: Record the sensor spectrum and the OPD (at least 300 data points).
- Step 4: Plot the OPD change.

Similar procedures were developed to evaluate the sensor for specific detection of DNA hybridization. ssDNA-B was used as the target sequence and ssDNA-C as the negative control.

4. DNA hybridization

   - Step 1: Immerse the sensor into sample solution (ssDNA-B or ssDNA-C) for 5 minutes.
   - Step 2: Rinse the sensor with DI water for 1 minute. Dry in air.
   - Step 3: Record the sensor spectrum and the OPD (at least 300 data points).
   - Step 4: Plot the OPD change.

All experiments were carried out at $23°C$. The experiment setup is shown in Figure 8.4. Since the sensor is so tiny that a little bit of environment disturbance, such as a person walking, may cause the signal instability, the film growth setup is stabilized onto an optical table (Newton, Inc.) by two magnets. No electrical equipment sits on the same table to minimize the vibration. The sensor is clamped by a fiber clamper, which is screwed onto a holder. The immersion depth is consistent for all the steps by controlling the holder. The immersion time is controlled by a timer. The light is launched through a coupler and the reflected signal is coupled back to the CTS. The data is finally transferred to a laptop by an Ethernet cable for data processing.

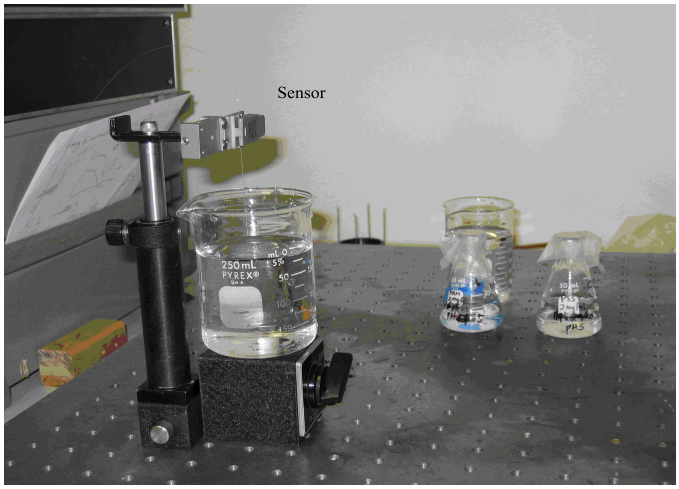

Figure 8.4: Experiment setup for film growth.

8.2 Hybridization detection with a 125 μm diameter sensor tip

To evaluate the effectiveness of the IFPI structure, the procedures developed above, but eliminating the etching step, were used to fabricate and test a 125 μ m Micro-IFPI Sensor.

8.2.1 Polymer growth

Figure 8.5 shows the change in sensor OPD as $[PAH/PSS]_{10.5}$ was grown onto the sensor tip. The x-axis indicates the number of polymer bilayers. The average film thickness per bilayer in the first 2 bilayers is about $\frac{10.5}{2 \times 1.45} = 3.6(nm)$, in the following five bilayers ($3 \sim 7$) about $\frac{8.5}{2 \times 1.45} = 2.9(nm)$, and the final three bilayers ($8 \sim 10$) about $\frac{8.7}{2 \times 1.45} = 3.0(nm)$.

The inconsistency occurred between the 7th and 8th bilayers was caused by a pause in the experiment. After the first 7.5 bialyers were grown, the sensor was dried in air overnight. The following 8th $\sim$ 10.5th bilayers were grown on the second day. However, after self-healing, the linearity was good which indicates that the polymer films were evenly grown onto the sensor and can serve as a precursor for the following DNA immobilization and hybridization.

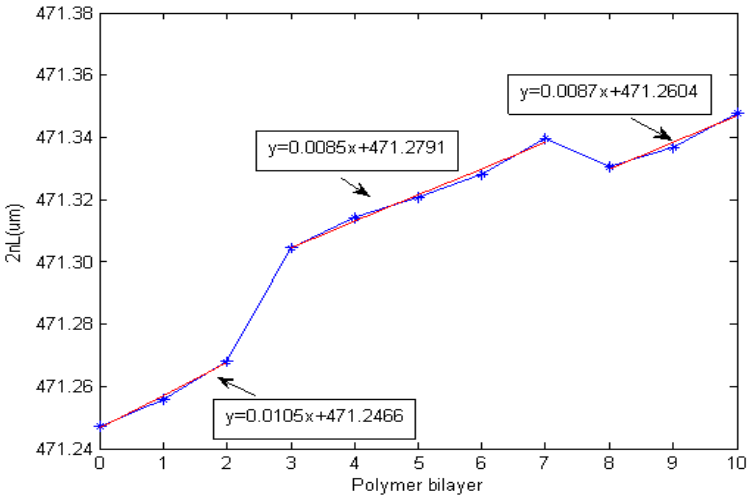

Figure 8.5: $[PAH/PSS]_{7.5}$ is grown onto sensor 15. The average film thickness per bilayer in bilayers $0 \sim 2$ is about 3.6 nm. The average film thickness per bilayer in bilayers $3 \sim 7$ is about 2.9 nm. The average film thickness per bilayer in bilayers $8 \sim 10$ is about 3.0 nm .

8.2.2 DNA immobilization (DNA immobilization thickness: 4.5nm)

Figure 8.6 shows that ssDNA-A was successfully immobilized onto the sensor tip. DNA growth on the fiber tip is $\frac{471.3629 - 471.3499}{2 \times 1.5} = 4.5(nm)$. This is larger than the unperturbed radius of gyration of the ssDNA chain of about 2 nm, and smaller than the end-to-end distance of about 5 nm, if a Gaussian coil of a Kuhn step length model is used for the unstretched conformation of the immobilized ssDNA. This may be caused by the salt concentration. At low NaCl concentrations, the negative charges on the DNA chain tend to repel each other, stretching the DNA strands. When the concentration of NaCl increases, the Na+ alleviate the repulsion, and the DNA strands may coil up. A further increase in NaCl may shield some of the phosphate groups on the DNA strands and make the DNA extend from the surface to form a brushlike structure. Slight differences in thickness may be caused by different ionic strengths of the DNA solution.

8.2.3 DNA hybridization

Figure 8.6 also indicates that complementary ssDNA-B was successfully hybridized onto the sensor tip. The thickness of the DNA hybridized on the fiber tip was: $\frac{471.3714 - 471.3629}{2 \times 1.45} = 2.9(nm)$.

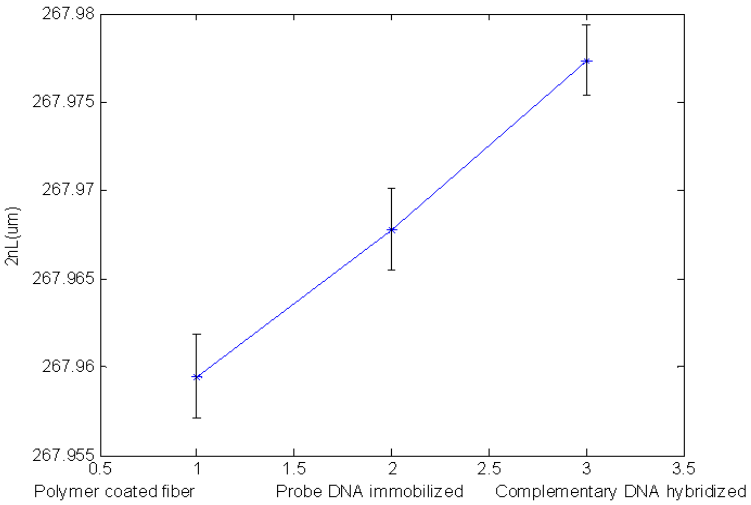

Figure 8.6: Complementary ssDNA-B was successfully hybridized onto the fiber tip.

8.3 Hybridization detection with a 25 μm diameter sensor tip

The feasibility of reducing the sensor tip size was demonstrated by using the procedures developed above to fabricate and test a $25\mu m$ Micro-IFPI Sensor.

8.3.1 Polymer growth

□ Linearity of polymer growth

Figure 8.7 shows the change in OPD of the sensor as $[PAH/PSS]_{5.5}$ was grown onto the sensor tip.

The x-axis indicates the number of polymer bilayers . In the top plot, the y-axis indicates the OPD. A linear trend with a slope of 13 nm/bilayer was observed. The average film thickness per bilayer is about $\frac{13}{2 \times 1.45} = 4.5(nm)$. In the lower plot, y-axis shows the residuals from the fitting line. We can see that the linearity is very good.

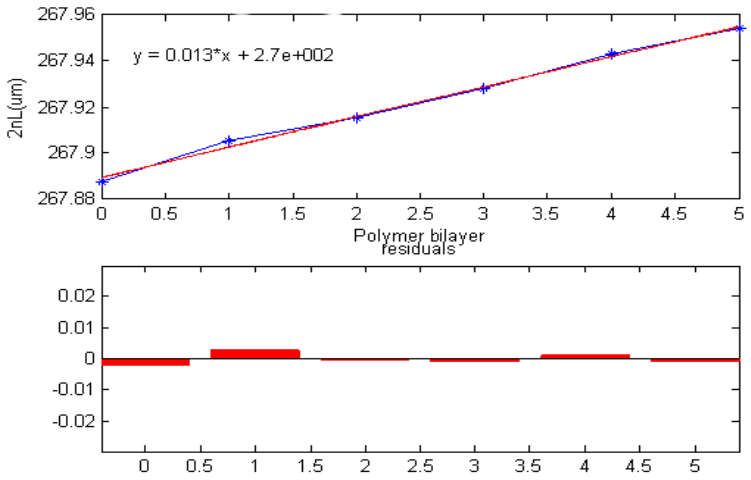

Figure 8.7: Change in sensor OPD as $[PAH/PSS]_{7.5}$ was grown onto the sensor ($25\mu m$ diameter). The average film thickness per bilayer is about 4.5 nm.

8.3.2 DNA immobilization (DNA immobilization thickness: 2.9nm)

Figure 8.8 shows that ssDNA-A was successfully immobilized onto the sensor tip.

DNA growth on the fiber tip was: $\frac{8.4}{2 \times 1.45} = 2.9(nm)$.

8.3.3 DNA hybridization

Figure 8.8 also indicates that complementary ssDNA-B was successfully hybridized onto the $25\mu m$ diameter sensor tip. The thickness of DNA hybridized on the fiber tip was: $\frac{9.6}{2 \times 1.45} = 3.3(nm)$.

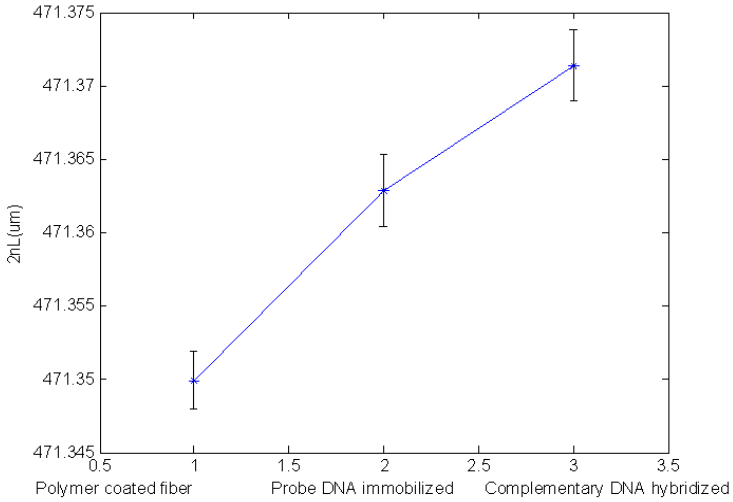

Figure 8.8: Complementary ssDNA-B was successfully hybridized onto the fiber tip.

8.4 Summary

In summary, label-free DNA sequence detection with a micrometric tip sensor was demonstrated. Using the L-b-L ESA method, single-stranded capture DNA was immobilized onto the sensor tip. When the target DNA sequence was present in the DNA sample tested, it was hybridized. The consequent increased optical thickness of the film was able to be detected; detection of this thickness change indicates successful hybridization.

Experiments show that the method is simple and cost-efficient. Moreover, a range of optical sensors with different FP cavity designs can be extrapolated. After optimization, the sensor probe size can be further minimized.

Chapter 9

Conclusions

9.1 Conclusions

The detection of DNA sequences plays an important role in molecular biology, genetics, pathology, criminology, pharmacogenetics, cancer diagnostics, food safety, environment monitoring, and many other fields. In this work, a label-free direct DNA sequence detection scheme was developed. Three kinds of novel fiber probe sensors with specific advantages have been demonstrated. Compared with the current available methods, which are usually cumbersome, time-consuming, and expensive, this approach features sequence specificity, cost efficiency, speed, and ease of use.

The principle is simple. With capture DNA immobilized onto the probe by layer-by-layer electrostatic self-assembly (L-b-L ESA), it is immersed in the sample. If the sequence of the sample is complementary to that of the capture DNA, hybridization occurs and the thickness of the probe increases. Otherwise, if the sample is not complementary, the remaining samples on the probe can be easily rinsed away. The difference among the three structures lies in the design of the Fabry-Prot (FP) interferometer formed inside the sensor for thin film thickness measurement. Demodulation of the output spectrum provides the detection results.

L-b-L ESA provides an effective and convenient method for DNA immobilization and hybridiza-

tion onto fiber optic biosensors. The long-term stability and low-absorption in NIR range of the polymers makes them suitable as a precursor film for optical biosensors where a 1310 nm or 1550 nm optical source is usually utilized. The effect of the characteristics of polymer and DNA solutions on the hybridization quality of silicon wafer samples was investigated by ellipsometry. The Taguchi method was applied to determine the relative effects of the factors. The optimum conditions for polymer self-assembly were obtained by systematic study of the multiple factors.

A multi-cavity Fabry-Perot fiber sensor with 125 μm diameter was used. The sensor has a short length of hollow tube sandwiched between two pieces of optical fiber, forming an air cavity between the lead-in and reflection fibers. By cleaving the reflection fiber, a fiber cavity can be formed in addition to the air-cavity. Multiple reflection signals from the interfaces of the air and fiber cavities form the interference fringe pattern. Demodulation of this spectrum can give out an accurate cavity length with high resolution. Therefore, the thickness of the fiber gap, which is our focus, can be obtained. After deposition of several bilayers of polymer films, capture DNA is immobilized onto the sensor tip. Hybridization of complementary target DNA onto the sensor tip increases the fiber gap, which can be obtained by the signal demodulation. Experiments demonstrate that the sensor has good specificity and high sensitivity with detection of target sample quantities as small as 1.7 ng.

For future in-cell direct detection, two novel structures that use etching to narrow the fiber tip into micrometric size were designed and developed. The differences lie in the in-fiber Fabry-Perot (FP) structure. These two structures feature unique advantages such as temperature compensation capability or durability, which can fulfill different application requirements. Both of them have high potential to be narrowed down to nanometric size. With such a tiny protrusion, the sensor can be inserted into micron size cells for intracellular measurements. The possibility of monitoring in-vivo biological processes within single living cells could greatly improve our understanding of cellular function. With the FP cavity inside the fiber, the change in optical path difference (OPD) caused by the environment can be demodulated. This label-free detection method is very useful in biological areas, such as DNA hybridization detection. Compared with currently available techniques that usually consist of fluorescent dyes, our method greatly reduces the cost and increases

the reliability. It provides a valuable tool for intracellular studies that have applications ranging from medicine to national security to energy production. In addition, the fabrication is simple including only cleaving, splicing, and etching. The signal is stable with high visibility. Last but not least, the structure shows great promise for nanometric protrusion. Once this goal is achieved, the sensor can be inserted into most cells with minimal invasiveness.

What's more, the idea of a nanoscale probe has a broad impact in Scanning Near-field Optical Microscopy (SNOM), intracellular surgery, in cell sensing, manipulation, and injection.

9.2 Summary of contributions

This section lists the main contributions of this dissertation.

- Demonstrated L-b-L ESA as an effective surface modification method for immobilization of DNA onto optical fibers.
- Optimized polyelectrolyte self-assembly for optical DNA detection by experiment design and analysis.
- Developed a label-free DNA detection scheme.
- Developed an optical fiber tip sensor for DNA detection.
- Demonstrated the good specificity and high sensitivity of the sensor for DNA detection.
- Designed and fabricated two micrometric biosensors, with high potential to be developed into nanometric ones.

9.3 Suggestions for future research

Future work is suggested here for increase of the sensitivity and improvement of the specificity of the DNA sensor, enhancement in the reliability of sensor fabrication for nanometric structure, diversification in the sensor structure, integration of the sensing system and reduction of cost. An outline of further investigations is described in the following.

9.3.1 Improvement of sensitivity and specificity

The nature of the capture DNA used for selective recognition can also exert significant effects on the selectivity and the sensitivity of hybridization assays. Factors such as probe length, mobility and charge can significantly affect the stability of hybrids formed in interfacial environments. [108] A relationship between immobilization density, probe accessibility, and hybridization yield, sensitivity and selectivity of an assay will be an interesting topic.

The thermal stability of double-stranded DNA is dependent on base composition, as illustrated by differences in Tm in oligomers of the same size the magnitude of this reduction depends on the number of mismatches and length of the duplex in question. In addition, the use of suitable blocking buffer may be useful to separate the DNA with the fiber tip, and increase the reliability of the sensor.

9.3.2 Nanoprobe design and fabrication

The nanobiosensor provides a valuable tool for intracellular studies, which allows scientists to physically probe inside a living cell without destroying it. It is of significance in applications ranging from medicine to national security to energy production. This area of research is truly at the nexus of nanotechnology, biology, engineering and information technology. Nanoprobe design will be another very interesting topic to continue. As reviewed in Chapter 3, there are many different methods to fabricate taper fiber probes. Among them, chemical etching is preferable.

Investigation of DNA immobilization and hybridization effects onto the nanoprobe will arouse great interest. The challenge will be the sensitivity of the sensor and signal detection, i.e., how low a concentration of the target DNA hybridized will be detected.

The smaller the size of the sensor tip, the relative roughness will be increased. More residual HF from the etching process may be stay on the surface. This surface treatment will greatly influence the following L-b-L ESA. The worst effect may be the complete failure of film growth. Therefore, the sensor needs to be thoroughly rinsed after etching. According to [109], PSS/PAH polymeric films typically have a roughness of 4.5A. Thanks to the self-healing effect of the L-b-L ESA, the roughness may be better after many bilayers film growth. A stable self-consistent growth requires that surface charge density and surface roughness reach the same equilibrium value after each adsorption cycle. [109]

Also, the rinsing and drying process are very critical for the L-b-L ESA. Other research groups [109] also have found out that the thickness may change a lot after overnight storage and longer time (two weeks') "cooling". The explanation is the removal and reentry of water. The estimation is that approximately of the film's mass is loosely bound water. In our case, when the sensor tip reaches much smaller size, the relative surface area will be much bigger. The percentage of water bound may significantly increase, which may be the cause for the increase of film thickness for the smaller size sensors.

As mentioned in the previous chapters, salt concentration has great influence on film thickness and roughness. Very high salt concentration may cause the failure of film growth due to the propagation of surface defects caused by increased roughness.

In addition, when the nanometric size diameter of the fiber-optic probe is much narrower than the 400nm wavelength of light, only target molecules bound to the bioreceptors at the tip are exposed to and excited by the evanescent field of a laser signal. Special waveguide analysis will be necessary.

9.3.3 Development of signal detection and processing instrumentation

Currently we are using a Micron Optics si720 Component Testing System (CTS) that operates at 1550nm for signal detection. To meet the requirements of program, the current system will require modification to further improve the SNR. The reflected signal from the nanoprobe may be too weak to be detected. The processing algorithm will also need to be tailored for this particular kind of sensor.

9.3.4 Packaging

Sensor packaging is very important to increase its robustness and ease of operation. For an on-site or point-of-care application, it would be advantageous to have a system in which the liquid handling, the detection, and the readout of the sensor would all be integrated in one system. This integration would minimize problems due to contamination or mechanical damage of the sensors, and it would also be possible to automate the process in order to save time and avoid human error.

9.3.5 Other sensor structure design

Based on this principle, a variety of DNA sensors can be developed, including those based on a FP cavity, which can be in-fiber or not. The sensor is not only applicable not only to the detection of DNA hybridization, but also to the other in situ monitoring of the binding process in biosensing applications such as antibody-antigen interactions. Varying the sensing material incorporated into the sensor may expand the application area into gas and chemical sensing.

Bibliography

[1] Y. L. Zhou and Y. Z. Li. Layer-by-layer self-assembly of multilayer films containing dna and eu3+: Their characteristics and interactions with small molecules. *Langmuir*, 20:7208–7214, 2004.

[2] D. B. Young and B.D. Robertson. Approaches to combat tuberculosis. *Current Opinion in Biotechnology*, 9:650–652, 1998.

[3] E.Cambau, C. Wichlacz, C.Truffot-Pernot, and V. Jarlier. Evaluation of the new mb redox system for detection of growth of mycobacteria. *Journal of clinical microbiology*, 37:2013–2015, 1999.

[4] S.Chanteau, L. Rahalison, L.Ralafiarisoa, J. Foulon, M.Ratsitorahina, L.Ratsifasoamanana, E.Carniel, and F. Nato. Development and testing of a rapid diagnostic test for bubonic and pneumonic plague. *Lancet*, 361:211–216, 2003.

[5] D.Jungkind. Molecular testing for infectious disease. *Science*, 294:1553–1555, 2001.

[6] E.Palecek, M.Fojta, and F.Jelen. New approaches in the development of dna sensors: hybridization and electrochemical detection of dna and rna at two different surfaces. *Bioelectrochemistry*, 56:85C90, 2002.

[7] J.L.DeRisi, V.R.Iyer, and P.O. Brown. Exploring the metabolic and genetic control of gene expression on a genomic scale. *Science*, 278:680–686, 1997.

[8] W. Tan, Z.Y. Shi, D. Birnbaum S. Smith, and R. Kopelman. Submicrometer intracellular chemical optical fiber sensors. *Science*, 258:778–781, 1992.

[9] W. Tan, Z.Y. Shi, and R. Kopelman. Development of submicron chemical fiber optic sensors. *Analytical chemistry*, 64:2985–2990, 1992.

[10] B.M.Cullum, G.D.Griffin, G.H.Miller, and T.Vo-Dinh. Intracellular measurements in mammary carcinoma cells using fiber-optic nanosensors. *Analytical Biochemistry*, 277:25–32, 2000.

[11] T.A. Taton, C. A. Mirkin, and R. L. Letsinger. Scanometric dna array detection with nanoparticle probes. *Science*, 289:1757–1760, 2000.

[12] S.Moses, S. H. Brewer, L. B.Lowe, S. E.Lappi, L. B. G.Gilvey, M.Sauthier; R. C.Tenent, D. L.Feldheim, and S.Franzen. Characterization of single- and double-stranded dna on gold surfaces. *Langmuir*, 20:11134–11140, 2004.

[13] E. Paleek, M. Fojta, M. Tomschik, and J. Wang. Electrochemical biosensors for dna hybridization and dna damage. *Biosensors & bioelectronics*, 13:621–628, 1998.

[14] G. Marrazza, I. Chianella, and M. Mascini. Disposable dna electrochemical sensor for hybridization detection. *Biosensors & bioelectronics*, 14:43–51, 1999.

[15] H. Zhang, H. Tan, R. Wang, W. Wei, and S. Yao. Immobilization of dna on silver surface of bulk acoustic wave sensor and its application to the study of uv-c damage. *Analytica chimica acta*, 374:31–38, 1998.

[16] E.Souteyrand, J. P.Cloarec, J. R.Martin, C.Wilson, I.Lawrence, S.Mikkelsen, and M. F.Lawrence. Direct detection of the hybridization of synthetic homo-oligomer dna sequences by field effect. *Journal of physical chemistry. B*, 101:2980–2985, 1997.

[17] R.Lenigk, M.Carles, N. Y.Ip, and N. J.Sucher. Surface characterization of a silicon-chip-based dna microarray. *Langmuir*, 17(8):2497–2501, 2001.

[18] A. P. Alivisatos, K. P. Johnsson, X. Peng, T. E. Wilson, C. J. Loweth, M. P. Bruchez, and P. G. Schultz. Organization of 'nanocrystal molecules' using dna. *Nature*, 382:609–611, 1996.

[19] S. Park, T. A. Taton, and C. A. Mirkin. Array-based electrical detection of dna with nanoparticle probes. *Science*, 295:1503–1506, 2002.

[20] R.Moller, A.Csaki, J. M.Kohler, and W.Fritzsche. Electrical classification of the concentration of bioconjugated metal colloids after surface adsorption and silver enhancement. *Langmuir*, 17(18):5426–5430, 2001.

[21] M. Urban, R. Moller, and W. Fritzsche. A paralleled readout system for an electrical dna-hybridization assay based on a microstructured electrode array. *Review of scientific instruments*, 74:1077–1081, 2003.

[22] E. Diessel, K. Grothe, H. Siebert, B. D. Warner, and J. Burmeister. Online resistance monitoring during autometallographic enhancement of colloidal au labels for dna analysis. *Biosensors & bioelectronics*, 19:1229–1235, 2004.

[23] L.Authier, C.Grossiord, P.Brossier, and B.Limoges. Gold nanoparticle-based quantitative electrochemical detection of amplified human cytomegalovirus dna using disposable microband electrodes. *Analytical chemistry*, 73(18):4450–4456, 2001.

[24] C. A. Mirkin, R. L. Letsinger, R. C. Mucic, and J. J. Storhoff. A dna-based method for rationally assembling nanoparticles into macroscopic materials. *Nature*, 382:607–609, 1996.

[25] R. Elghanian, R. C. Mucic J. J. Storhoff, R. L. Letsinger, and C. A. Mirkin. Selective colorimetric detection of polynucleotides based on the distance-dependent optical properties of gold nanoparticles. *Science*, 277:1078–1081, 1997.

[26] J. J.Storhoff, R.Elghanian, R. C.Mucic, C. A.Mirkin, and R. L.Letsinger. One-pot colorimetric differentiation of polynucleotides with single base imperfections using gold nanoparticle probes. *Journal of American Chemical Society*, 120(9):1959–1964, 1998.

[27] L.A. Chrisey, G.U. Lee, and C.E. O'Ferrall. Covalent attachment of synthetic dna to self-assembled monolayer films. *Nucleic acids research*, 24:3031–3039, 1996.

[28] M.Dequaire, C.Degrand, and B.Limoges. An electrochemical metalloimmunoassay based on a colloidal gold label. *Analytical chemistry*, 72(22):5521–5528, 2000.

[29] M.Ozsoz, A.Erdem, K.Kerman, D.Ozkan, B.Tugrul, N. Topcuoglu, H.Ekren, and M.Taylan. Electrochemical genosensor based on colloidal gold nanoparticles for the detection of factor v leiden mutation using disposable pencil graphite electrodes. *Analytical chemistry*, 75(9):2181–2187, 2003.

[30] J.Wang, D.Xu, A.-N.Kawde, and R.Polsky. Metal nanoparticle-based electrochemical stripping potentiometric detection of dna hybridization. *Analytical chemistry*, 73(22):5576–5581, 2001.

[31] J.Wang, G.Liu, and A.Merkoci. Electrochemical coding technology for simultaneous detection of multiple dna targets. *Journal of American Chemical Society*, 125(11):3214–3215, 2003.

[32] C. J.Yu, Y.Wan, H.Yowanto, J.Li, C.Tao, M. D.James, C. L.Tan, G. F.Blackburn, and T. J.Meade. Electronic detection of single-base mismatches in dna with ferrocene-modified probes. *Journal of American Chemical Society*, 123(45):11155–11161, 2001.

[33] E. M. Boon and J. K. Barton. Charge transport in dna. *Current opinion in structural biology*, 12:320–329, 2002.

[34] R.D. Mitra and G.M. Church. In situ localized amplification and contact replication of many individual dna molecules. *Nucleic Acids Research*, 27:4830–4837, 1999.

[35] K. Hashimoto, K. Ito, and Y. Ishimori. Sequence-specific gene detection with a gold electrode modified with dna probes and an electrochemically active dye. *Analytical chemistry*, 66(21):3830–3833, 1994.

[36] E.Souteyrand, J. P.Cloarec, J. R.Martin, C.Wilson, I.Lawrence, S.Mikkelsen, and M. F.Lawrence. Direct detection of the hybridization of synthetic homo-oligomer dna sequences by field effect. *Journal of Physical Chemistry B*, 101(15):2980–2985, 1996.

[37] S. Hashioka, M. Saito, E. Tamiya, and H. Matsumura. Deoxyribonucleic acid sensing device with 40-nm-gap-electrodes fabricated by low-cost conventional techniques. *Applied physics letters*, 85:687–688, 2004.

[38] Y.Okahata, M.Kawase, K.Niikura, F.Ohtake, H.Furusawa, and Y.Ebara. Kinetic measurements of dna hybridization on an oligonucleotide-immobilized 27-mhz quartz crystal microbalance. *Analytical chemistry*, 70(7):1288–1296, 1998.

[39] R. Berger, E. Delamarche, H. P. Lang, C. Gerber, J. K. Gimzewski, E. Meyer, and H. Gntherodt. Surface stress in the self-assembly of alkanethiols on gold. *Science*, 276:2021–2024, 1997.

[40] J. Fritz, M. K. Baller, H. P. Lang, H. Rothuizen, P. Vettiger, E. Meyer, H. J. Gntherodt, Ch. Gerber, and J. K. Gimzewski. Translating biomolecular recognition into nanomechanics. *Science*, 288:316–318, 2000.

[41] K. Miyamoto, K. Ishibashi, K. Hiroi, Y. Kimura, H. Ishii, and M. Niwano. Label-free detection and classification of dna by surface vibration spectroscopy in conjugation with electrophoresis. *Applied Physics Letters*, 86:053902, 2005.

[42] J.Wang and A. J.Bard. Monitoring dna immobilization and hybridization on surfaces by atomic force microscopy force measurements. *Analytical chemistry*, 73(10):2207–2212, 2001.

[43] M. Nagel, P. H. Bolivar, M. Brucherseifer, H. Kurz, A. Bosserhoff, and R. Bttner. Integrated thz technology for label-free genetic diagnostics. *Applied Physics Letters*, 80:154–156, 2002.

[44] M. Su, S. Li, and V. P. Dravid. Microcantilever resonance-based dna detection with nanoparticle probes. *Applied Physics Letters*, 82:3562–3564, 2003.

[45] M. Ueda, M. Takai, K. Taniguchi, Y. Takamura, Y. Horiike, and Yoshinobu Baba. Fluorescence modulation of long dna molecules adsorbed onto a microelectrode surface. *Applied Physics Letters*, 83:5086–5088, 2003.

[46] P. Hoffmann, B. Dutoit, and R. Salath. Comparison of mechanically drawn and protection layer chemically etched optical fiber tips. *Ultramicroscopy*, 61:165–170, 1995.

[47] B. A. F. Puygranier, S. Montgomery, J. Ashe, R. J. Turner, and P. Dawson. Imaging tip formation in single-mode optical fibres. *Ultramicroscopy*, 86:233–239, 2001.

[48] S. I. Hosain, Y. Lacroute, and J. P. Goudonnet. A simple low-cost highly reproducible method of fabricating optical fiber tips for a photon scanning tunneling microscope. *Microwave and Optical Technology Letters*, 13:243–248, 1996.

[49] T. Held, S. Emonin, O. Marti, and O. Hollricher. Method to produce high-resolution scanning near-field optical microscope probes by beveling optical fibers. *Review of Scientific Instruments*, 71:3118–3122, 2000.

[50] T.H.W. Pak, K.Wong, and C. Ho. *Optical Fiber Tip Fabricated by Surface Tension Controlled Etching*. Hilton Head Island, South Carolina, 2002.

[51] S.Mononobe and M. Ohtsu. Fabrication of a pencil-shaped fiber probe for near-field optics by selective chemical etching. *Journal of Lightwave Technology*, 14:2231–2235, 1996.

[52] R.U.Maheswari, S.Mononobe, and M.Ohtsu. Control of apex shape of the fiber probe employed in photon scanning tunneling microscope by a multistep etching method. *Journal of Lightwave Technology*, 13:2308–2313, 1995.

[53] S.Mononobe and M.Ohtsu. A model based on geometrical construction in designing a pencil-shaped fiber probe for near-field optics. *Journal of Lightwave Technology*, 15:1051–1055, 1997.

[54] T.Pangaribuan, S.Jiang, and M.Ohtsu. Two-step etching method for fabrication of fibre probe for photon scanning tunneling microscope. *Electronics letters*, 29:1978–1979, 1993.

[55] Y.Belosludtsev, B.Iverson, S.Lemeshko, R.Eggers, R. Wiese, S.Lee, T.Powdrill, and M. Hogan. Dna microarrays based on noncovalent oligonucleotide attachment and hybridization in two dimensions. *Analytical biochemistry*, 292:250–256, 2001.

[56] G.U. Lee, L.A. Chrisey, and R.J. Colton. Direct measurement of the forces between complementary strands of dna. *Science*, 266:771–773, 1994.

[57] Z. Guo, R. A. Guilfoyle, A. J. Thiel, R. Wang, and L. M. Smith. Direct fluorescence analysis of genetic polymorphisms by hybridization with oligonucleotide arrays on glass supports. *Nucleic Acids Research*, 22:5456–5465, 1994.

[58] M. Boncheva, L. Scheibler, P. Lincoln, H. Vogel, and B. Akerman. Design of oligonucleotide arrays at interfaces. *Langmuir*, 15:4317 – 4320, 1999.

[59] T.-Y.Lee and Y.-B.Shim. Direct dna hybridization detection based on the oligonucleotide-functionalized conductive polymer. *Analytical chemistry*, 73(22):5629–5632, 2001.

[60] Y. Liu, A. Rosidian, K. Lenahan, Y. Wang, T. Zeng, and R. O. Claus. Characterization of electrostatically self-assembled nanocomposite thin films. *Smart materials and structures*, 8:100–105, 1999.

[61] G. Decher. Fuzzy nanoassemblies: Toward layered polymeric multicomposites. *Science*, 277:1232–1237, 1997.

[62] Y. Lvov, K. Ariga, I. Ichinose, and T. Kunitake. Assembly of multicomponent protein films by means of electrostatic layer-by-layer adsorption. *Journal of the American Chemical Society*, 117(22):6117–6123, 1995.

[63] Y. Lvov, G. Decher, and G. Sukhorukov. Assembly of thin films by means of successive deposition of alternate layers of dna and poly(allylamine). *Macromolecules*, 26(20):5396–5399, 1993.

[64] Y. M.Lvov, Z.Lu, J. B.Schenkman, X.Zu, and J. F.Rusling. Direct electrochemistry of myoglobin and cytochrome p450cam in alternate layer-by-layer films with dna and other polyions. *Journal of the American Chemical Society*, 120(17):4073–4080, 1998.

[65] S. Watanabe and S. L. Regen. Dendrimers as building blocks for multilayer construction. *Journal of the American Chemical Society*, 116(19):8855–8856, 1994.

[66] D. L.Feldheim, K. C.Grabar, M. J.Natan, and T. E.Mallouk. Electron transfer in self-assembled inorganic polyelectrolyte/metal nanoparticle heterostructures. *Journal of the American Chemical Society*, 118(32):7640–7641, 1996.

[67] Y. Liu, A. Wang, and R. O. Claus. Layer-by-layer electrostatic self-assembly of nanoscale fe3o4 particles and polyimide precursor on silicon and silica surfaces. *Applied Physics Letters*, 71:2265–2267, 1997.

[68] K. M. Lenahan, Y. Wang, Y. Liu, R. O. Claus, J. R. Heflin, D. Marciu, and C. Figura. Novel polymer dyes for nonlinear optical applications using ionic self-assembled monolayer technology. *Advanced Materials*, 10:853–855, 1998.

[69] Y.Lvov, K.Ariga, M. Onda, I.Ichinose, and T.Kunitake. Alternate assembly of ordered multilayers of sio2 and other nanoparticles and polyions. *Langmuir*, 13(23):6195–6203, 1997.

[70] N. A. Kotov, I. Dekany, and J. H. Fendler. Layer-by-layer self-assembly of polyelectrolyte-semiconductor nanoparticle composite films. *Journal of Physical Chemistry*, 99(35):13065–13069, 1995.

[71] P. Stroeve, V. Vasquez, M. A. N. Coelho, and J. F. Rabolt. Gas transfer in supported films made by molecular self-assembly of ionic polymers. *Thin solid films*, 284:708–712, 1996.

[72] J.-M.Levasalmi and T. J.McCarthy. Poly(4-methyl-1-pentene)-supported polyelectrolyte multilayer films: Preparation and gas permeability. *Macromolecules*, 30(6):1752–1757, 1997.

[73] M. Onda, Y. Lvov, K. Ariga, and T. Kunitake. Sequential actions of glucose oxidase and peroxidase in molecular films assembled by layer-by-layer alternate adsorption. *Biotechnology and Bioengineering*, 51:163–167, 1996.

[74] P. T. Hammond and G. M. Whitesides. Formation of polymer microstructures by selective deposition of polyion multilayers using patterned self-assembled monolayers as a template. *Macromolecules*, 28(22):7569–7571, 1995.

[75] D.Laurent and J. B.Schlenoff. Multilayer assemblies of redox polyelectrolytes. *Langmuir*, 13(6):1552–1557, 1997.

[76] A. Laschewsky, B. Mayer, E. Wischerhoff, X. Arys, P. Bertrand, A. Delcorte, and A. Jonas. A new route to thin polymeric, non-centrosymmetric coatings. *Thin solid films*, 284:334–337, 1996.

[77] G. Decher, J. D. Hong, and J. Schmitt. Buildup of ultrathin multilayer films by a self-assembly process: Iii. consecutively alternating adsorption of anionic and cationic polyelectrolytes on charged surfaces. *Thin solid films*, 210:831–835, 1992.

[78] S. W. Keller, H. Kim, and T. E. Mallouk. Layer-by-layer assembly of intercalation compounds and heterostructures on surfaces: Toward molecular.

[79] J. Schmitt, T. Gruenewald, G. Decher, P. S. Pershan, K. Kjaer, and M. Loesche. Internal structure of layer-by-layer adsorbed polyelectrolyte films: a neutron and x-ray reflectivity study. *Macromolecules*, 26(25):7058–7063, 1993.

[80] C. Bariin, I. R. Matłas, F. J. Arregui, and M. Lpez-Amo. Optical fiber humidity sensor based on a tapered fiber coated with agarose gel. *Sensors and actuators. B*, 69:127–131, 2000.

[81] M. A.; Fleer G. J.; Bohmer M. R. Hoogeveen, N. G.; Cohen Stuart. Formation and stability of multilayers of polyelectrolytes. *Langmuir*, 12(15):3675–3681, 1996.

[82] K.Lowack and C. A.Helm. Molecular mechanisms controlling the self-assembly process of polyelectrolyte multilayers. *Macromolecules*, 31(3):823–833, 1998.

[83] D.Yoo, S. S.Shiratori, and M. F.Rubner. Controlling bilayer composition and surface wettability of sequentially adsorbed multilayers of weak polyelectrolytes. *Macromolecules*, 31(13):4309–4318, 1998.

[84] D.Yoo, S. S.Shiratori, and M. F.Rubner. Controlling bilayer composition and surface wettability of sequentially adsorbed multilayers of weak polyelectrolytes. *Macromolecules*, 31(13):4309–4318, 1998.

[85] S. S.Shiratori and M. F.Rubner. ph-dependent thickness behavior of sequentially adsorbed layers of weak polyelectrolytes. *Macromolecules*, 33(11):4213–4219, 2000.

[86] Richard G. Miekka Alan S. Michaels. Polycation-polyanion complexes: Preparation and properties of poly-(vinylbenzyltrimethylammonium) poly-(styrenesulfonate). *Journal of Physical Chemistry*, 65(10):1765–1773, 1961.

[87] F. A. M.; Koopal L. K. Vermeer, A. W. P.; Leermakers. Adsorption of weak polyelectrolytes on surfaces with a variable charge. self-consistent-field calculations. *Langmuir*, 13(16):4413–4421, 1997.

[88] S. T.Dubas and J. B.Schlenoff. Factors controlling the growth of polyelectrolyte multilayers. *Macromolecules*, 32(24):8153–8160, 1999.

[89] J. B.Schlenoff, H.Ly, and M.Li. Charge and mass balance in polyelectrolyte multilayers. *Journal of the American Chemical Society*, 120(30):7626–7634, 1998.

[90] B. Giese, J. Amaudrut, A. Kohler, M. Spormann, and S. Wessely. Direct observation of hole transfer through dna by hopping between adenine bases and by tunnelling. *Nature*, 412:318–320, 2001.

[91] D. Porath, A. Bezryadin, S. Vries, and Cees Dekker. Direct measurement of electrical transport through dna molecules. *Nature*, 403:635–638, 2000.

[92] Y. A.Berlin, A. L.Burin, and M. A.Ratner. Charge hopping in dna. *Journal of the American Chemical Society*, 123(2):260–268, 2001.

[93] A.B.Steel, T. M.Herne, and M. J.Tarlov. Electrochemical quantitation of dna immobilized on gold. *Analytical chemistry*, 70:4670–4677, 1998.

[94] D.Yoo, S. S.Shiratori, and M. F.Rubner. Controlling bilayer composition and surface wettability of sequentially adsorbed multilayers of weak polyelectrolytes. *Macromolecules*, 31:4309–4318, 1998.

[95] P. Bertrand, A. Jonas, A. Laschewsky, and R. Legras. Ultrathin polymer coatings by complexation of polyelectrolytes at interfaces: suitable materials, structure and properties. *Macromolecular Rapid Communications*, 21:319–348, 2000.

[96] S. T.Dubas and J. B.Schlenoff. Factors controlling the growth of polyelectrolyte multilayers. *Macromolecules*, 32:8153–8160, 1999.

[97] Y. Lvov, G. Decher, and H. Moehwald. Assembly, structural characterization, and thermal behavior of layer-by-layer deposited ultrathin films of poly(vinyl sulfate) and poly(allylamine). *Langmuir*, 9:481–486, 1993.

[98] S. L.Clark, M. F.Montague, and P. T.Hammond. Ionic effects of sodium chloride on the templated deposition of polyelectrolytes using layer-by-layer ionic assembly. *Macromolecules*, 30:7237–7244, 1997.

[99] L.Krasemann and B.Tieke. Selective ion transport across self-assembled alternating multilayers of cationic and anionic polyelectrolytes. *Langmuir*, 16:287–290, 2000.

[100] N. G.Hoogeveen, M. A.Cohen Stuart, G. J.Fleer, and M. R.Bohmer. Formation and stability of multilayers of polyelectrolytes. *Langmuir*, 12:3675–3681, 1996.

[101] Y. Zhang, K.L.Cooper, and A. Wang. Multicavity fabry-perot interferometric thin-film sensor with built-in temperature compensation. *IEEE Photonics Technology Letters*, 17(2):2712–2714, 2005.

[102] Y. Lvov, G. Decher, and G. Sukhorukov. Assembly of thin films by means of successive deposition of alternate layers of dna and poly(allylamine). *Macromolecules*, 26:5396–5399, 1993.

[103] D. T. Dennis, T. V. Inglesby, D. A. Henderson, J. G. Bartlett, M. S. Ascher, E. Eitzen, A. D. Fine, A. M. Friedlander, J. Hauer, M. Layton, S. R. Lillibridge, J. E. McDade, M. T. Osterholm, T. O'Toole, G. Parker, T. M. Perl, P. K. Russell, and K. Tonat. Tularemia as a biological weapon. *JAMA*, 285:2763–2773, 2001.

[104] D.J.Markos, B.L.Ipson, K.H.Smith, S.M.Schultz, R.H.Selfridge, T.D. Monte, R. B. Dyott, and G. Miller. Controlled core removal from a d-shaped optical fiber. *Applied Optics*, 5:7121–7125, 1996.

[105] K.R.Williams and R.S.Muller. Etch rates for micromachining processing. *Journal of micromechanics and microengineering*, 5:256–269, 1996.

[106] A. Grosse, M. Grewe, and H. Fouckhardt. Deep wet etching of fused silica glass for hollow capillary optical leaky waveguides in microfluidic devices. *Journal of micromechanics and microengineering*, 11:257–262, 2001.

[107] Z. Huang, X. Chen, and A. Wang. Intrinsic fabry-pe/spl acute/rot fiber sensor for temperature and strain measurements. *IEEE photonics technology letters*, 17:2403– 2405, 2005.

[108] L. M.Demers, L. A.Mirkin, R. C.Mucic, R. A.Reynolds, R. L.Letsinger, R.Elghanian, and G.Viswanadham. A fluorescence-based method for determining the surface coverage and hybridization efficiency of thiol-capped oligonucleotides bound to gold thin films and nanoparticles. *Analytical chemistry*, 72:5535–5541, 2000.

[109] Y. Lvov, G. Decher, and H. Moehwald. Assembly, structural characterization, and thermal behavior of layer-by-layer deposited ultrathin films of poly(vinyl sulfate) and poly(allylamine). *Langmuir*, 9:481–486, 1993.

Vita

Xingwei Wang was born in Guangzhou, P.R. China, in 1978. She received her B.S. degree in Electrical Engineering with a minor in Computer Software from Zhongshan University (Sun Yat-sen University), Guangzhou, P.R. China, in September 2000. She received her M.S. degree in Electrical Engineering from Virginia Polytechnic Institute and State University (Virginia Tech), Blacksburg, VA, USA, in 2004. She is expecting her Ph.D. degree in Electrical Engineering in August, 2006, from Virginia Tech.

She joined the Center of Optoelectronics at Zhongshan University in 2000, focusing on research about erbium doped fiber amplifiers, and liquid crystal Fabry-Perot tunable filters. In January 2003, she joined the Center for Photonics Technology at Virginia Tech as a graduate research assistant. She has authored or co-authored more than 20 journal and conference papers, and 8 patent disclosures. She has also contributed to the writing of 9 proposals. Her current research interests include optical sensors for medical, chemical and industrial applications; nanoprobe design and fabrication; self-assembled nanostructures; optical biosensing and biomedical devices; optical imaging; MEMS technology and electromagnetic wave propagation. Her previous research experience includes temperature, pressure, acoustic, strain, and chemical sensors.

Ms. Wang is a student member of IEEE and OSA.